

The Contribution of  $\beta$ -Hexosaminidase and Hyaluronidase 1 to  
Hyaluronan Turnover

by

Lara E.M. Gushulak

Thesis submitted to the Faculty of Graduate Studies of

The University of Manitoba

In partial fulfilment of the requirements of the degree of

MASTER OF SCIENCE

Department of Biochemistry and Medical Genetics

University of Manitoba

Winnipeg

Copyright © 2012 Lara E.M. Gushulak

## Abstract

Hyaluronan, a member of the glycosaminoglycan family, is a critical component of the extracellular matrix. A model for hyaluronan degradation has been advanced that invokes the activity of both hyaluronidases and exoglycosidases. However, no *in vivo* studies have been done to determine the extent to which these enzymes contribute to hyaluronan breakdown. Herein, we have used several mouse models to investigate the contributions of the exoglycosidase,  $\beta$ -hexosaminidase, and the endoglycosidase, hyaluronidase 1, to the lysosomal degradation of hyaluronan. We employed immunohistochemistry and fluorophore assisted carbohydrate electrophoresis to determine the degree of hyaluronan accumulation in mice deficient in one or both enzyme activities.  $\beta$ -Hexosaminidase-deficient mice displayed only low levels of hyaluronan accumulation, limited to the liver and lymph node. The distribution and levels of hyaluronan in hyaluronidase 1-deficient mice were similar to that observed in  $\beta$ -hexosaminidase-deficient mice. Interestingly, extensive global hyaluronan accumulation was present in mice deficient in both enzymes, with the highest levels found in liver and lymph node. Chondroitin, a glycosaminoglycan similar in structure to hyaluronan, was also broadly accumulating in mice deficient in both enzymes. Further, the accumulation of chondroitin sulphate derivatives was detected in mice deficient in both enzymes, as well as in  $\beta$ -hexosaminidase-deficient mice, indicating that both enzymes play a significant role in chondroitin sulphate breakdown. Extensive accumulation of hyaluronan and chondroitin when both enzymes are lacking suggests  $\beta$ -hexosaminidase and hyaluronidase 1 are functionally redundant in hyaluronan and chondroitin breakdown, as broad extensive accumulation was not observed in mice deficient in only one of these enzymes.

## Acknowledgements

I would first and foremost like to thank my supervisor, Dr. Barbara Triggs-Raine, for giving me the opportunity to complete a Master's degree in her lab. Barb is an amazing teacher, mentor, and scientist who has achieved a lab environment that actually feels like a second home. She is one of the most patient and helpful people I have had the pleasure to work with. Her willingness to listen, lend a hand, and provide support throughout the completion of my degree was unprecedented. Furthermore, Barb's capability to balance work, life, and family is a model to which I will strive to achieve.

Secondly, I would like to acknowledge my committee and lab members. Thank you to Dr. Steve Pind and Dr. Sabine Hombach-Klonish for your experimental and scientific writing advice and your belief in my Master's project. To my past and present lab members, especially Rick Hemming and Joy Armistead, I appreciate all your suggestions, support, and help throughout my project and troubleshooting struggles. Joy has an amazing gift to make a person smile, laugh, and recognize the bright side of a situation. She is a remarkable young scientist and a true friend who can tell it how it is. I would also like to acknowledge Xiaoli Wu from the Ding lab for answering my wealth of technical questions and her assistance with unfamiliar laboratory equipment.

Furthermore, I would like to give gratitude to my parents, my brother, my future sister-in-law Meagan, and my best friend Ashley Furlong, for the many hours they endured while listening to me proof read and practice for presentations. Thank you for always being there for me, encouraging me to always do my best, and for providing me a personal thesaurus. I am sure all of them cringe when they hear "What word can I use instead of....".

Last but certainly not least, I would like to thank Ben Barber. Ben gave me daily strength, encouragement, and ideas to keep troubleshooting with experiments. He is an incredible individual who is inspiring, compassionate, and definitely keeps me on my toes. I cannot express in words the appreciation I have for his tender personality, character, and his ability to make me smile.

## Table of contents:

### Preface:

Abstract .....	ii
Acknowledgements .....	iii
Table of contents .....	v
List of abbreviations .....	vii
List of tables .....	viii
List of figures .....	ix

### Chapter 1: Introduction ..... 1

1.1 Glycosaminoglycans .....	2
1.2 Hyaluronan .....	4
1.2.1 HA structure and distribution .....	4
1.2.2 HA functions .....	4
1.2.3 Hyaladherins .....	6
1.2.4 HA synthesis .....	8
1.2.5 HA degrading enzymes .....	9
1.2.5.1 Endoglycosidases .....	9
1.2.5.1.1 HYAL1 and HYAL2 .....	10
1.2.5.1.2 Other Hyals .....	11
1.2.5.2 Exoglycosidases .....	12
1.2.6 Model of HA turnover .....	14
1.2.7 Tissues involved in HA degradation .....	16
1.3 Lysosomal storage diseases .....	16
1.4 Human deficiencies in enzymes relevant to HA degradation .....	18
1.4.1 Human hyaluronidase deficiency .....	18
1.4.2 Human exoglycosidase deficiencies .....	19
1.4.2.1 Human $\beta$ -glucuronidase deficiency .....	19
1.4.2.2 Human $\beta$ -hexosaminidase deficiencies .....	19
1.5 Animal models of deficiency .....	20
1.5.1 Murine mucopolysaccharidosis IX .....	20
1.5.2 Murine HYAL2 deficiency .....	21
1.5.3 Murine $\beta$ -glucuronidase deficiency .....	22
1.5.4 Murine $\beta$ -hexosaminidase deficiencies .....	22
1.5.4.1 Murine Tay-Sachs and Sandhoff Disease .....	22
1.5.4.2 Murine model deficient in all isoforms of $\beta$ -hexosaminidase .....	23
1.6 Rationale .....	25
1.7 Hypothesis .....	25

### Chapter 2: Materials and Methods ..... 26

2.1 Generation of <i>Hexa</i> <sup>-/-</sup> <i>Hexb</i> <sup>-/-</sup> mice .....	27
2.2 Generation of <i>Hexa</i> <sup>-/-</sup> <i>Hexb</i> <sup>-/-</sup> <i>Hyal1</i> <sup>-/-</sup> mice .....	27
2.3 DNA isolation .....	27
2.4 Genotyping of <i>Hexa</i> <sup>-/-</sup> <i>Hexb</i> <sup>-/-</sup> mice .....	28
2.5 Genotyping of <i>Hexa</i> <sup>-/-</sup> <i>Hexb</i> <sup>-/-</sup> <i>Hyal1</i> <sup>-/-</sup> mice .....	30

2.6 Dissection and tissue preservation .....	30
2.7 Tissue processing, embedding, and microtomy .....	31
2.8 Histological staining .....	31
2.8.1 Hematoxylin and Eosin (H&E) staining .....	32
2.8.2 Alcian blue staining .....	32
2.8.3 Hyaluronan-binding protein (HABP) staining .....	33
2.9 Fluorophore assisted carbohydrate electrophoresis .....	34
2.10 Statistical analysis .....	35
<b>Chapter 3: Results Part 1 .....</b>	<b>36</b>
3.1 Description of the $\beta$ -hexosaminidase-deficient/ <i>Hexa</i> <sup>-/-</sup> <i>Hexb</i> <sup>-/-</sup> (DKO) mice .....	37
3.2 Tissue morphology and substrate accumulation in DKO mice .....	37
3.3 HABP staining of DKO mice .....	43
3.4 Fluorophore assisted carbohydrate electrophoresis of DKO tissues .....	47
3.4.1 GAG analysis in high HA turnover tissues of DKO mice .....	47
3.4.2 GAG analysis in other DKO tissues .....	51
3.5 Summary of results part 1 .....	52
<b>Chapter 4: Results Part 2 .....</b>	<b>55</b>
4.1 Rationale .....	56
4.2 Hypothesis .....	56
4.3 Phenotype of <i>Hexa</i> <sup>-/-</sup> <i>Hexb</i> <sup>-/-</sup> <i>Hyal1</i> <sup>-/-</sup> (TKO) mice .....	57
4.4 Tissue morphology and substrate accumulation in TKO tissues .....	57
4.5 Localization and accumulation of HA in TKO tissues .....	60
4.6 Identification and quantification of GAGs in TKO tissues using FACE .....	68
4.7 Quantification of GAGs in <i>C57BL6</i> and <i>C57BL6;C129</i> HYAL1-deficient mice .....	73
4.8 Summary of results part 2 .....	74
<b>Chapter 5: Discussion and Future Directions .....</b>	<b>78</b>
5.1 Discussion .....	79
5.1.1 Functional redundancy between $\beta$ -hexosaminidase and HYAL1 .....	79
5.1.2 Clinical relevance of a functional redundancy .....	80
5.1.3 Major tissues involved in HA metabolism .....	80
5.1.4 Role of HYAL1 in brain .....	82
5.1.5 $\beta$ -hexosaminidase and HYAL1 take part in the degradation of multiple GAGs .....	83
5.1.6 Substrate specificity of the $\beta$ -hexosaminidase isoforms .....	84
5.2 Conclusion .....	85
5.3 Future directions .....	86
<b>References .....</b>	<b>89</b>

## List of abbreviations:

ABC	ATP-binding cassette
ANOVA	analysis of variance
DAB	diaminobenzidine
DKO	double knockout
ECM	extracellular matrix
EDTA	ethylenediaminetetraacetic acid
FACE	fluorophore assisted carbohydrate electrophoresis
GAG	glycosaminoglycan
GalNAc	N-acetylgalactosamine
GlcA	glucuronic acid
GlcNAc	N-acetylglucosamine
GlcNS	N-sulfoglucosamine
GPI	glycosylphosphatidyl-inositol
HA	hyaluronan
HABP	hyaluronan binding protein
HAS	hyaluronan synthase
HARE	hyaluronan receptor of endocytosis
HEK	human embryonic kidney
HMW	high molecular weight
H&E	hematoxylin and eosin
Hyal	hyaluronidase
IdoA	iduronic acid
LMW	low molecular weight
LYVE-1	lymphatic vessel endothelial hyaluronan receptor-1
NaCl	sodium chloride
PBS	phosphate-buffered saline
PCR	polymerase-chain reaction
PLP	paraformaldehyde lysine periodate
RHAMM	receptor of hyaluronan-mediated motility
S <sub>B</sub>	dermatan sulphate
S <sub>D</sub>	chondroitin type D
SDS	sodium dodecyl sulphate
S <sub>E</sub>	chondroitin type E
TBST	tris buffered saline tween
TKO	triple knockout
UA2S	chondroitin-2-sulphate
UDP	uridine diphosphate
WT	wild-type
OS	non-sulphated chondroitin

**List of tables:**

<b>Table 1. Defining characteristics of glycosaminoglycans .....</b>	<b>3</b>
<b>Table 2. Primers used for PCR-based genotyping .....</b>	<b>29</b>

## List of figures:

Figure 1: Schematic of the HA disaccharide repeating unit .....	5
Figure 2: A proposed model of HA degradation .....	15
Figure 3: Analysis of tissue morphology in DKO, WT, and <i>HexB</i> <sup>-/-</sup> mice .....	38
Figure 4: Distribution of GAGs in DKO, WT, and <i>HexB</i> <sup>-/-</sup> mice .....	41
Figure 5: HA localization in high HA turnover tissues of DKO, WT, and <i>HexB</i> <sup>-/-</sup> mice .....	44
Figure 6: HA localization in other tissues of DKO, WT, and <i>HexB</i> <sup>-/-</sup> mice .....	45
Figure 7: Representative FACE gel of various GAG disaccharides in DKO and WT mice .....	48
Figure 8: Quantification of GAG levels in high HA turnover tissues in DKO, WT, and <i>HexB</i> <sup>-/-</sup> mice .....	50
Figure 9: Quantification of GAG levels in other tissues from DKO, WT, and <i>HexB</i> <sup>-/-</sup> mice .....	53
Figure 10: Analysis of tissue morphology in TKO mice and DKO controls .....	58
Figure 11: GAG distribution in TKO mice and DKO controls .....	61
Figure 12: HA localization in vascular tissues of TKO mice and DKO controls .....	63
Figure 13: HA localization in avascular tissues of TKO mice and DKO controls .....	66
Figure 14: FACE of various GAG disaccharides in TKO and DKO mouse tissue .....	69
Figure 15: Quantification of GAGs in TKO high HA turnover tissues .....	70
Figure 16: Quantification of GAG accumulation in other TKO tissues .....	72
Figure 17: Analysis of HA and chondroitin sulphate levels in <i>C57BL6</i> ; <i>C129</i> HYAL1-deficient tissues .....	76
Figure 18: Analysis of HA and chondroitin sulphate levels in <i>C57BL6</i> HYAL1-deficient tissues .....	77

## **Chapter 1: Introduction**

## 1.1 Glycosaminoglycans:

Glycosaminoglycans (GAGs) are a family of polysaccharides rich in uronic acids and amino sugars. They are primarily found in the extracellular matrix (ECM) where they have important structural and functional roles. Individually characterized by a unique repeating disaccharide unit, to date there have been 6 types of GAGs identified<sup>1, 2</sup>. GAGs can contain either glucuronic acid (GlcA) or iduronic acid (IdoA) as their uronic acid component and N-acetyl-glucosamine (GlcNAc), N-acetyl-galactosamine (GalNAc), or N-sulfoglucosamine (GlcNS) as their amino sugar component. GAGs vary from each other not only based on their disaccharide unit, but also by their glycosidic linkages, their degree of sulphation on their carbon sugar ring, and whether or not they are attached to a protein core. Table 1 provides a summary of the structural differences observed between members of the GAG family. Information in Table 1 was summarized from Essentials of Glycobiology<sup>1,2</sup>.

The function of GAGs varies immensely, from providing structural support<sup>3</sup> to being an anticoagulant released from immune cells<sup>4</sup>. Most GAGs are covalently attached to a protein and are referred to as proteoglycans. Proteoglycans have known roles in cellular structure and function, some of which include being a component of the basement membrane<sup>5</sup>, ECM organization and lubrication<sup>6</sup>, and the binding/release of ligands that regulate signalling pathways<sup>7</sup>. The simplest member of the GAG family is hyaluronan (HA), which has often been overlooked because of its basic structure and lack of a protein core. However, as described below, HA has numerous cellular functions that are governed by its simple structure.

**Table 1:** Defining characteristics of glycosaminoglycans

<b>GAG type</b>	<b>Most common repeating unit with glycosidic bonds</b>	<b>Potential sulphate locations on carbon ring</b>	<b>Protein core</b>	<b>Primary location</b>
Hyaluronan	GlcNAc $\beta$ 1-4GlcA $\beta$ 1-3	NONE (HA)	NO	Ubiquitous
Chondroitin and its sulphated derivatives	GalNAc $\beta$ 1-4GlcA $\beta$ 1-3	NONE (0S) GalNAc <ul style="list-style-type: none"> <li>• 4S, (type A)</li> <li>• 6S, (type C)</li> <li>• 2S and 6S, (type D; S<sub>D</sub>)</li> <li>• 4S and 6S, (type E; S<sub>E</sub>)</li> </ul> GlcA <ul style="list-style-type: none"> <li>• 2S, (chondroitin-2-sulphate; UA2S)</li> </ul>	YES	Ubiquitous
Dermatan Sulphate	GalNAc $\beta$ 1-4IdoA* $\beta$ 1-3 *or GlcA	GalNAc/IdoA <ul style="list-style-type: none"> <li>• 46/2S, (S<sub>B</sub>)</li> </ul>	YES	Skin
Keratan Sulphate	Gal $\beta$ 1-4GlcNAc $\beta$ 1-3	GlcNAc <ul style="list-style-type: none"> <li>• 6S</li> </ul> Gal <ul style="list-style-type: none"> <li>• 6S</li> </ul>	YES	Eye, Cartilage
Heparan Sulphate	GlcNAc $\alpha$ 1-4GlcA* $\beta$ 1-4 *or IdoA	GlcNAc <ul style="list-style-type: none"> <li>• 6S</li> </ul> IdoA <ul style="list-style-type: none"> <li>• 2S</li> </ul>	YES	Basement membrane
Heparin	GlcNS $\alpha$ 1-4IdoA* $\alpha$ 1-4 *or GlcA	GlcNAc <ul style="list-style-type: none"> <li>• 6S</li> </ul> IdoA <ul style="list-style-type: none"> <li>• 2S</li> </ul>	YES	Mast cells Basophils

## **1.2 Hyaluronan:**

### **1.2.1 HA structure and distribution:**

HA was discovered by Karl Meyer in 1934 and was found to be composed of a repeating disaccharide unit containing GlcNAc and GlcA as shown in Figure 1<sup>8</sup>. HA can range in size from tetrasaccharides to high molecular weights (HMW), containing more than  $10^5$  saccharide units<sup>9</sup>. Due to the anionic structure of the glucuronic acid component, HA attracts water molecules, creating a hydrated sphere in the shape of a random coil<sup>10</sup>. Unlike other GAGs, HA is not sulphated and is not covalently bound to a core protein. However, HA does interact with other proteoglycans through the assistance of a link protein that is discussed below<sup>11</sup>.

The distribution of HA in rat tissues was previously analyzed<sup>12</sup>, demonstrating that HA is broadly distributed. Skin was found to have the highest concentration of HA, whereas liver was found to have the lowest. Furthermore, lymph was found to have a higher concentration of HA when compared to blood plasma<sup>13</sup>. Given the range of HA concentrations and its broad distribution, HA has been suggested/shown to have many functions.

### **1.2.2 HA functions:**

HA is abundant in the ECM of vertebrate tissues, where its primary function is to provide structural integrity at both the tissue and cellular level. The ability of HA to attract water molecules allows it to hydrate tissues, lubricate areas under high stress, such as the knee joint, and act as a space filler<sup>14</sup>. More recently, HA has been shown to also

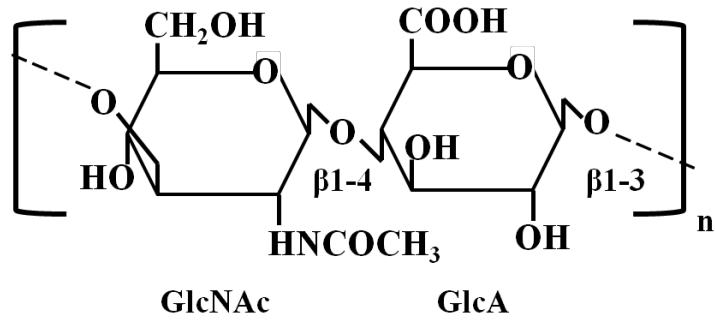


**Figure 1: Schematic of the HA disaccharide repeating unit.** HA is composed of repeating units of GlcNAc and GlcA linked by  $\beta$ 1-4 and  $\beta$ 1-3 glycosidic bonds, respectively. HA can range in size from a tetrasaccharide to more than  $10^5$  saccharides.

have functional capabilities, including a role in inflammation <sup>15</sup>, and ovulation <sup>16</sup>. Moreover, HA is used in medical devices, primarily in ophthalmology, and in the treatment of childhood and adult diseases <sup>17</sup>.

Interestingly, unlike other macromolecules, the function of HA greatly depends on its size. For example, the formation of new blood vessels is inhibited in the presence of HMW HA <sup>18</sup>, whereas angiogenesis is up-regulated in the presence of HA fragments composed of approximately 16 saccharides <sup>19</sup>. Further, several additional functions of HA were determined through analysis of a mouse model that was deficient in the major HA synthesizing enzyme, hyaluronan synthase 2 or HAS2 <sup>20</sup>. Some of those functions included cardiac development and morphogenesis. In order for HA to participate in its numerous structural and functional roles, some of which are mentioned above, HA-binding proteins and HA receptors collectively known as hyaladherins are required.

### **1.2.3 Hyaladherins:**

Hyaladherins can be classified as a group of proteins that have the ability to bind HA and either play a structural role or act as a receptor <sup>21</sup>. Many of these proteins are known to contain a link domain composed of two alpha helices and two anti-parallel beta-sheets harbouring an area of positively charged amino acids for the binding of HA <sup>22</sup>. In order for optimal binding, HA fragments of a decasaccharide or more are required. The link domain has been found to be a component of the protein core found in many proteoglycans including aggrecan, brevican, neurocan, and versican. It is the interaction between the link protein and HA that creates stabilized aggregates of proteoglycans in tissues <sup>23</sup>.

The receptors known to bind HA that contain a link domain include CD44, LYVE-1 (Lymphatic Vessel Endothelial HA receptor-1), and HARE (HA receptor of endocytosis). The most broadly expressed receptor, CD44, is known to be involved in the turnover of HA, specifically in the receptor mediated endocytosis of HA <sup>24, 25</sup>. Interactions of CD44 with HA have also been implicated in lymphocyte rolling <sup>26</sup> and angiogenesis <sup>27</sup>. LYVE-1 is structurally similar to CD44, however, expression of this receptor has only been found in the lymphatic endothelium <sup>28</sup>, liver sinusoids <sup>29</sup>, blood vessels <sup>30</sup>, and the lymphatic vessels of the kidney <sup>31</sup>. Like CD44, LYVE-1 also has the ability to facilitate the uptake HA <sup>32</sup>. HARE has been found in the liver, lymph node sinusoids, and spleen <sup>33, 34</sup>. Parallel to that of CD44 and LYVE-1, HARE has also been shown to mediate the internalization of HA <sup>35</sup>. Although all 3 of the above receptors have been shown to be involved in HA metabolism, the relative contribution of each receptor is unknown. However, lack of HA accumulation in LYVE-1 deficient mice <sup>36</sup> suggests a functional redundancy may exist among these HA receptors.

There have been several HA binding proteins identified that do not contain a link domain, including the receptor for HA-mediated motility (RHAMM) <sup>37</sup>. Localized intracellularly, some RHAMM-HA interactions have been characterized and include cell locomotion <sup>38</sup>, cytoskeleton assembly <sup>39</sup>, and tissue repair <sup>40</sup>. RHAMM-HA interactions have also been associated with several types of cancer, as cell migration is a requirement for metastasis <sup>41, 42</sup>. Given that HA and some of its receptors are found both intracellularly and extracellularly, how HA is synthesized is another interesting property that is unique among the GAGs.

#### 1.2.4 HA synthesis:

HA synthesis has been demonstrated to take place at the plasma membrane<sup>43</sup>, in contrast to that of most GAGs, which takes place intracellularly within the Golgi apparatus. Speculations as to why HA is synthesized at the plasma membrane have been made. Unlike other GAGs, HA is not covalently attached to a protein, and therefore does not require its synthesis to be linked to the endoplasmic reticulum. Further, given the massive size that HA can reach, its hydrophilic properties would cause tremendous cell swelling and potentially cause the cell to burst<sup>17</sup>. HA synthases (HAS) are embedded in the plasma membrane and function to sequentially add GlcNAc and GlcA, in the form of UDP-GlcNAc and UDP-GlcA, respectively<sup>43</sup>. At the inner plasma membrane, upon addition of the above sugars to the reducing end of the growing HA molecule, the UDP molecule is released resulting in the formation of a glycosidic bond between GlcNAc and GlcA<sup>43</sup>. Previous work completed in bacteria and in human embryonic kidney (HEK) 293 cells suggests that as HA is being synthesized, it is exported from the cell by an ATP-binding cassette (ABC) transporter<sup>44, 45</sup>. However, whether a transporter is required for mammalian HA synthesis *in vivo* is still unknown.

To date there have been three enzyme isoforms found to synthesize HA in mammals; they are known as HAS1, HAS2, and HAS3. These enzymes are embedded in the plasma membrane and have been characterized as integral proteins which all have the ability to produce newly synthesized HA. Furthermore, it has been suggested that the three isoforms of HAS, however similar, produce HA of distinct sizes and at different rates<sup>46</sup>. It was found that whereas HAS1 and HAS2 produce HA in the range of  $2 \times 10^5$  to  $2 \times 10^6$  Da, the HA generated by HAS3 was smaller in size, approximately  $1 \times 10^5$  Da. In

addition, of the three HAS isoforms, HAS3 has the greatest activity in the production of HA, whereas HAS1 is the least active<sup>46</sup>. The different sizes of HA, and the varying rates of its production, may permit for the diverse roles that HA plays within an organism.

The importance of HASs and their varying roles has been shown through knockout mouse studies<sup>20, 47, 48</sup>. The most severe phenotype was observed in a HAS2-deficient mouse model<sup>20</sup>. A deficiency of HAS2 resulted in embryonic lethality at approximately E9.5. The lethality of the HAS2-deficient embryos was attributed to abnormal heart morphogenesis because of a failure to form the endocardial cushion and a deficiency in endothelial-mesenchymal transition in the heart<sup>20</sup>. The extreme phenotype provides evidence that HAS2 plays an essential role in providing HA for development. Further, given that HAS1, HAS3, and a combined deficiency of both HAS1 and HAS3 resulted in viable and fertile mice<sup>20, 48</sup>, it is likely that HAS2 is the major HA synthesizing enzyme. In order to maintain HA homeostasis, while new HA is being synthesized, the degradation of HA must also be occurring.

### **1.2.5 HA degrading enzymes:**

#### **1.2.5.1 Endoglycosidases:**

There are two families of HA degrading enzymes, the endoglycosidases and the exoglycosidases. Hyaluronidases (Hyal) are endoglycosidases that belong to the glycosidase 56 family and are endo- $\beta$ -acetyl-hexosaminidases which function to cleave internal  $\beta$ 1-4 glycosidic bonds between GlcNAc and GlcA of HA<sup>49</sup>. Humans have been shown to have six hyaluronidase-like genes found in two clusters. The first cluster on chromosome 3, contains *HYAL1*, *HYAL2*, and *HYAL3* and a second cluster on

chromosome 7 contains *HYALP1*, *HYAL4*, and *PH-20*<sup>50</sup>. These hyaluronidase-like genes are also present in mice, with the first cluster residing on chromosome 9 and the second cluster found on chromosome 6<sup>51, 52</sup>. Unlike humans, another hyaluronidase gene has been found in mice, *Hyal5*, which clusters with the hyaluronidase-like genes on chromosome 6<sup>53</sup>.

Of the genes named above, *HYAL1* and *HYAL2* displayed broad tissue expression at relatively high levels after northern blotting was completed on numerous human tissues<sup>50, 54</sup>. Thus, *HYAL1* and *HYAL2* have been deemed as the major Hyals involved in the overall turnover of HA<sup>55</sup>, and therefore are described in detail below. The other Hyals listed above are either expressed at low levels, and/or in a tissue-specific manner, therefore, although they may be able to degrade HA they are not considered major HA turnover enzymes and consequently are only briefly described below.

#### **1.2.5.1.1 HYAL1 and HYAL2:**

*HYAL1* was first identified in 1997 in human plasma using antibody purification and was shown to cleave HA at its  $\beta$ 1-4 glycosidic bonds at an optimal working pH of approximately 4.5<sup>56</sup>. It was further shown that *HYAL1* is continuously removed from the plasma through endocytosis by endothelial cells and can actively function to degrade HA in lysosomes<sup>57</sup>. Studies have also shown that *HYAL1* can cleave HA of any size to tetrasaccharide units<sup>56</sup>. However, the ability of *HYAL1* to cleave intracellular HA is CD44 dependent in HEK 293 cells, as degradation was inhibited when CD44 was absent<sup>25</sup>. As HEK 293 cells are not of endothelial origin they may not express LYVE-1 or HARE which would explain the sole dependency of *HYAL1* on CD44 in the above

experimental system. Similar studies using cells of endothelial origin have not been completed and therefore it is possible that the dependency exhibited by HYAL1 on CD44 could be alleviated by the presence of LYVE-1 or HARE.

HYAL2 was first identified in 1998 and characterized as an acidic lysosomal enzyme<sup>58</sup>. More recently however, using site-directed mutagenesis, it was determined that HYAL2 is actually a glycosylphosphatidylinositol (GPI) anchored enzyme at the cell surface<sup>59</sup>. HYAL2 optimally functions in lipid rafts<sup>60</sup> in a slightly acidic environment thought to be maintained by a Na<sup>+</sup>/H<sup>+</sup> exchanger<sup>61</sup>. It has been shown that HYAL2 functions *in vitro* to cleave HMW HA (10<sup>6</sup> Da) to low molecular weight (LMW) HA (10<sup>4</sup> Da)<sup>58</sup> and similarly to HYAL1, CD44 is required for degradation of HA by HYAL2 in HEK 293 cells<sup>25</sup>. Again, LYVE-1 and HARE may not be expressed on HEK 293 cells therefore, it is unknown if this dependency would still exist if other HA receptors are present.

Besides their implicated role in the overall turnover of HA, the involvement of HYAL1 and HYAL2 in other processes has also been suggested; these include inflammation<sup>62</sup>, angiogenesis<sup>63</sup>, and metastasis<sup>64, 65</sup>.

#### **1.2.5.1.2 Other Hyals**

*HYAL3* is expressed broadly at low levels, with its highest expression in the testis and bone marrow<sup>50</sup>. Its general function is still unknown, however, given its expression profile, there has been speculation that HYAL3 has a role in regulating the properties of germ and stem cells<sup>52</sup>. In addition, it has been shown that the overexpression of *Hyal3* in cell culture resulted in an increase in HYAL1 protein levels, suggesting that HYAL3 may

play an indirect role in HA degradation by enhancing the level of HYAL1<sup>66</sup>. Further, a mouse model deficient in HYAL3 activity was created<sup>67</sup>, and *Hyal3*<sup>-/-</sup> mice were viable, fertile, and lacked any noticeable abnormalities. Upon histological examination, no mucopolysaccharidosis-like characteristics were evident and tissue GAG content was similar to wild-type mice, suggesting that HYAL3 is not directly involved in GAG turnover.

*Hyal5*, found only in mouse, and *PH-20*, found in both mice and humans, are expressed in only a few tissues, including the testis<sup>53</sup>. These genes produce enzymes with Hyal activity that are active at a neutral pH and function to assist sperm in penetrating the HA-rich cumulus of the oocyte during fertilization<sup>53, 68</sup>. *HYAL4*, unlike the other Hyals, is thought to lack Hyal activity and only function as a chondroitinase<sup>52, 69</sup>.

Lastly, HYALP1 is a pseudogene with multiple mutations in humans, resulting in no protein product<sup>50</sup>. In mice however, mutations in HYALP1 are absent and therefore a functional Hyal is possible<sup>52</sup>.

#### **1.2.5.2 Exoglycosidases:**

Two lysosomal exoglycosidases,  $\beta$ -glucuronidase and  $\beta$ -hexosaminidase, have also been shown *in vitro* to contribute to the degradation of HA by removing individual terminal sugar units<sup>70</sup>.  $\beta$ -Glucuronidase is coded for by *GUS*, found on chromosome 7 in humans<sup>71</sup> and chromosome 5 in mice<sup>72</sup>.  $\beta$ -glucuronidase expression has been shown in all tissues and the glycoprotein enzyme has been localized to lysosomes<sup>73</sup>. It is thought that when *GUS* is translated, a single subunit is produced which then forms a functional tetrameric structure to create the active lysosomal  $\beta$ -glucuronidase<sup>74</sup>. HA has been shown

as a substrate of  $\beta$ -glucuronidase<sup>70,75</sup> as it contains  $\beta$ 1-3 glycosidic bonds between GlcA and GlcNAc, a characteristic required by  $\beta$ -glucuronidase for cleavage.

$\beta$ -Hexosaminidase is coded for by *HEXA* and *HEXB*, which are located on chromosomes 15 and 5 in humans and on chromosomes 9 and 13 in mice, respectively<sup>76</sup>. Northern blot analysis displayed that *HEXA* is ubiquitously expressed in tissues, *HEXB* expression is more variable. *HEXB* is highly expressed in heart, brain, spleen, and kidney, with lower levels observed in lung, liver, and testis<sup>76</sup>. *HEXA* and *HEXB* produce an  $\alpha$ -subunit and  $\beta$ -subunit, respectively. Isoforms of the enzyme consist of an  $\alpha$ -subunit homodimer ( $\beta$ -hexosaminidase S), a  $\beta$ -subunit homodimer ( $\beta$ -hexosaminidase B), and a heterodimer of both subunits ( $\beta$ -hexosaminidase A)<sup>76</sup>. Previous studies have shown substrate specificity between isoforms;  $\beta$ -hexosaminidase A degrades neutral and charged substrates including GAGs and GM2 gangliosides, whereas  $\beta$ -hexosaminidase B degrades only neutral substrates<sup>77</sup>. *In vitro*,  $\beta$ -hexosaminidase S has the ability to cleave anionic GAGs including chondroitin sulphate and dermatan sulphate<sup>78</sup>.  $\beta$ -Hexosaminidase's ability to cleave GAGs occurs through the release of a terminal hexosamine by the hydrolysis of glycosidic bonds with a  $\beta$ 1-4 orientation. Given that HA contains a  $\beta$ 1-4 glycosidic bond between GlcNAc and GlcA, this allows HA to be a substrate of  $\beta$ -hexosaminidase *in vitro*<sup>70</sup>. Further, chondroitin and its derivatives are also *in vitro* substrates of  $\beta$ -hexosaminidase given that its amino component is GalNAc linked with  $\beta$ 1-4 glycosidic bonds<sup>78</sup>.

### 1.2.6 Model of HA turnover:

Despite the broad distribution of HA and its diverse roles in tissues, its pathway of breakdown is still not completely understood. A model for HA degradation was initially proposed by Hascall <sup>79</sup> and further advanced by Stern <sup>55</sup>. As shown in Figure 2, the model begins with cleavage of HMW HA ( $10^6$  Da) to LMW HA ( $10^4$  Da) through the action of the previously described extracellular enzyme, HYAL2. HA is internalized through ligand-receptor interactions with a cell surface receptor such as CD44 <sup>24, 25</sup>, LYVE-1 <sup>80</sup>, or HARE <sup>33</sup>. Once internalized, the endosome matures to a lysosome where HYAL1 breaks down HA to generate short oligosaccharides that are putative substrates for the lysosomal exoglycosidases,  $\beta$ -glucuronidase and  $\beta$ -hexosaminidase <sup>55</sup>.

Strong evidence supporting the lysosomal degradation of HA proposed in this model comes from studies using inhibitors of lysosomal function which disrupt HA degradation <sup>24, 81</sup>. However, within the lysosome, the contribution of individual Hyals and exoglycosidases to the breakdown of HA is still to be defined.

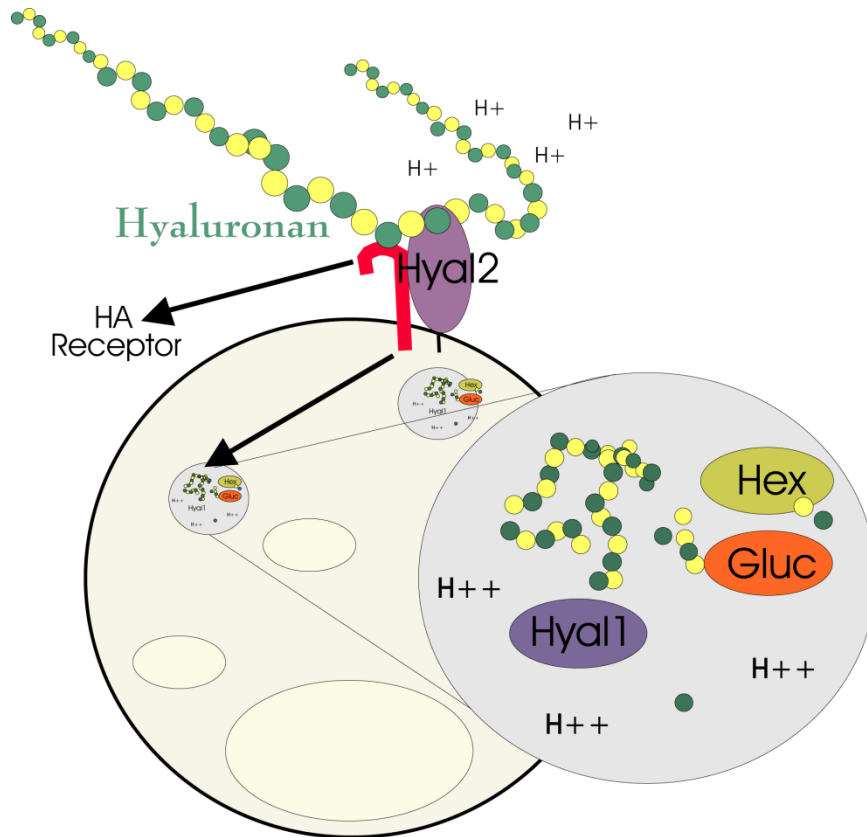


**Figure 2: A proposed model of HA degradation**<sup>55, 79</sup>. Breakdown of HA begins at the plasma membrane where HYAL2, a GPI-anchored enzyme, cleaves HMW HA ( $10^6$  Da) to LMW HA ( $10^4$  Da). The HA is then internalized through ligand-receptor interactions with CD44, LYVE-1, or HARE. Once internalized, HA is further degraded in the lysosome by HYAL1 to generate short HA oligosaccharides. These short HA oligosaccharides are then putative substrates for the exoglycosidases,  $\beta$ -glucuronidase and  $\beta$ -hexosaminidase, which cleave HA to single sugar units that are then recycled and reused in the cell. Figure courtesy of Dr. Barbara Triggs-Raine.

### **1.2.7 Tissues involved in HA degradation:**

For decades, the organ systems involved in HA catabolism has been a focal point in the turnover of this interesting GAG. It is thought that the proposed model takes place locally in avascular tissues<sup>82</sup>, whereas in vascular tissues, the majority of HA is displaced and transported to multiple organs for degradation<sup>13</sup>.

Studies in many model systems have identified the lymph node and liver as principal sites of HA uptake and turnover after the injection of radio- or fluorescently-labelled HA<sup>12, 13, 83-85</sup>. HA turnover studies further suggest that peripheral tissue HA is first brought to the lymph node where it is degraded and recycled. If there is residual HA within the efferent lymph it will then reach the blood where it is sequestered by the liver and degraded<sup>13, 86</sup>. As mentioned earlier, receptors that mediate the endocytosis of HA including CD44<sup>24</sup>, LYVE-1<sup>28, 29</sup>, and HARE<sup>34</sup>, are found in both the sinuses of the lymph node and liver. Thus, it has been speculated that it is the endothelial cells that line the sinusoids of the lymph node and liver that take up circulating HA by endocytosis, followed by the subsequent degradation of HA in the lysosome. Enzymatic intracellular degradation is tightly regulated, such that if the process goes awry devastating lysosomal storage diseases can result.

### **1.3 Lysosomal storage diseases:**

Lysosomal storage diseases are caused by a loss of function of a lysosomal enzyme required for the degradation of a particular substrate, typically due to a mutation in the coding gene. As normal synthesis of the substrate continues, it begins to accumulate within the lysosome because the degradation has been compromised<sup>87</sup>. Although rare, there are many different types of lysosomal storage disorders categorized

based on the affected enzyme and the accumulating substrate. Two groups found under the umbrella of lysosomal storage diseases, and that are relevant to the degradation of HA, include mucopolysaccharidoses and gangliosidoses<sup>87</sup>.

Mucopolysaccharidoses result from the loss of a lysosomal enzyme required for the degradation of GAGs<sup>88</sup>. The accumulation of one or more GAGs can result in skeletal, connective tissue, neurological, and organ abnormalities. Physical characteristics or symptoms of mucopolysaccharidoses include, but are not limited to, coarse facial features, short stature, joint anomalies, developmental delay, mental retardation, and abnormal motor function. Cellular changes noted by histological techniques include cell swelling and intracellular vacuolization, which if extensive, can lead to cell death. To date, gene mutations coding for 11 enzymes have been characterized and are categorized into 7 types of mucopolysaccharidoses<sup>88</sup>.

Gangliosidoses result from the loss of a lysosomal enzyme required in the degradation of gangliosides, a lipid component in cell membranes that is turned over through a well known enzymatic pathway<sup>89</sup>. Physical and cellular abnormalities resulting from gangliosidoses are similar to those described for mucopolysaccharidoses, except the neurological effects are far more severe and are often fatal at a very young age. There are two known types of gangliosidoses, GM1 and GM2 gangliosidosis, which differ in the structure of the accumulating lipid<sup>89</sup>. GM1 gangliosidosis is caused by a lack of  $\beta$ -galactosidase, an enzyme which removes a galactose sugar unit to create a GM2 ganglioside. GM2 gangliosidosis is caused by a lack of  $\beta$ -hexosaminidase, an enzyme which removes a GalNAc sugar unit to create a GM3 ganglioside<sup>90</sup>. Since  $\beta$ -

hexosaminidase has been suggested as a key player in the breakdown of HA, the genetics of GM2 gangliosidosis is explained below (1.4.2.2).

#### **1.4 Human deficiencies in enzymes relevant to HA degradation:**

##### **1.4.1 Human hyaluronidase deficiency:**

Mutations in *HYAL* genes leading to deficiencies are rare; in fact, to date there have only been 4 documented cases worldwide <sup>54, 91</sup>. All 4 of the Hyal deficiencies have been the result of mutations in *HYAL1*. Human HYAL1 deficiency has been categorized as mucopolysaccharidosis IX (OMIM 601492). The first patient to display a HYAL deficiency was characterized in 1996 <sup>92</sup> and was later diagnosed with mucopolysaccharidosis IX when mutations in *HYAL1* were reported as the cause of the deficiency <sup>54</sup>. This patient presented with short stature, non-calcified periarticular masses, and swelling. However, there was no report of developmental delay as all neurological examinations were normal. Histologically, the periarticular masses contained vacuolated cells which prominently stained with alcian blue and colloidal iron, indicating the presence of GAGs. HA was suggested as one of the GAGs as prior treatment with a hyaluronidase diminished the above staining. Upon biochemical analysis, plasma HYAL activity was not detected and coincided with an increase in HA plasma levels <sup>92</sup>.

Since the first case of mucopolysaccharidosis IX, 3 more cases have been reported. In 2011, three siblings of a consanguineous marriage were found to have a deletion in the coding region of *HYAL1*, creating a premature stop codon <sup>91</sup>. All 3 patients had normal stature with joint pain and swelling. Like the first reported case, cells from

biopsies stained positive for GAGs using alcian blue staining. The patients lacked serum HYAL activity but, the level of plasma HA was not measured <sup>91</sup>.

#### **1.4.2 Human exoglycosidase deficiencies:**

##### **1.4.2.1 Human $\beta$ -glucuronidase deficiency:**

$\beta$ -Glucuronidase deficiency, first described in 1973 by Dr. W. Sly <sup>93</sup>, is also known as Sly syndrome or mucopolysaccharidosis VII (OMIM 253220). Mucopolysaccharidosis VII is caused by various mutations in *GUS*, the coding gene for  $\beta$ -glucuronidase. The partial or full loss of  $\beta$ -glucuronidase activity results in a decreased lifespan, due to the accumulation of multiple GAGs including keratan, dermatan, and chondroitin sulphates <sup>94</sup>. Physical symptoms of this deficiency can range from mild to severe and can include skeletal anomalies, organomegaly, corneal clouding, fetal hydrops, developmental delay, and mental retardation <sup>95,96</sup>. Samples recovered from autopsy show intracellular vacuolization in multiple tissues with GAG storage, however, the accumulation of HA was not specifically queried. Further, cardiac lesions with valve thickening were apparent <sup>97</sup>.

##### **1.4.2.2 Human $\beta$ -hexosaminidase deficiencies:**

$\beta$ -Hexosaminidase deficiency can result in GM2 gangliosidosis. As explained in section 1.2.5.2, there are three isoforms of  $\beta$ -hexosaminidase coded for by *HEXA* and *HEXB*. Tay-Sachs disease (OMIM# 272800) and Sandhoff disease (OMIM# 268800) result from mutations in *HEXA* and *HEXB*, respectively <sup>89</sup>. Tay-Sachs and Sandhoff disease are categorized into infantile, juvenile, and adult forms depending on the age of onset. All forms display lysosomal storage of GM2 gangliosides that can cause mental

retardation, little to no muscle tone, and loss of motor control. Symptoms of infantile and juvenile forms also include seizures and loss of sight <sup>98</sup>. Oligosacchariduria and extensive accumulation resulting in neuronal cell body swelling has also been documented <sup>99, 100</sup>.

### **1.5 Animal models of deficiency:**

A common method used to better understand the function and/or affects of an enzyme in scientific studies is to remove the activity of that enzyme from a model system. In order to gain further knowledge of the breakdown pathway of HA, multiple hyaluronidase and exoglycosidase deficient mouse models have been generated and the phenotype of each model is described below.

#### **1.5.1 Murine mucopolysaccharidosis IX:**

A mouse knockout model of mucopolysaccharidosis IX was previously characterized <sup>101</sup>. Briefly, a neomycin resistance cassette was inserted into exon 2 of the *Hyal1* gene to create a null allele, *Hyal1*<sup>-/-</sup>, which was inherited with normal Mendelian ratios. Loss of HYAL1 activity was confirmed by western blot and zymography. *Hyal1*<sup>-/-</sup> mice, both male and female, appeared normal, were viable, and fertile. *Hyal1*<sup>-/-</sup> mice were similar in size to wild-type littermates and did not display any skeletal defects or organomegaly. Upon necropsy at 3 and 12 months of age, *Hyal1*<sup>-/-</sup> mice presented with articular cartilage loss and an increase in periarticular and epiphyseal HA <sup>101</sup>. Thus, joint involvement and indications of osteoarthritis were consistent with human HYAL1 deficiency. There was no evidence of mucopolysaccharidosis-like characteristics outside the cartilaginous knee joint in the *Hyal1*<sup>-/-</sup> mice and total GAG levels in multiple tissues were similar to wild-type controls. Unlike patients affected with mucopolysaccharidosis

IX, the murine model did not present with elevated HA serum levels. *Hyal3* transcript levels were elevated in the *Hyal1*<sup>-/-</sup> mice but the levels of *Hyal2* and  $\beta$ -hexosaminidase transcripts were normal<sup>101</sup>.

### **1.5.2 Murine HYAL2 deficiency:**

A cre-lox conditional knockout system removing the majority of the *Hyal2* coding sequence was used to explore the effects of a loss of HYAL2 activity<sup>102</sup>. *Hyal2*<sup>-/-</sup> mice were viable and fertile, however, they did display craniofacial abnormalities. These abnormalities included a shortened nose and extra bony protrusions, consistent with a mucopolysaccharidosis-like phenotype. HA accumulation was only detected in liver sinusoids, an area known for HA uptake and turnover<sup>13</sup>. In addition, a 10 fold increase in HA plasma levels was observed, coinciding with a two-fold increase in plasma hyaluronidase activity. It was suggested that the uptake and clearance of HA was hindered by the loss of HYAL2 activity<sup>102</sup>, which is consistent with the model of HA degradation proposed<sup>55, 103</sup>. *Hyal1* transcript levels were elevated in the kidney of *Hyal2*<sup>-/-</sup> mice, although not in the liver. *Hyal3* transcripts were similar to controls;  $\beta$ -hexosaminidase transcripts were not analyzed. Other abnormalities seen in the *Hyal2*<sup>-/-</sup> mice and not present in wild-type mice included iron deposition in some tissues and mild anemia<sup>102</sup>. To date, a mutation causing HYAL2-deficiency has not been identified in humans.

### **1.5.3 Murine $\beta$ -glucuronidase deficiency:**

Several murine model systems of mucopolysaccharidosis VII or Sly syndrome have been previously characterized<sup>104, 105</sup>. Mice deficient in  $\beta$ -glucuronidase displayed many gross mucopolysaccharidosis-like characteristics which became apparent at approximately 21 days of age. These characteristics included craniofacial anomalies, skeletal abnormalities, stunted growth, and splenomegaly. Similar to human patients, mutant mice displayed a decreased lifespan. Upon histological analysis, multiple tissues displayed cellular enlargement and intracellular vacuolization including the endothelial cells in the liver, cerebral cortex, cardiac valves, and skin fibroblasts. The presence of GAGs was confirmed using alcian blue staining however, individual GAG analysis has not been completed. Further, isolated knee joints displayed abnormal articular cartilage with vacuolated chondrocytes<sup>104, 105</sup>.

### **1.5.4 Murine $\beta$ -hexosaminidase deficiencies:**

Given that  $\beta$ -hexosaminidase is coded for by 2 genes, there have been 3 different mouse models generated. These included a Tay Sachs disease model with mutations in *Hexa*, a Sandhoff disease model with mutations in *Hexb*, and a double knockout mouse model with mutations in both *Hexa* and *Hexb*.

#### **1.5.4.1 Murine Tay-Sachs and Sandhoff disease:**

Targeted gene disruption was used to insert a neomycin resistance cassette into exon 11 of *Hexa* to generate a mouse deficient in the activity of  $\beta$ -hexosaminidase A. A similar strategy was used to create a mouse with mutations in *Hexb* except the neomycin resistance cassette was inserted into exon 2<sup>106</sup>; these mice were deficient in both  $\beta$ -

hexosaminidase A and B. *Hexa*<sup>-/-</sup> mice were viable, phenotypically normal, and fertile. Further, they were not stunted in growth, nor did they display behavioural abnormalities up to one year of age. In contrast, *Hexb*<sup>-/-</sup> mice were phenotypically normal until approximately 4 months of age. At this age, *Hexb*<sup>-/-</sup> mice had reduced feeding resulting in weight loss, muscle weakness, tremors, and seizure like episodes, soon after resulting in death. Both *Hexa*<sup>-/-</sup> and *Hexb*<sup>-/-</sup> mice showed accumulation of gangliosides in neuronal cell bodies. However, *Hexb*<sup>-/-</sup> mice displayed more extensive accumulation that was also apparent in the liver<sup>106</sup>. Histological studies revealed that morphologically, *Hexa*<sup>-/-</sup> mice were indistinguishable from wild-type mice when comparing visceral organs. However, *Hexb*<sup>-/-</sup> mice displayed intracellular vacuolization in several tissues. The striking difference between the Tay-Sachs and Sandhoff disease models can be attributed to a sialidase that is present in mice, but absent in humans, allowing the formation of a GA2-ganglioside that can then be further degraded by  $\beta$ -hexosaminidase B, thus  $\beta$ -hexosaminidase A is not required<sup>106, 107</sup>.

#### **1.5.4.2 Murine model deficient in all isoforms of $\beta$ -hexosaminidase:**

Mice heterozygous for *Hexa*<sup>+/-</sup> and *Hexb*<sup>+/-</sup> gene disruptions were bred to yield double knockout mice (*Hexa*<sup>-/-</sup>*Hexb*<sup>-/-</sup>), deficient in all  $\beta$ -hexosaminidase isoforms<sup>108, 109</sup>. At approximately 4 weeks, *Hexa*<sup>-/-</sup>*Hexb*<sup>-/-</sup> mice were noticeably smaller in size than their littermates, they displayed coarse facial features, and they showed symptoms of neurological deterioration. Similar to *Hexb*<sup>-/-</sup> mice, *Hexa*<sup>-/-</sup>*Hexb*<sup>-/-</sup> mice displayed abnormal neuronal cell bodies with accumulation of substrate. However, severe hypomyelination was also observed and supporting cells in the brain were also vacuolated. A striking mucopolysaccharidosis-like phenotype, with prominent storage of

GAGs in multiple tissues was noted in the *Hexa*<sup>-/-</sup>*Hexb*<sup>-/-</sup> mice<sup>108, 109</sup>, which was absent in wild-type, *Hexa*<sup>-/-</sup>, and *Hexb*<sup>-/-</sup> mice. Monosaccharide analysis completed on mouse urine revealed that *Hexa*<sup>-/-</sup>*Hexb*<sup>-/-</sup> mice were excreting elevated levels of GalNAc and IdoA. It was suggested that these mice were accumulating dermatan sulphate, as GalNAc and IdoA are the primary components of this GAG<sup>108</sup>. Given that the severe accumulation of GAGs is not displayed by human patients with *HEXA* or *HEXB* mutations and was not observed in *HEXA* or *HEXB*-deficient mice, it was further suggested that a functional redundancy exists among the  $\beta$ -hexosaminidase isoforms toward GAGs<sup>108, 109</sup>.

## **1.6 Rationale:**

Unlike other mucopolysaccharidoses, symptoms displayed in patients with mucopolysaccharidosis IX are relatively mild and for the most part limited to the joints<sup>91, 92</sup>. Furthermore, broad HA accumulation was not identified in mice deficient in any one hyaluronidase<sup>67, 101, 102</sup>. Together, these findings suggest that other enzymes are important in HA degradation and are potentially compensating for the loss of individual hyaluronidase activities.

Interestingly, mice lacking all isoforms of  $\beta$ -hexosaminidase displayed a prominent mucopolysaccharidosis-like phenotype, with evident GAG accumulation in multiple tissues<sup>108, 109</sup>. The identity of these GAGs was not fully investigated, and could therefore include HA. Monosaccharide analysis completed on urine excreted from mice deficient in all isoforms  $\beta$ -hexosaminidase displayed extensive accumulation of two monosaccharides common to the structure of dermatan sulphate<sup>108</sup>. However, it has previously been shown that excretion of HA through the urinary system accounts for only 1% of normal HA turnover<sup>13</sup>. Therefore, accumulation of HA in  $\beta$ -hexosaminidase-deficient mice may have been missed as the identity of individual GAGs were not assayed for in tissues.

## **1.7 Hypothesis:**

The lysosomal exoglycosidase,  $\beta$ -hexosaminidase, contributes significantly to the constitutive degradation of HA. Therefore, mice deficient in all isoforms of  $\beta$ -hexosaminidase will display tissue accumulation of HA.

## **Chapter 2: Materials and Methods**

## **2.1 Generation of *Hexa*<sup>-/-</sup> *Hexb*<sup>-/-</sup> mice:**

*C57BL6;C129* mice heterozygous for gene disruptions in *Hexa* and *Hexb*, were kindly provided by our collaborators Drs. Alexey Pshezhetsky and Roy Gravel<sup>106</sup>. Gene disruptions creating *Hexa*<sup>+/-</sup> and *Hexb*<sup>+/-</sup> were generated through the insertion of a neomycin-resistant cassette in exon 11 and 2, respectively. These mice were crossed to produce *Hexa*<sup>-/-</sup> *Hexb*<sup>-/-</sup> (DKO) mice, deficient in all isoforms of  $\beta$ -hexosaminidase. At 14 days of age, ear punches were taken from progeny of the above crosses and used to isolate DNA for PCR-based genotyping. DKO mice were age and sex-matched to wild-type (WT) and *Hexb*<sup>-/-</sup> littermates to serve as controls.

## **2.2 Generation of *Hexa*<sup>-/-</sup> *Hexb*<sup>-/-</sup> *Hyal1*<sup>-/-</sup> mice:**

Mice heterozygous for *Hexa* and *Hexb* gene disruptions, *Hexa*<sup>+/-</sup> *Hexb*<sup>+/-</sup>, described above, were bred with *C57BL6* mice heterozygous for a deletion in the coding region of *Hyal1*, *Hyal1*<sup>+/-</sup>, previously described<sup>101</sup>. Mice heterozygous at all three loci *Hexa*<sup>+/-</sup> *Hexb*<sup>+/-</sup> *Hyal1*<sup>+/-</sup> were then bred to generate triple knockout mice, *Hexa*<sup>-/-</sup> *Hexb*<sup>-/-</sup> *Hyal1*<sup>-/-</sup> (TKO). Similar to above, ear punches were used for routine genotyping. TKO mice were age and sex-matched to DKO littermates to serve as controls.

## **2.3 DNA isolation:**

Ear samples were lysed overnight at 55°C in 500  $\mu$ l of lysis buffer containing 1 M Tris, pH 8.5, 0.5 M EDTA, 10% SDS, 5 M NaCl, autoclaved distilled water, and 20  $\mu$ g/ $\mu$ l of Proteinase K (Sigma). Debris was separated from the samples by centrifugation for 10 minutes at 16 100 g, and the supernatant containing DNA was collected. DNA was precipitated using isopropanol to a final volume of 50%, and the DNA was pelleted via

centrifugation for 10 minutes at 16 100 g. The supernatant was discarded and the DNA was resuspended in 300  $\mu$ l of autoclaved distilled water. Tubes were placed in a 37°C water bath for 30 minutes to evaporate residual isopropanol. DNA was then stored at 4°C until the genotype was determined using PCR.

#### **2.4 Genotyping of *Hexa*<sup>-/-</sup> *Hexb*<sup>-/-</sup> mice:**

Isolated DNA was used to determine the genotypes of progeny. Approximately 650 mice were genotyped from the *Hexa*<sup>+/-</sup> *Hexb*<sup>+/-</sup> breedings. A standard PCR master mix containing 40.75  $\mu$ l of ultra pure water (Invitrogen), 5  $\mu$ l of 10x ThermoPol reaction buffer (New England Biolabs), 1  $\mu$ l of 10 mM dNTPs, 1  $\mu$ l of 100 ng/ $\mu$ l forward primer, 1  $\mu$ l of 100 ng/ $\mu$ l reverse primer, and 0.25  $\mu$ l of *Taq* DNA polymerase (New England Biolabs) was added to 2  $\mu$ l of sample DNA. The *Hexa* WT allele was amplified using primers WPG 672 (see Table 2) and WPG 673 to produce a 420 bp product. The *Hexa* mutant allele with an incorporated neomycin-resistance cassette was amplified using primers WPG 672 and WPG 658 to produce a 219 bp product. The *Hexb* WT allele was amplified using primers WPG 656 and WPG 657 to generate a product of 141 bp. The disrupted *Hexb* allele was amplified using primers WPG 657 and WPG 659 and produced a 700 bp product. The corresponding primer sequence for each primer listed above is available in Table 2. PCR conditions for the above reactions included a 5 minute incubation at 95°C, followed by 35 cycles of a 1 minute denaturation step at 94°C, a 1 minute annealing step at 55°C, and a 1 minute elongation step at 72°C. PCR products were separated on a 1.2% agarose gel containing 50  $\mu$ g of ethidium bromide per 100 mL of 40 mM tris acetate 1 mM EDTA buffer. The gel was then visualized in an AlphaImager2000 using Alpha imager software.

**Table 2:** Primers used for PCR-based genotyping

<b>Primer ID</b>	<b>Primer sequence</b>	<b>Targeted alleles</b>
WPG 672	5'-GGCCAGATACAATCATACAG-3'	<i>Hexa</i> WT and disrupted
WPG 673	5'-CTGTCCACATACTCTCCCCACAT-3'	
WPG 658	5'-CACCAAAGAAGGGAGCCGGT-3'	
WPG 657	5'-CAATCGGTGCTTACAGGTTTCATC-3'	<i>Hexb</i> WT and disrupted
WPG 656	5'-GGTTTCTACAAGAGACATCATGGC-3'	
WPG 659	5'-GATATTGCTGAAGAGCTTGGCGGC-3'	
WPG 612	5'-CTGGGACAGCAAGGACATTT-3'	<i>Hyal1</i> WT
WPG 613	5'-CAGTGCTGCAGGCAAATAAA-3'	
WPG 617	5' ATCGCCTTCTATCGCCTT 3'	<i>Hyal1</i> mutated
WPG 619	5' GAGACATGCCTTGA ACTCTGCCTCC 3'	

## **2.5 Genotyping of *Hexa*<sup>-/-</sup> *Hexb*<sup>-/-</sup> *Hyal1*<sup>-/-</sup> mice:**

Isolated DNA was used to genotype the progeny from the triple heterozygous breedings following the procedures for *Hexa* and *Hexb* described above. Approximately 700 mice were genotyped from the *Hexa*<sup>+/-</sup> *Hexb*<sup>+/-</sup> *Hyal1*<sup>+/-</sup> breedings. The *Hyal1* WT allele was PCR-amplified using primers WPG 612 and WPG 613 to produce a 340 bp product. To amplify the *Hyal1* WT allele the conditions used were as stated for *Hexa* and *Hexb* amplification. The mutated *Hyal1* allele was amplified using WPG 617 and WPG 619 as primers, which resulted in a 450 bp product. PCR amplification conditions for this allele included a 2 minute denaturation at 94°C, followed by 35 cycles of a 1 minute denaturation step at 94°C, a 1 minute annealing step at 52°C, and a 1 minute elongation step at 70°C. Primer sequences for the above are available in Table 2. The PCR product was visualized as described earlier.

## **2.6 Dissection and tissue preservation:**

All procedures and care of the animals were in compliance with the Canadian Council on Animal Care and approved by the Animal Protocol Management and Review Committee at the University of Manitoba.

When mutant mice reached the predetermined end point requiring euthanasia, the mice, along with controls were asphyxiated using isoflurane, (Baxter Corporation), and immediately dissected. Tissues, including brain, eyes, heart, lungs, trachea, liver, kidney, spleen, lymph nodes, skin, knee joints, and rib cartilage, were rapidly collected and either frozen on dry ice and then stored at -80°C for biochemical studies or placed in fixative for histological studies. All tissues, excluding knee joints, rib cartilage and trachea, were

fixed in 10% formalin (Fisher Scientific) containing 0.5% cetylpyridinium chloride (Sigma) overnight at room temperature. The tissues were then washed 3 times for 5 minutes in phosphate-buffered saline (PBS; 137 mM NaCl, 2.7 mM KCl, 10 mM Na<sub>2</sub>P0<sub>4</sub>, 2 mM KH<sub>2</sub>P0<sub>4</sub>, pH 7.4) and once in 70% ethanol for 5 minutes prior to being stored in 70% ethanol until processing. Knee joints, rib cartilage, and trachea were fixed in 0.01 M periodate and 0.075 M lysine in 2% paraformaldehyde (PLP; Sigma) overnight at room temperature followed by a 10 minute wash with distilled water. Decalcification of the cartilaginous tissues was completed using Immunocal (Decal Chemical Corporation) for 1 week. Tissues were then stored in 70% ethanol until processing.

## **2.7 Tissue processing, embedding, and microtomy:**

Fixed tissues were processed for paraffin embedding using a Citadel 1000 tissue processor under vacuum. Tissues were dehydrated using 70% ethanol for 1 hour, 95% ethanol for 3 hours, 100% ethanol for 6 hours, and xylene for 2.5 hours. The tissues were then equilibrated in two melted paraffin baths, each for 6 hours. Tissues were then embedded in paraffin blocks using a Histocentre 3 embedder. Blocks were incubated at 4°C for approximately 4 hours prior to removing block molds. Tissue sections (5µm) were then cut using a Leica RM2245 microtome, and adhered to glass slides.

## **2.8 Histological staining:**

Paraffin embedded tissue sections were used for all histological staining. Unless otherwise noted, all steps occurred at room temperature.

### **2.8.1 Hematoxylin and eosin (H&E) staining:**

Tissue sections were deparaffinized using 2 xylene incubations of 5 minutes each. Following deparaffinization, slides were rehydrated to water using decreasing concentrations of ethanol. Slides were then stained for 3 minutes in Mayer's hematoxylin (Sigma) followed by blueing under running tap water for 6 minutes. Incubation in 80% ethanol for 1 minute was then used to equilibrate the slides for eosin staining. Eosin Y stain (Sigma) was then applied to the slides for 40 seconds followed by a 3 minute incubation in 70% ethanol. Slides were then dehydrated by incubations of increasing concentrations of ethanol, followed by xylene, before mounting in the toluene-based mounting medium, Permount (Fisher Scientific). Slides were then visualized using light microscopy and images were taken using AxioVision software.

### **2.8.2 Alcian blue staining:**

Tissue sections were deparaffinized and rehydrated to water as in H&E staining. Following rehydration, slides were then incubated in 3% acetic acid for 3 minutes. Sections were then stained with Alcian 8GX (1 g/ml) in 3% acetic acid pH 2.5 for 30 minutes. Running tap water was used to wash the slides for 10 minutes, followed by a 3 minute incubation in distilled water. Nuclear Fast Red (ScyTeK Laboratories) was then applied to the slides as a counterstain for 1.5 minutes, followed by a wash in distilled water for 1 minute. Dehydration, mounting, visualization, and imaging occurred as in H&E staining above.

### **2.8.3 Hyaluronan-binding protein (HABP) staining:**

Tissue sections were deparaffinized and rehydrated to water. In parallel to experimental slides, control slides of each tissue were produced to monitor binding specificity. Control slides received overnight treatment at 37°C with hyaluronidase from *Streptomyces hyalurolyticus* (Sigma) at a concentration of 50 U/ml in sodium acetate pH 6.0. Experimental slides received the same treatment except hyaluronidase was omitted. After overnight incubation, tissue sections were washed with PBS followed by quenching for endogenous peroxidases using 3% hydrogen peroxide in distilled water for 30 minutes. Tissue sections were washed again in PBS prior to being incubated in 10% Fetal Bovine Serum in Tris Buffered Saline Tween (TBST; 50 mM Tris, 150 mM NaCl, 0.1% Tween 20, pH 7.4) for 30 minutes. To block for endogenous biotin, sections were then incubated with Avidin D, followed by biotin, according to the instructions of the manufacturer (Vector Laboratories). Following a TBST wash, sections were incubated at 4°C overnight with a biotinylated-HABP (Calbiochem) at a concentration of 6.67 µg/ml in TBST. Sections were washed in TBST and incubated with an avidin-horseradish peroxidase complex from Vector Laboratories for 1 hour. Following washing the sections in TBST, a DAB substrate was applied for 10 minutes and then the slides were immersed in water for 5 minutes. The DAB substrate (prepared without nickel) was made according to Vector Laboratories. Slides were counterstained with Mayer's hematoxylin (Sigma) for 2 minutes followed by blueing under running tap water for 6 minutes. Dehydration, mounting, visualization, and imaging occurred as in H&E staining.

## **2.9 Fluorophore assisted carbohydrate electrophoresis:**

HA and other GAG levels in mouse tissues were quantified using fluorophore assisted carbohydrate electrophoresis (FACE). Frozen mouse tissue samples were lyophilized until dry and degraded in an ammonium acetate buffer pH 7.0, containing 50  $\mu\text{g}/\mu\text{l}$  of Proteinase K (Sigma), overnight at 55°C. The amount of buffer used was proportional to the dry weight of the individual tissue sample. For example, if sample A weighed 5mg and sample B weighed 10 mg, 100  $\mu\text{l}$  and 200  $\mu\text{l}$  of buffer with Proteinase K respectively would be added to each sample. Samples were then boiled for 5 minutes to deactivate the Proteinase K. Tissue debris was removed by centrifugation for 10 minutes at 16 100 g and an equal volume of supernatant was collected from each sample. To defat the samples, acetone was added (3 parts acetone/1 part sample) and samples were stored at -20°C for 2 hours. Precipitates were pelleted through centrifugation at 1500 g for 20 minutes. The supernatant was removed, and the precipitant was air dried. The pellets were reconstituted in ultra pure water and 100% ice cold ethanol was added to a final ethanol concentration of 75%. Samples were then stored at -20°C for 4 hours. Precipitates were then pelleted by centrifugation at 10 000 g for 15 minutes at 4°C. The supernatant was removed and the precipitate was air dried. The samples were then reconstituted with ultra pure water and divided into 3 aliquots. Individual aliquots were treated with 5 mU of Hyaluronidase SD (Seikagaku) or Chondroitinase ABC (Sigma) in 200 mM ammonium acetate buffer using the pH recommended by the supplier. The last aliquot received no enzyme and served as a negative control. Samples were incubated overnight at 37°C for the production of disaccharide units. Digests were cooled on ice and 100% ice cold ethanol was added to a final ethanol concentration of 95%, followed by incubation for 2

hours at -20°C. Following centrifugation for 20 minutes at 10 000 g, the supernatant was collected and dried in a speed vacuum. When samples were completely dry, 5 µl of 0.1 M 2-aminoacridone (Sigma) was added and kept at room temperature for 15 minutes, followed by the addition of 5 µl of 1 M sodium cyanoborohydrite (Sigma). Samples were then incubated overnight at 37°C, followed by the addition of 10 µl of 25% glycerol. Labeled disaccharide units were then separated on a 20% acrylamide gel using previously described conditions<sup>110</sup>. Fluorescent signals were quantified using a Fluor-S MultiImager (BioRad) by comparison to fluorescently labeled standards (Seikagaku) of a known concentration using Quantity One software. For quantification, the volume analysis tool in Quantity One was used to create a standard curve from lanes loaded with known concentrations of standards. The equation generated from the standard curve was then used to determine the concentration of samples. To account for background, local background subtraction was employed.

## **2.10 Statistical analysis:**

GraphPad Prism software was used to perform unpaired student t-tests and one way ANOVA tests to test for statistical significance. To determine which means were significantly deviating from each other, post ANOVA analysis was performed using Tukey's Multiple Comparison Test. Values of  $p < 0.05$  were considered significant.

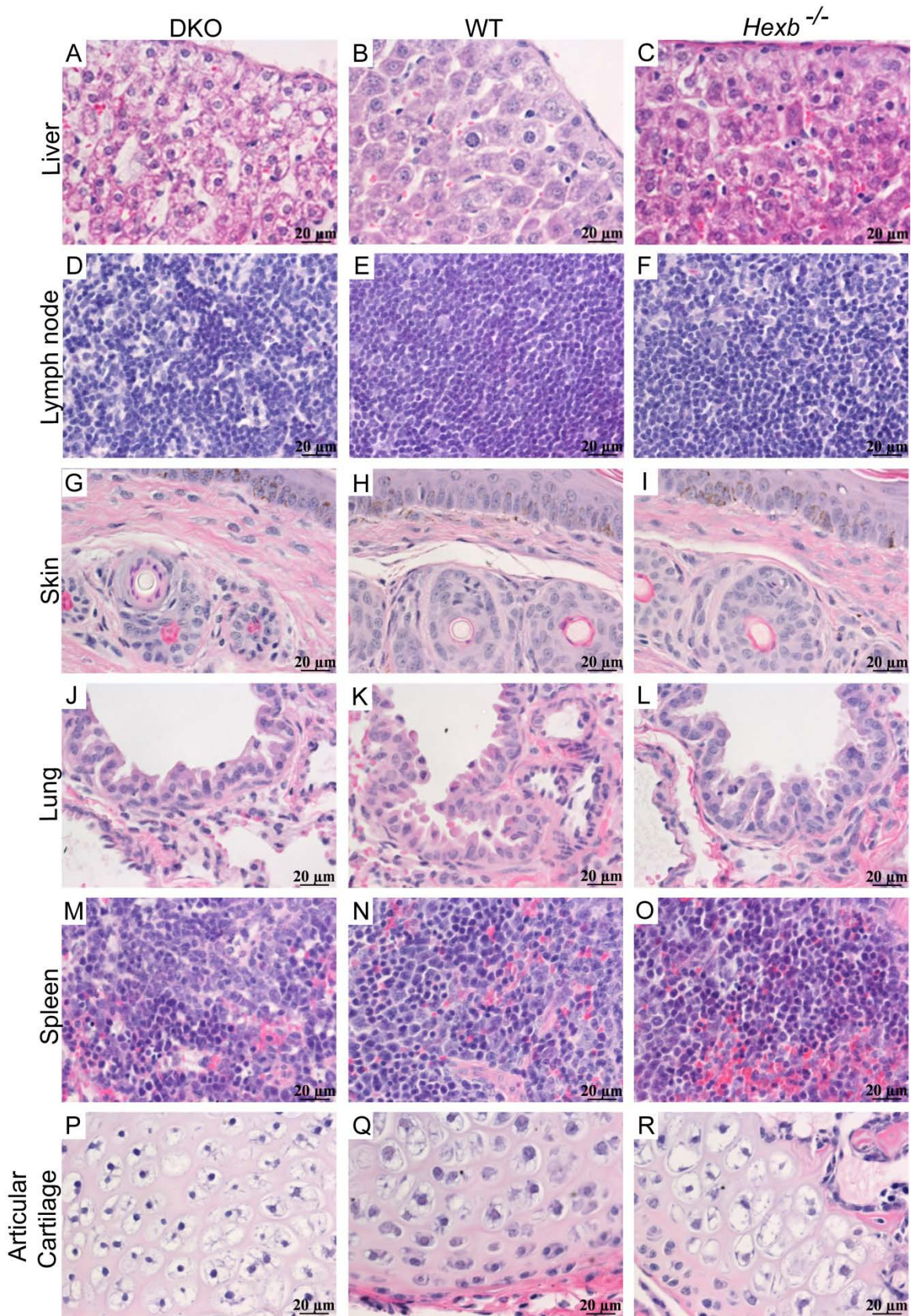
## **Chapter 3: Results Part 1**

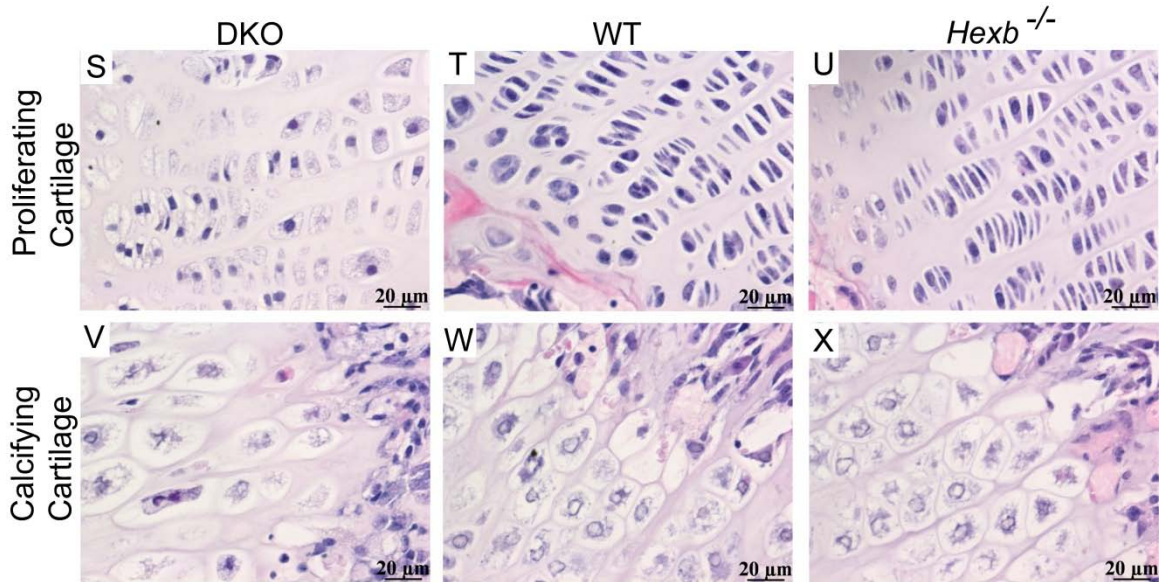
### 3.1 Description of the $\beta$ -hexosaminidase-deficient/*Hexa*<sup>-/-</sup>*Hexb*<sup>-/-</sup> (DKO) mice:

Mice with a *Hexa*<sup>-/-</sup>*Hexb*<sup>-/-</sup> (DKO) genotype displayed a Mendelian inheritance pattern of autosomal recessive with an occurrence of approximately 1/16, suggesting no early lethality occurred. The average age at which DKO mice reached the predetermined endpoint (inability to feed/reduced mobility) was approximately 33 days (n=14). All DKO mice were smaller in size when compared to their wild-type (WT) and *Hexb*<sup>-/-</sup> littermates, although formal weights were not documented. Features exhibited by the DKO mice included laboured breathing, tremors, and seizure-like episodes. Unlike controls, DKO mice displayed coarse features, including a broad nose, and a hunched posture.

### 3.2 Tissue morphology and substrate accumulation in DKO mice:

To assess tissue morphology in  $\beta$ -hexosaminidase-deficient mice, H&E staining was performed on paraffin sections from DKO, WT, and *Hexb*<sup>-/-</sup> mice. Vacuolization resulting from the accumulation of substrates that are normally degraded by  $\beta$ -hexosaminidase, including gangliosides and GAGs, have previously been observed in the DKO mice<sup>108, 109</sup>. As expected, the DKO tissues displayed increased vacuolization in multiple tissues. These included liver, lymph node, spleen, and chondrocytes of the articular, proliferating, and calcifying cartilage when compared to WT controls (Fig. 3). Similar to previous studies<sup>106, 108, 109</sup>, *Hexb*<sup>-/-</sup> mice also displayed intracellular vacuolization, albeit less extensive than that found in DKO mice (Fig. 3). An increase in vacuole size and number, apparent in the DKO and *Hexb*<sup>-/-</sup> mice, are both characteristics

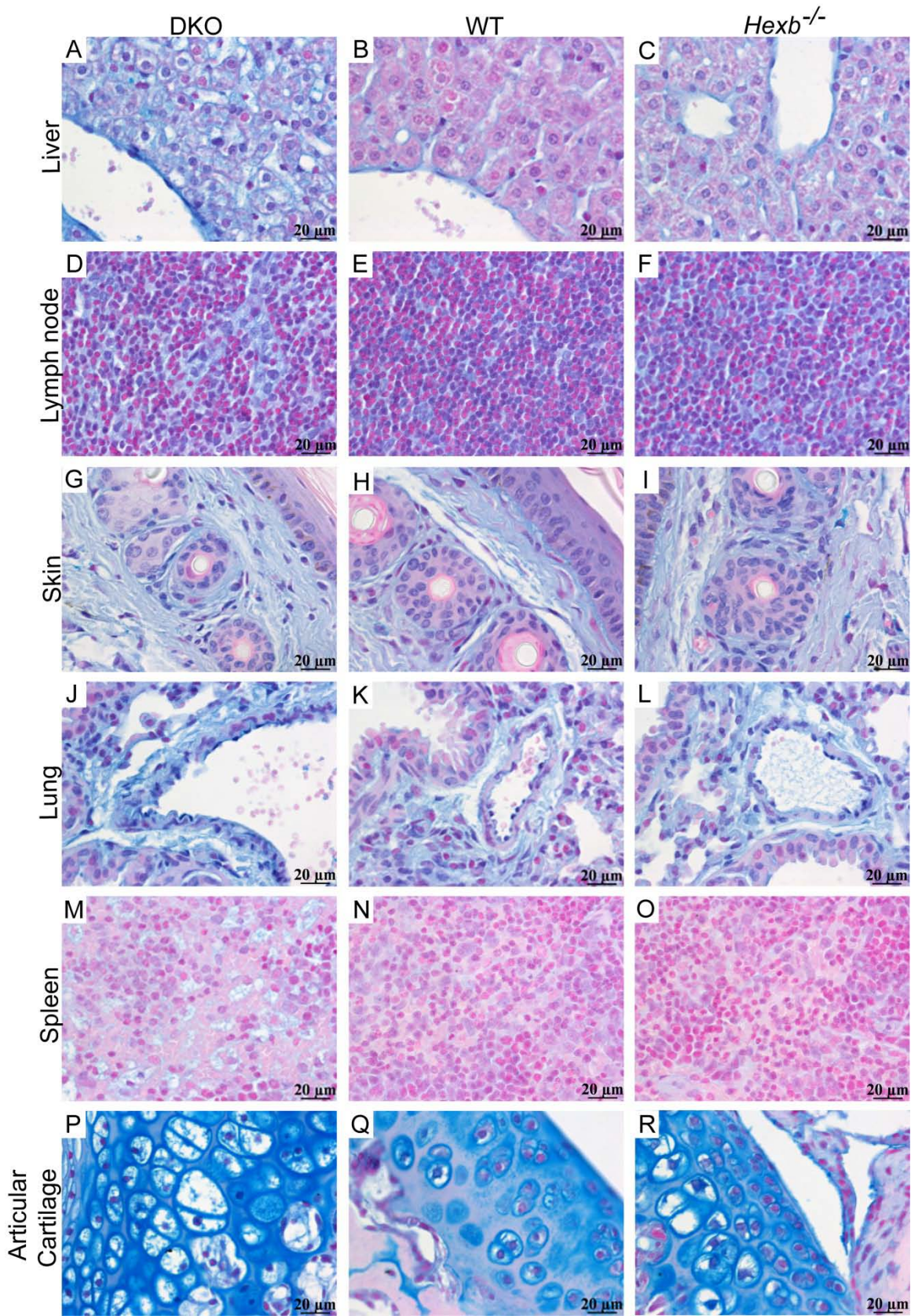




**Figure 3: Analysis of tissue morphology in DKO, WT, and *Hexb*<sup>-/-</sup> mice.** (A-X) H&E staining was completed to assess tissue morphology at 63x magnification. Intracellular vacuolization was apparent in DKO and *Hexb*<sup>-/-</sup> sections in many tissues including liver (A and C), lymph node (D and F), spleen (M and O) and in the cartilage of the knee joint (P, R, S, and U), when compared to the respective WT tissue controls. The observed vacuolization appeared more prominent in the DKO mice compared to *Hexb*<sup>-/-</sup> littermates, suggesting the accumulation of additional substrates. Pyknotic nuclei appeared to be more prominent in DKO articular cartilage compared to WT (Q) and *Hexb*<sup>-/-</sup> (R) sections. Further, lacunae in the proliferative cartilage (S) and calcifying chondrocytes (V) in the DKO mice appeared less organized than in the WT (T and W) and *Hexb*<sup>-/-</sup> (U and X) sections, respectively. Intracellular vacuolization was not observed in skin (G and I) or lung (J and L) of the DKO and *Hexb*<sup>-/-</sup> mice when compared to WT skin (H) and lung (K) sections.

of a lysosomal storage disorder, suggesting that substrates of  $\beta$ -hexosaminidase are in fact accumulating. Further, lacunae in the proliferative cartilage (Fig. 3S) and calcifying chondrocytes (Fig. 3V) in the DKO mice appeared less organized than in the WT (Fig. 3T and W) and *Hexb*<sup>-/-</sup> (Fig. 3U and X) sections, respectively. Unlike other tissues, skin (Fig. 3G-I) and lung (Fig. 3J-L) sections from DKO and *Hexb*<sup>-/-</sup> mice did not show intracellular vacuolization and appeared similar to WT skin and lung.

To confirm and extend previous work indicating that GAGs were accumulating in DKO mice, tissue sections were stained with alcian blue to detect GAGs. Since GAGs are a component of all tissues, DKO, WT, and *Hexb*<sup>-/-</sup> tissues stained positive (blue staining) for GAGs. However, the DKO tissues, including liver, lymph node, lung, spleen, articular cartilage, and proliferating cartilage of the epiphyseal plate, showed increased blue staining compared to WT tissues, suggesting there are more GAGs present (Figure 4). With the exception of liver and lymph node, *Hexb*<sup>-/-</sup> tissues displayed intensity levels similar to those of WT. *Hexb*<sup>-/-</sup> liver (Fig. 4C), and lymph node (Fig. 4F), had an intermediate staining intensity, between that of DKO and WT. This suggested more GAGs are present, however not to the extent seen in DKO mice. Sections from DKO, WT, and *Hexb*<sup>-/-</sup> skin (Fig. 4G-I), and calcifying cartilage of the epiphyseal plate (Fig. 4V-X), had similar staining intensities, indicating that these tissues contained similar levels of GAGs.



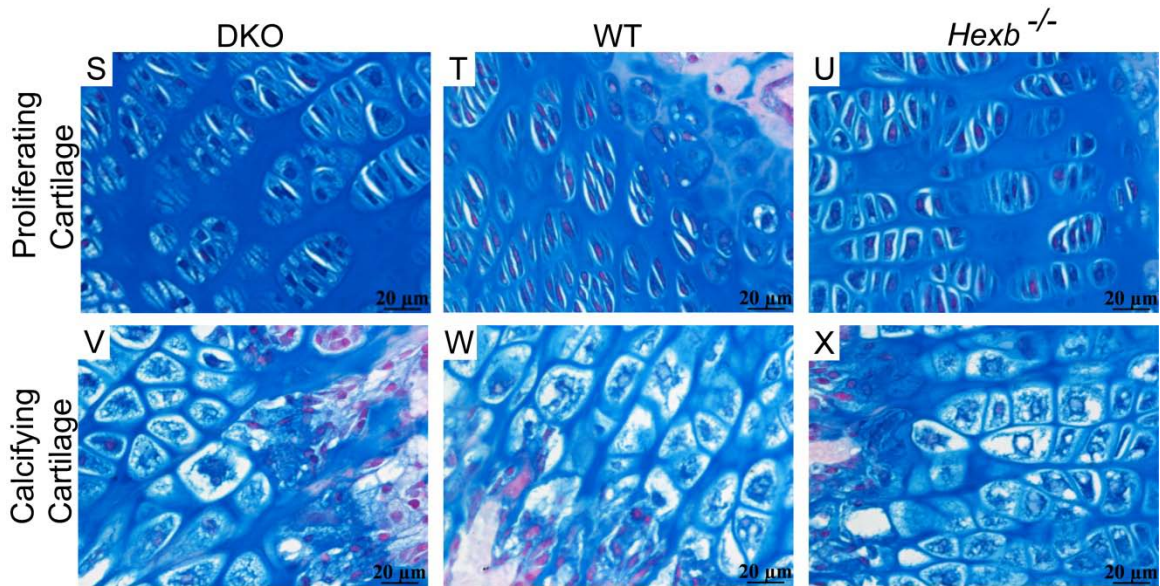
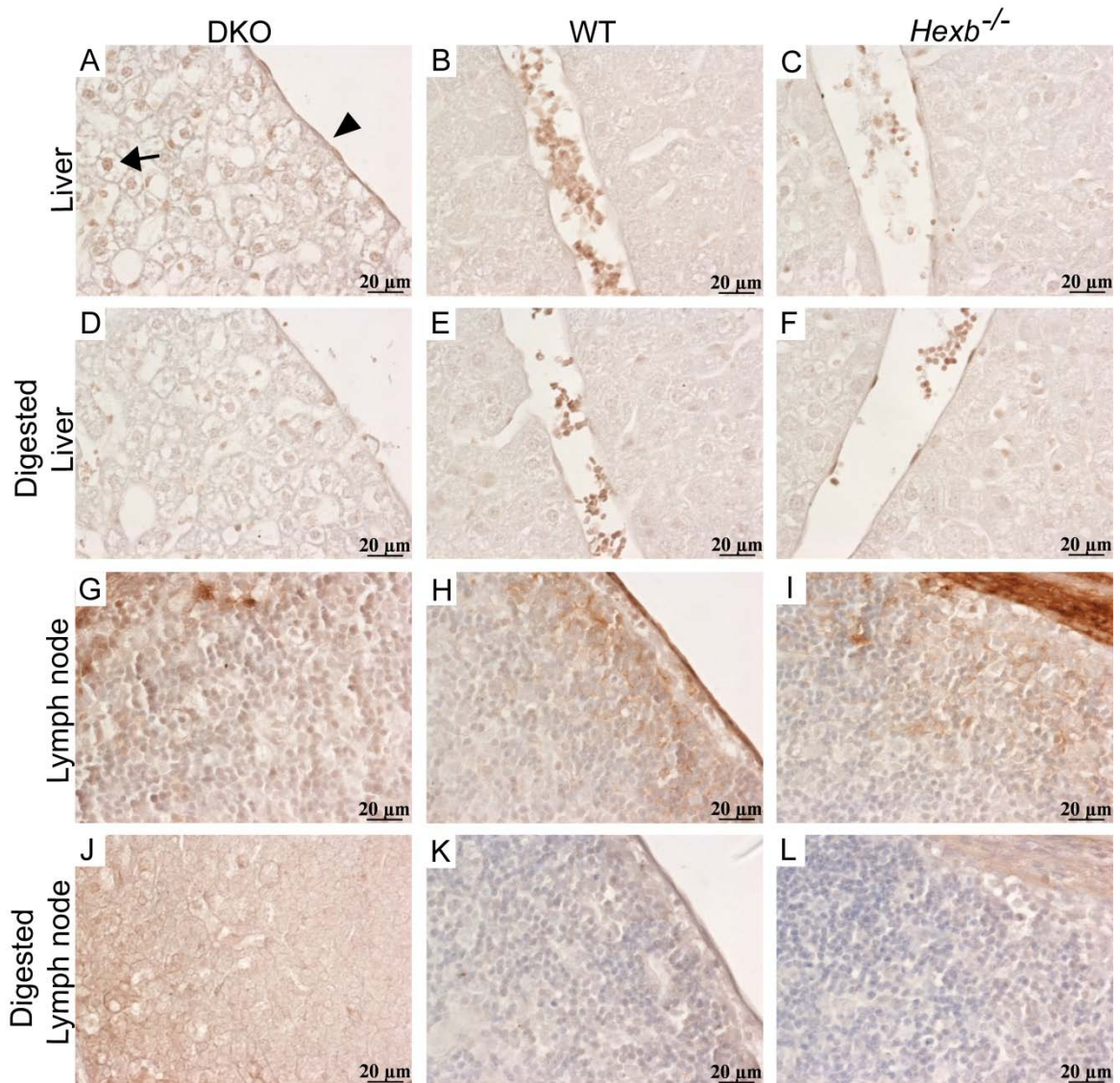


**Figure 4: Distribution of GAGs in DKO, WT, and *Hexb*<sup>-/-</sup> mice.** (A-X) Tissue sections were stained with alcian blue and the presence of GAGs was observed (blue staining) at 63x magnification. Compared to the corresponding WT controls, DKO mice displayed more intense staining in several tissues including liver (A), lymph node (D), lung (J), spleen (M), and some areas in the cartilage of the knee joint (P and S) suggesting the presence of more GAGs. However, similar intensities of staining were seen in skin (G-I) sections from the DKO, WT, and *Hexb*<sup>-/-</sup> mice. With less intensity than DKO sections, *Hexb*<sup>-/-</sup> liver (C) and lymph node (F) also displayed a greater staining intensity compared to WT liver (B) and lymph node (E) sections suggesting GAGs are accumulating at lower levels than in DKO mice.

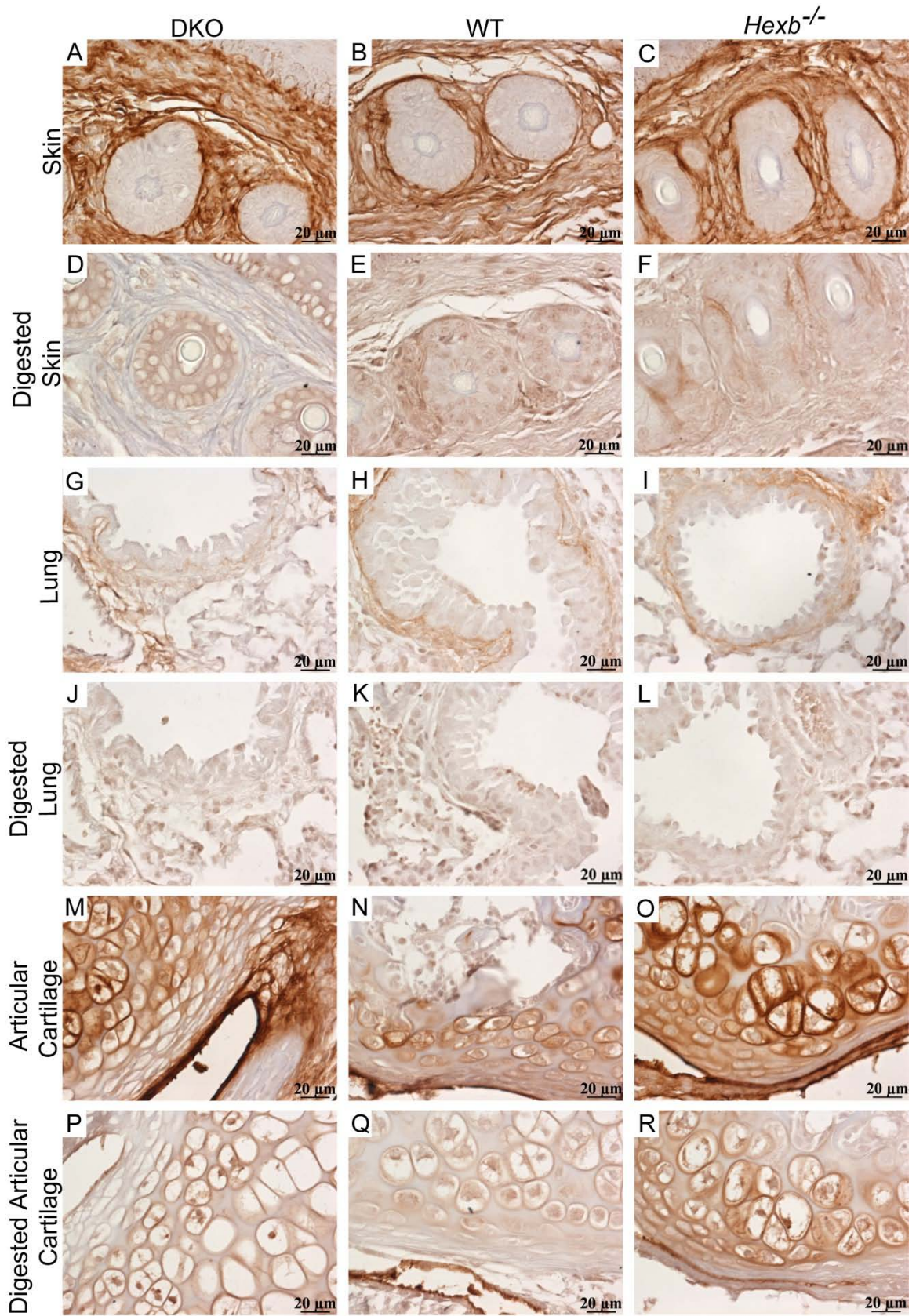
### 3.3 HABP staining of DKO mice:

To assess whether HA was one of the accumulating GAGs, immunohistochemistry with HABP was completed on paraffin-embedded tissue sections. Initially we focused on liver and lymph node because they are considered to be tissues with high levels of HA degradation; the distribution of HA (brown staining) is shown in Figure 5. DKO liver (Fig. 5A) displayed HA endothelial cell staining that was not observed in WT (Fig. 5B) or *Hexb*<sup>-/-</sup> (Fig. 5C) mice. This suggests that DKO liver endothelial cells are accumulating HA. Further, an increase in nuclear staining was also apparent in DKO hepatocytes (Fig. 5A) compared to WT (Fig. 5B) and *Hexb*<sup>-/-</sup> (Fig. 5C) sections. Stained lymph node sections showed similar intensities among DKO, WT, and *Hexb*<sup>-/-</sup> sections (Fig. 5G-I). Hyaluronidase digested sections of liver (Fig. 5D-F) and lymph node (Fig. 5J-L) were completed to ensure the binding specificity of the HABP, and served as a negative control.

Other tissues that are not considered high HA turnover areas were also stained with HABP, and are shown in Figure 6. Skin (Fig. 6A-C) and lung (Fig. 6G-I) sections from DKO, WT, and *Hexb*<sup>-/-</sup> mice displayed similar levels of HA. In contrast, an apparent increase in intracellular and pericellular staining was found in the articular cartilage (Fig. 6M-O) and the proliferating cartilage of the epiphyseal plate (Fig. 6S-U) in the DKO and *Hexb*<sup>-/-</sup> mice when compared to WT sections. Further, *Hexb*<sup>-/-</sup> mice displayed increased staining in the calcifying cartilage of the epiphyseal plate (Fig. 6AA) compared to DKO and WT mice (Fig. 6Y and Z). The lower intensity seen in the DKO mice could potentially be due to the disorganized structure observed in the DKO epiphyseal plate. Negative controls for skin (Fig. 6D-F), lung (Fig. 6J-L), articular



**Figure 5: HA localization in high HA turnover tissues of DKO, WT, and *Hexb*<sup>-/-</sup> mice.** (A-L) HA was detected in liver and lymph node tissue sections of DKO, WT, and *Hexb*<sup>-/-</sup> mice by staining with HABP, followed by viewing at 63x magnification. Liver sections from DKO mice (A) displayed increased endothelial cell (arrowhead) and hepatic nuclei (arrow) staining when compared to WT (B) and *Hexb*<sup>-/-</sup> (C) sections. Lymph node sections (G-I) displayed diffuse HA staining, with overall levels appearing similar in DKO, WT, and *Hexb*<sup>-/-</sup> tissue sections. Liver (D-F) and lymph node (J-K) sections treated with a hyaluronidase from *Streptomyces hyalurolyticus* served as negative controls as the HA signal was not present after treatment.



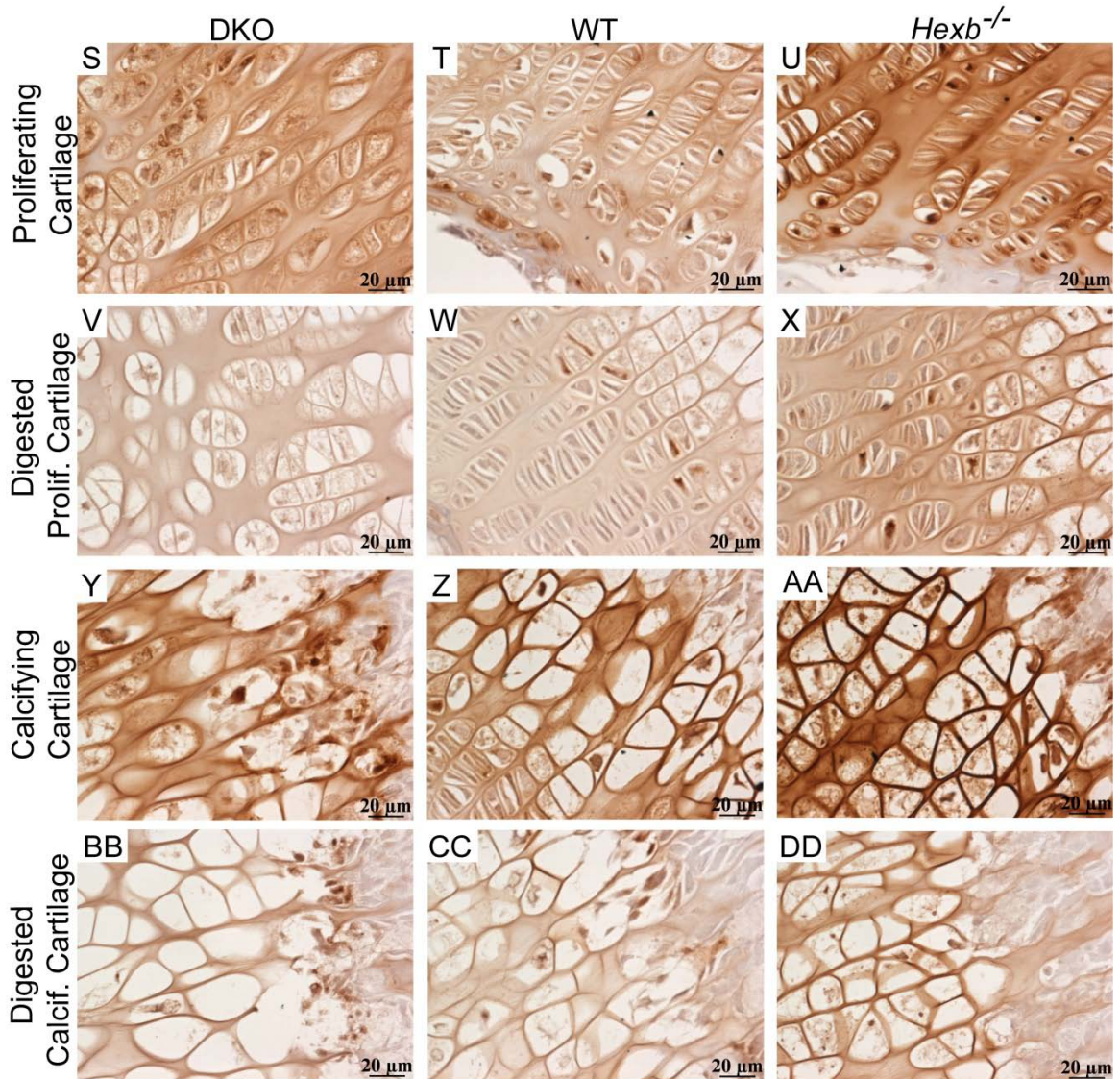


**Figure 6: HA localization in other tissues of DKO, WT, and *Hexb*<sup>-/-</sup> mice.** (A-DD) HA was detected in tissue sections of DKO, WT, and *Hexb*<sup>-/-</sup> mice by staining with HABP, followed by viewing at 63x magnification. Skin (A-C) and lung (G-I) sections from DKO, WT, and *Hexb*<sup>-/-</sup> mice showed similar levels of HA. In contrast, articular cartilage sections from DKO (M) and *Hexb*<sup>-/-</sup> (O) mice displayed increased extracellular, pericellular, and intracellular staining when compared to WT sections (N). Proliferating cartilage was positive for HA in the DKO (S), WT (T), and *Hexb*<sup>-/-</sup> (U) sections, but DKO and *Hexb*<sup>-/-</sup> sections displayed a greater intensity suggesting the presence of more HA. Further, an increase in pericellular staining in the calcifying cartilage was apparent in of the *Hexb*<sup>-/-</sup> mice (AA) when compared to DKO (Y) and WT (Z) sections. Tissue sections digested with hyaluronidase from *Streptomyces hyalurolyticus* served as a negative cartilage (Fig. 6P-R), proliferating cartilage (Fig. 6V-X), and calcifying cartilage (Fig. 6BB-DD) show the signal remaining after treatment with hyaluronidase from *Streptomyces hyalurolyticus*.

cartilage (Fig. 6P-R), proliferating cartilage (Fig. 6V-X), and calcifying cartilage (Fig. 6BB-DD) show the loss of signal after treatment with hyaluronidase from *Streptomyces hyalurolyticus*.

### **3.4 Fluorophore assisted carbohydrate electrophoresis of DKO tissues:**

To analyze the levels of individual GAGs biochemically, and to determine if and what GAGs were accumulating in DKO tissues, FACE was completed on a subset of tissues including liver, lymph node, skin, brain, and lung. Figure 7 depicts a representative FACE gel of various disaccharides found in DKO and WT mouse tissues. Similar gels were used to analyze *Hexb*<sup>-/-</sup> tissues; the results of all of these studies are summarized graphically.

#### **3.4.1 GAG analysis in high HA turnover tissues of DKO mice:**

Levels of HA and other GAGs were expected to accumulate to the highest levels in those tissues that have been shown to have high levels of HA turnover, liver and lymph node. Therefore, these were the first tissues that we assayed in the  $\beta$ -hexosaminidase-deficient mice. As shown in Fig. 8A, although the levels of HA were low in DKO liver (0.13 ng/mg), they were significantly higher ( $p=0.04$ ,  $n=6$ ) than those in the liver of WT control mice (0.02 ng/mg,  $n=5$ ). The levels of HA in liver from *Hexb*<sup>-/-</sup> mice (0.07 ng/mg) was between that of the DKO and WT mice, and did not differ significantly from either level ( $p=0.08$ ). DKO lymph node also displayed significant accumulation of HA ( $p=0.02$ ,  $n=4$ ) with average levels of 1.2 ng/mg compared to 0.4 ng/mg in WT controls (Fig. 8C). The accumulation of HA in DKO lymph node, albeit higher than DKO liver, was still relatively low. Only one sample of *Hexb*<sup>-/-</sup> lymph node was available at the time of analysis and therefore statistics could not be completed.

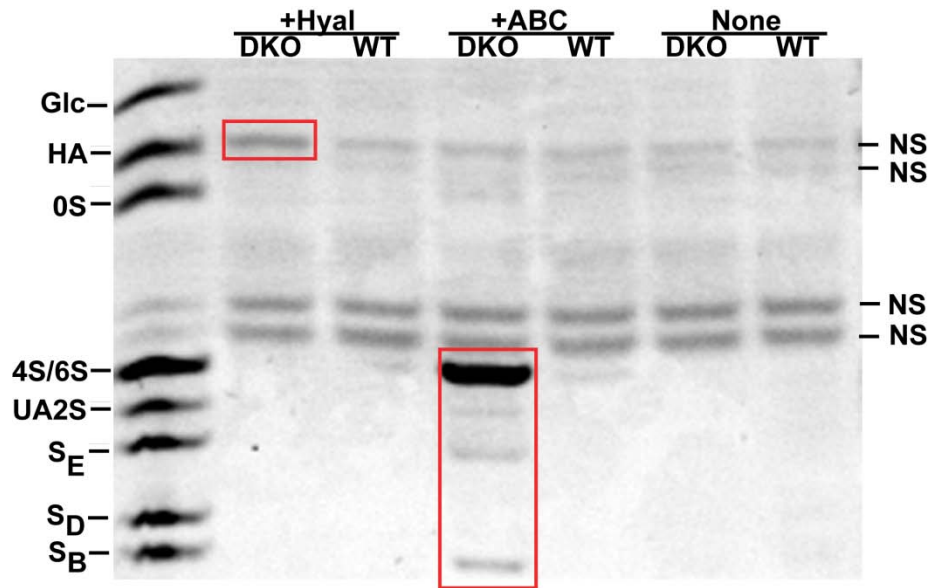


**Figure 7: Representative FACE gel of various GAG disaccharides in DKO and WT mice.** GAG disaccharides in DKO and WT mouse tissue samples were analyzed using FACE (*Hexb*<sup>-/-</sup> not shown). Tissue homogenates were digested with hyaluronidase SD (+Hyal) to produce HA disaccharides. Chondroitinase ABC (+ABC) was used to generate disaccharides of chondroitin (OS), and its sulphated derivatives including, type A (4S), type C (6S), chondroitin-2-sulphate (UA2S), type E (S<sub>E</sub>), type D (S<sub>D</sub>) and dermatan sulphate (S<sub>B</sub>). To serve as a negative control, an aliquot of the tissue homogenate was not digested (None). Bands labeled as NS are non-specific and are a result of the labeling agent 2-aminoacridone. GAG levels were quantified based on a standard curve generated from three or more lanes containing fluorescently labeled standards of known concentrations.

Given the low level of HA accumulation observed, and that  $\beta$ -hexosaminidase can cleave either GlcNAc or GalNAc with  $\beta$ 1-4 bonds, accumulation of other GAGs was expected in DKO mice, and therefore was first assayed in liver and lymph node. DKO liver presented with significant accumulation of both chondroitin type A/C (4S/6S;  $p=0.01$ ,  $n=5$ ) and type E ( $S_E$ ;  $p=0.02$ ,  $n=5$ ) compared to WT controls ( $n=4$ ) as shown in Figure 8B. Unlike the low levels of HA accumulation seen in DKO liver (0.13 ng/mg), average levels of accumulating chondroitin in DKO liver reached approximately 8.5 ng/mg of liver. Chondroitin-2-sulphate (UA2S) was also detected in DKO ( $n=5$ ) and WT ( $n=4$ ) liver, but the levels were comparable ( $p=0.09$ ). Chondroitin 4S/6S ( $p=0.01$ ), UA2S ( $p=0.3$ ), and  $S_E$  ( $p=0.03$ ) were detected in *Hexb*<sup>-/-</sup> liver at levels consistently higher than that of WT liver. However, post-ANOVA analysis determined that the average levels observed in *Hexb*<sup>-/-</sup> liver were not significantly different from WT or DKO (Fig. 8B), suggesting a full loss of  $\beta$ -hexosaminidase is required to fully disrupt GAG turnover.

The accumulation of sulphated chondroitin in DKO lymph node was similar to DKO liver, however with the addition of another chondroitin sulphate type, dermatan sulphate ( $S_B$ ). Chondroitin 4S/6S ( $p=0.0005$ ,  $n=5$ ),  $S_E$  ( $p=0.047$ ,  $n=4$ ), and  $S_B$  ( $p=0.001$ ,  $n=4$ ) were significantly accumulating compared to WT lymph node as shown in Figure 8D. Again, average levels of accumulating chondroitin in DKO mice reached 13.8 ng/mg of lymph node, which was much higher than the HA accumulation seen in DKO lymph node (1.2 ng/mg of lymph node). Similarly, statistics could not be completed on levels of chondroitin sulphate in *Hexb*<sup>-/-</sup> lymph node as FACE was completed using only one mouse set. However, as in DKO liver, chondroitin sulphate levels in *Hexb*<sup>-/-</sup> lymph node were consistently higher than average levels observed in WT lymph node. *In vivo*

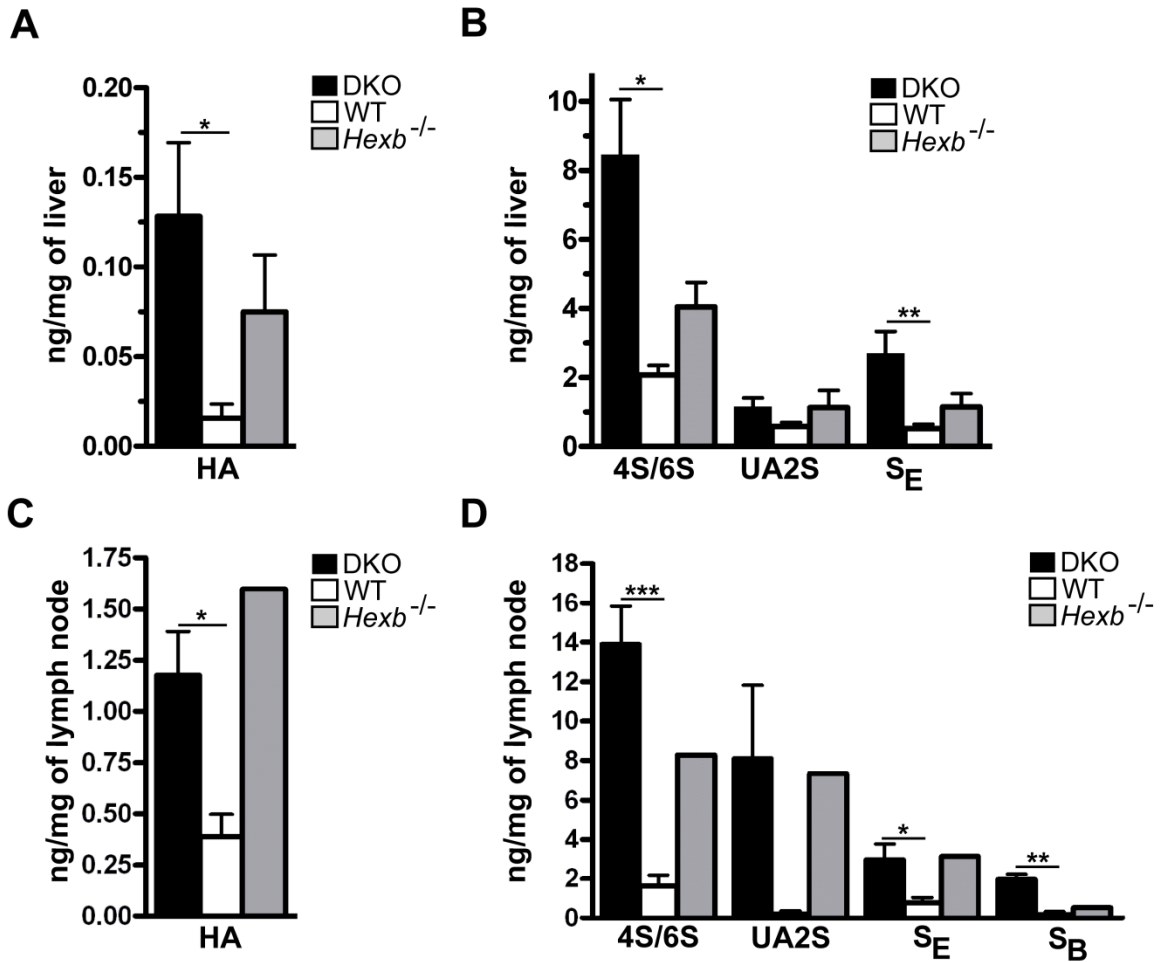


**Figure 8: Quantification of GAG levels in high HA turnover tissues in DKO, WT, and *Hexb*<sup>-/-</sup> mice.** (A-D) HA and chondroitin sulphate levels were determined using FACE. (A) DKO liver (p=0.04, n=6) and (C) lymph node (p=0.02, n=4) displayed increased levels of HA compared to liver (n=5) and lymph node (n=4) of WT controls. Levels of HA in *Hexb*<sup>-/-</sup> liver (A) did not differ significantly from either DKO or WT samples. (B) DKO liver was also accumulating chondroitin 4S/6S (p=0.01, n=5) and S<sub>E</sub> (p=0.02, n=5) compared to WT liver (n=4). UA2S levels were not significantly different from controls (p=0.09). (D) Lymph node was also accumulating high levels of various sulphated forms of chondroitin, including 4S/6S (p=0.0005, n=5), S<sub>E</sub> (p=0.047, n=4), and S<sub>B</sub> (p=0.001, n=4). UA2S levels in the DKO lymph node samples were not significantly different from WT controls (p=0.1, n=3). Average levels of GAGs are shown in ng/mg of tissue with standard error of the mean (\*p<0.05, \*\*p<0.01, \*\*\*p<0.001).

accumulation of several chondroitin sulphate derivatives suggests that  $\beta$ -hexosaminidase has multiple substrates in the GAG family.

### 3.4.2 GAG analysis in other DKO tissues:

Since the accumulation of multiple GAGs was observed in both DKO liver and lymph node, we wanted to determine if tissues that are not considered major players in overall HA turnover were also affected by the loss of  $\beta$ -hexosaminidase. Unlike DKO liver and lymph node, levels of HA in DKO lung ( $p=0.6$ ,  $n=5$ ), skin ( $p=0.4$ ,  $n=5$ ), and brain ( $p=1.0$ ,  $n=3$ ) did not significantly differ from WT controls, as shown in Figure 9A, C, and E. Similarly, average HA levels in *Hexb*<sup>-/-</sup> lung ( $p=0.6$ ), skin ( $p=0.5$ ), and brain ( $p=0.4$ ) samples were not significantly different from either DKO or WT (Fig. 9A, C, and E). It is important to note that the average WT level of HA found in skin was approximately 3.6 ng/mg of skin, which was 70 and 7.5 fold higher than the levels of accumulating HA found in DKO liver and lymph node, respectively.

Given that the majority of the GAG accumulation observed in liver and lymph node was due to various sulphated derivatives of chondroitin, levels of these GAGs were also analyzed in lung, skin, and brain (Fig. 9B, D, and F). Similar to DKO liver and lymph node, DKO lung displayed extensive accumulation of multiple derivatives of sulphated chondroitin including 4S/6S ( $p=0.005$ ,  $n=5$ ), UA2S ( $p=0.003$ ,  $n=5$ ), S<sub>E</sub> ( $p=0.0006$ ,  $n=5$ ), and S<sub>B</sub> ( $p=0.009$ ,  $n=4$ ) when compared to WT controls. Average levels reached 31 ng/mg of DKO lung, a striking level compared to the corresponding WT average level of 5 ng/mg of lung. The same derivatives of sulphated chondroitin were also detected in *Hexb*<sup>-/-</sup> lung samples, but only levels of chondroitin 4S/6S ( $p=0.0006$ ,  $n=4$ ) were significantly different from the levels in WT lung (Fig. 9B). It was determined by post ANOVA analysis that *Hexb*<sup>-/-</sup> average lung levels of UA2S, S<sub>E</sub>, and S<sub>B</sub> did not

significantly vary from average DKO or WT values ( $p>0.5$ ). However, average levels of the GAGs were still consistently higher than WT levels. As shown in Figure 9D, several types of sulphated chondroitin were detected in DKO, WT, and *Hexb*<sup>-/-</sup> skin including chondroitin 4S/6S ( $p=0.4$ ), UA2S, S<sub>E</sub>, and S<sub>B</sub> ( $p=0.2$ ), however, average levels were similar to one another. ANOVA values were not calculated for levels of UA2S or S<sub>E</sub> in skin since they were only detected in 2 of the 4 mouse sets. Likewise, similar levels of chondroitin 4S/6S were detected in brain samples from DKO, WT, and *Hexb*<sup>-/-</sup> mice ( $p=0.6$ ,  $n=3$ ), shown in Figure 9F.

### **3.5 Summary of results part 1:**

Cellular vacuolization due to the accumulation of gangliosides and GAGs was apparent in several DKO tissues when compared to WT controls. *Hexb*<sup>-/-</sup> tissues also displayed vacuolization, however, not to the extent seen in the DKO tissues. Further, DKO tissues displayed an increase in alcian blue staining, suggesting the presence of more GAGs. *Hexb*<sup>-/-</sup> mice displayed a staining intensity between that of DKO and WT suggesting that GAGs were accumulating, but not at the level seen in the DKO mice. Accumulation of HA was apparent in liver endothelial cells, in the nuclei of the hepatocytes and in the cartilage of the knee joint. Of the tissues tested, DKO liver and lymph node were shown to be accumulating, significant, but low levels of HA when compared to WT levels. Further, high levels of sulphated derivatives of chondroitin were found to be accumulating in DKO liver, lymph node, and lung samples. Whereas, levels of HA and chondroitin sulphate derivatives in *Hexb*<sup>-/-</sup> mice were not significantly different from either DKO or WT levels. However, a trend was present such that *Hexb*<sup>-/-</sup> samples displayed intermediate levels of GAGs, between that of DKO and WT, suggesting that there was still activity present to degrade GAGs.

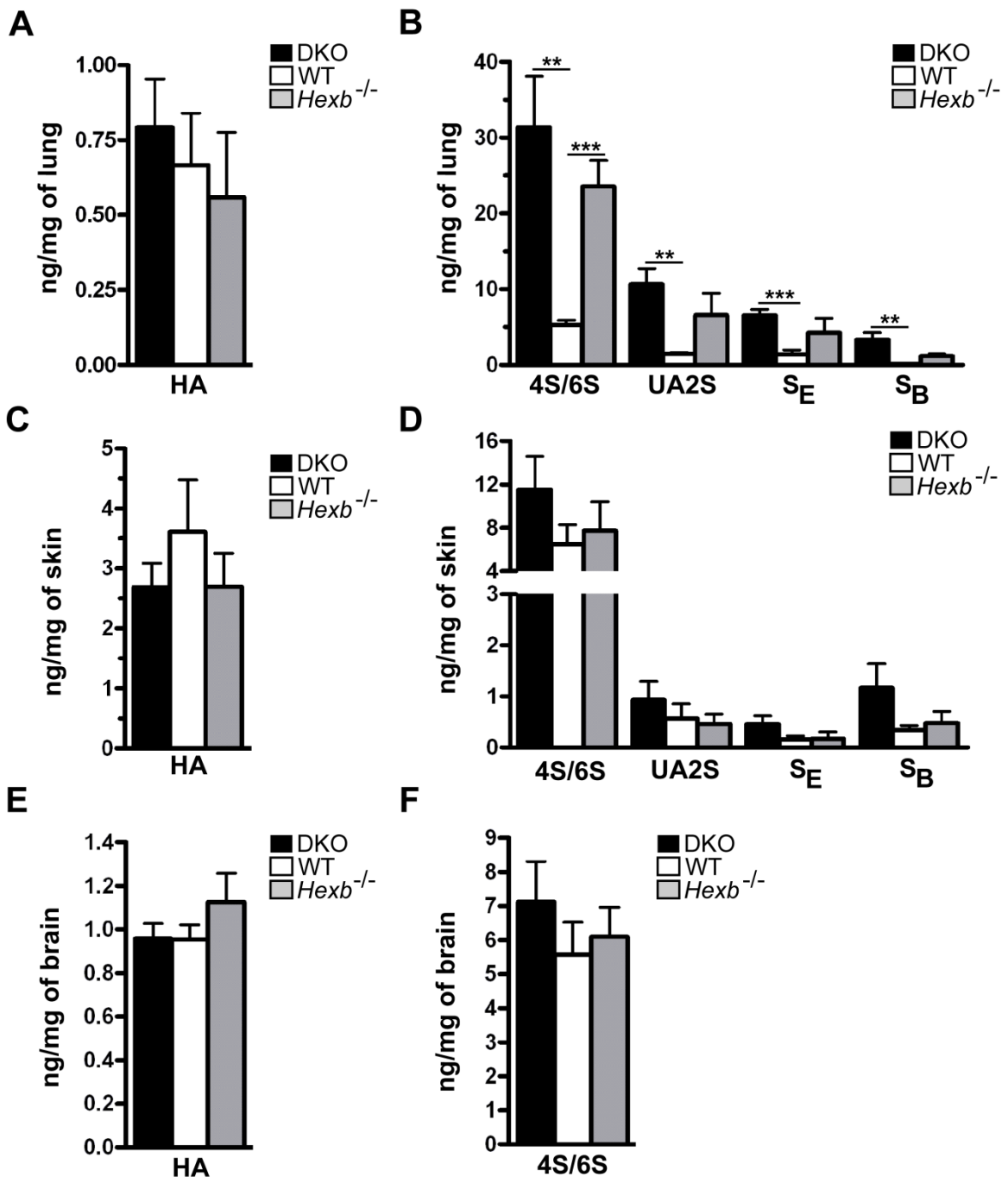


**Figure 9: Quantification of GAG levels in other tissues from DKO, WT, and *Hexb*<sup>-/-</sup> mice.** (A-F) HA and chondroitin sulphate levels were determined using FACE. (A, C, and E) There was no significant difference in HA levels between DKO and WT lung (p=0.6, n=5), skin (p=0.4, n=5), or brain (p=1.0, n=3). Similarly, HA levels in *Hexb*<sup>-/-</sup> samples were not significantly different from either DKO or WT values. (B) Levels of chondroitin 4S/6S in lung samples from DKO (p=0.005, n=5) and *Hexb*<sup>-/-</sup> (p=0.0006, n=

4) were significantly greater than those observed in WT samples. DKO lung (n=5) was also accumulating statistically significant levels of UA2S (p=0.003), S<sub>E</sub> (p=0.0006), and S<sub>B</sub> (p=0.009). *Hexb*<sup>-/-</sup> lung UA2S, S<sub>E</sub>, and S<sub>B</sub> were not significantly different from either DKO or WT samples. (D) Various derivatives of chondroitin sulphate were detected in DKO, WT, and *Hexb*<sup>-/-</sup> skin, however, there was no significant difference between sample means. (F) Similar levels of chondroitin 4S/6S was detected in brain samples from DKO, WT, and *Hexb*<sup>-/-</sup> mice. Average levels of GAGs are shown in ng/mg of tissue with standard error of the mean (\*\*p<0.01, \*\*\*p<0.001).

## **Chapter 4: Results Part 2**

#### **4.1 Rationale:**

The rapid turnover of HA in some tissues<sup>17</sup>, combined with the previous evidence of GAG accumulation in DKO mice, led us to expect extensive accumulation of HA after the loss of  $\beta$ -hexosaminidase as it was previously thought that HYAL1 only digested HA down to short oligosaccharides that were then digested by  $\beta$ -hexosaminidase<sup>55</sup>. However, FACE analysis of tissues from DKO mice demonstrated only low levels of HA accumulation, and this was limited to the liver and lymph node. This lack of broad HA accumulation could be explained by a functional redundancy between  $\beta$ -hexosaminidase and another lysosomal HA degrading enzyme. We predict HYAL1 as the best candidate to compensate for the loss of  $\beta$ -hexosaminidase as it is broadly expressed in tissues at high levels<sup>54</sup>, and also functions within the lysosome at an acidic pH<sup>103</sup>. Thus, *Hexa*<sup>-/-</sup> *Hexb*<sup>-/-</sup> *Hyal1*<sup>-/-</sup> mice were generated to test for functional redundancy. A drastic increase in HA accumulation observed in the triple knockout would suggest that HYAL1 and  $\beta$ -hexosaminidase are functionally redundant in the turnover of HA, and thus, explain the lack of extensive HA accumulation in  $\beta$ -hexosaminidase-deficient mice.

#### **4.2 Hypothesis:**

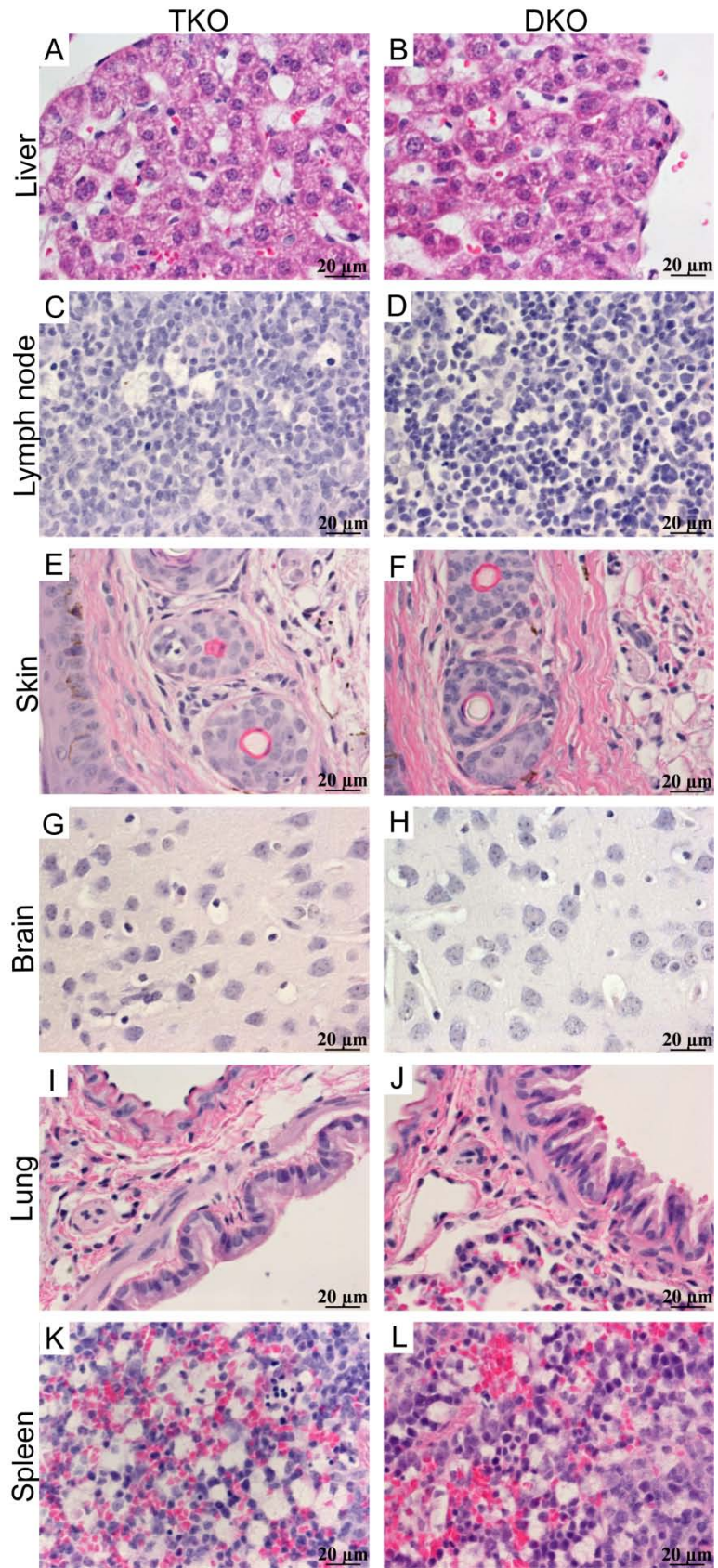
A mouse model with a combined deficiency of the lysosomal enzymes, HYAL1 and  $\beta$ -hexosaminidase, will display global tissue accumulation of HA, as all known active intracellular HA degrading enzymes would then be lacking.

#### **4.3 Phenotype of *Hexa*<sup>-/-</sup> *Hexb*<sup>-/-</sup> *Hyal1*<sup>-/-</sup> (TKO) mice:**

The phenotype of the TKO mice was found to be similar to that described previously for the DKO (*Hexa*<sup>-/-</sup> *Hexb*<sup>-/-</sup>) mice (3.1)<sup>108, 109</sup>, but more severe. At approximately 23 days, the TKO mice (n=7) reached the predetermined humane endpoint of inability to feed and/or reduced mobility compared to an average of 33 days in the DKO mice. The difference between the life span of the TKO and DKO mice was significant (p=0.04). The TKO mice were smaller than their DKO littermates, and leading up to the humane endpoint they displayed tremors, seizure-like episodes, and laboured breathing. Similar to DKO littermates, TKO mice displayed a broad nose, a characteristic of mucopolysaccharidoses in mouse models<sup>102, 105, 111</sup>.

#### **4.4 Tissue morphology and substrate accumulation in TKO tissues:**

To determine if the loss of both HYAL1 and  $\beta$ -hexosaminidase caused a change in tissue morphology, H&E staining was completed on several TKO and DKO tissues. Tissue sections from 4 week old TKO and DKO mice stained with H&E showed pronounced cellular vacuolization consistent with intracellular macromolecule accumulation (Fig. 10). Intracellular vacuoles were prominent in liver, lymph node, brain, spleen, kidney, and in chondrocytes of the articular, proliferating, and calcifying cartilage. There was no apparent difference in the overall vacuolization of the TKO mouse tissues when compared to DKO tissues. However, the lacunae of the proliferative cartilage in the TKO mice (Fig. 10Q) appeared less organized than in the DKO mice (Fig. 10R). Unlike other tissues, skin (Fig. 10E and F) and lung (Fig. 10I and J) sections of the TKO and DKO mice did not display intracellular vacuolization.



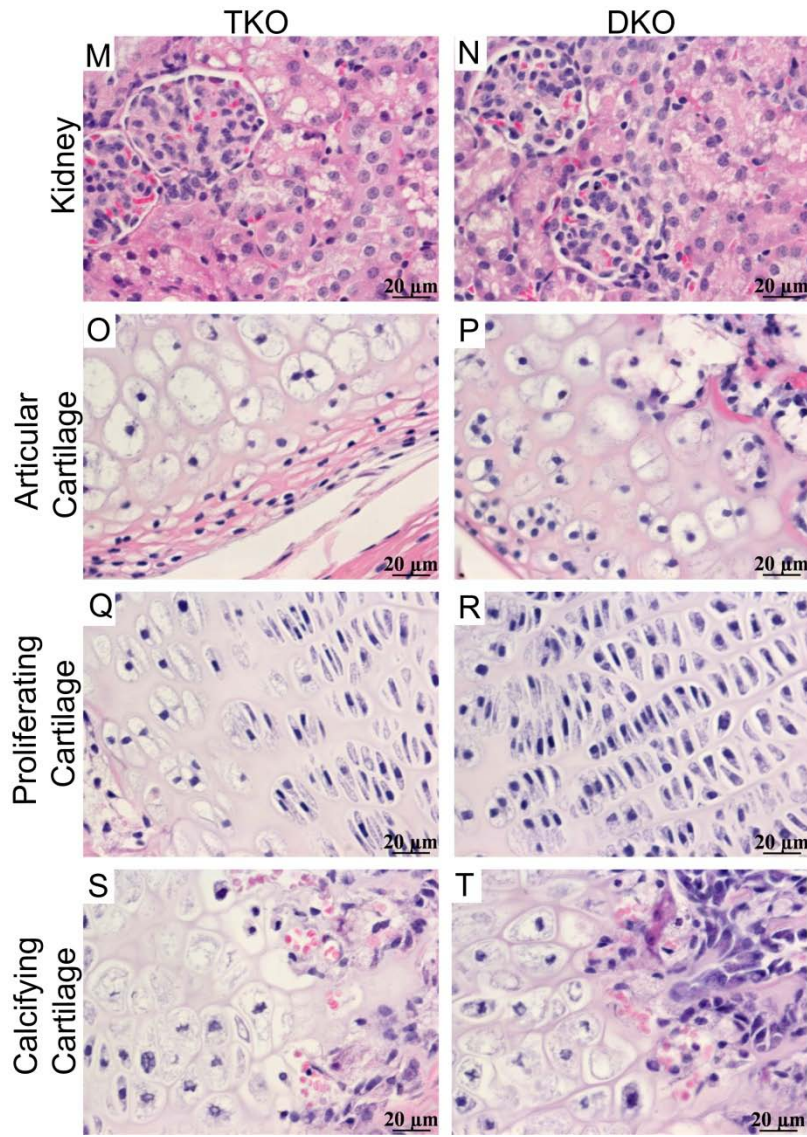
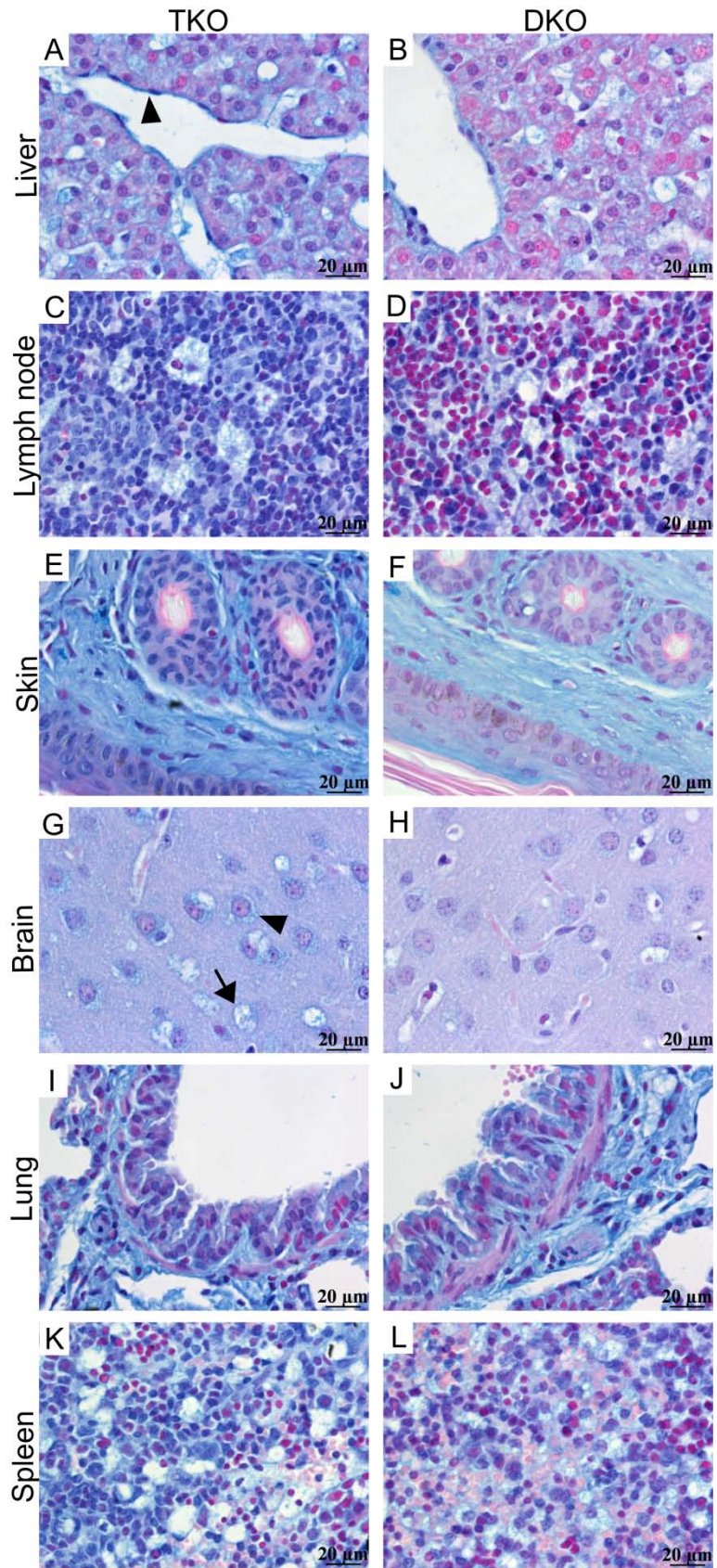


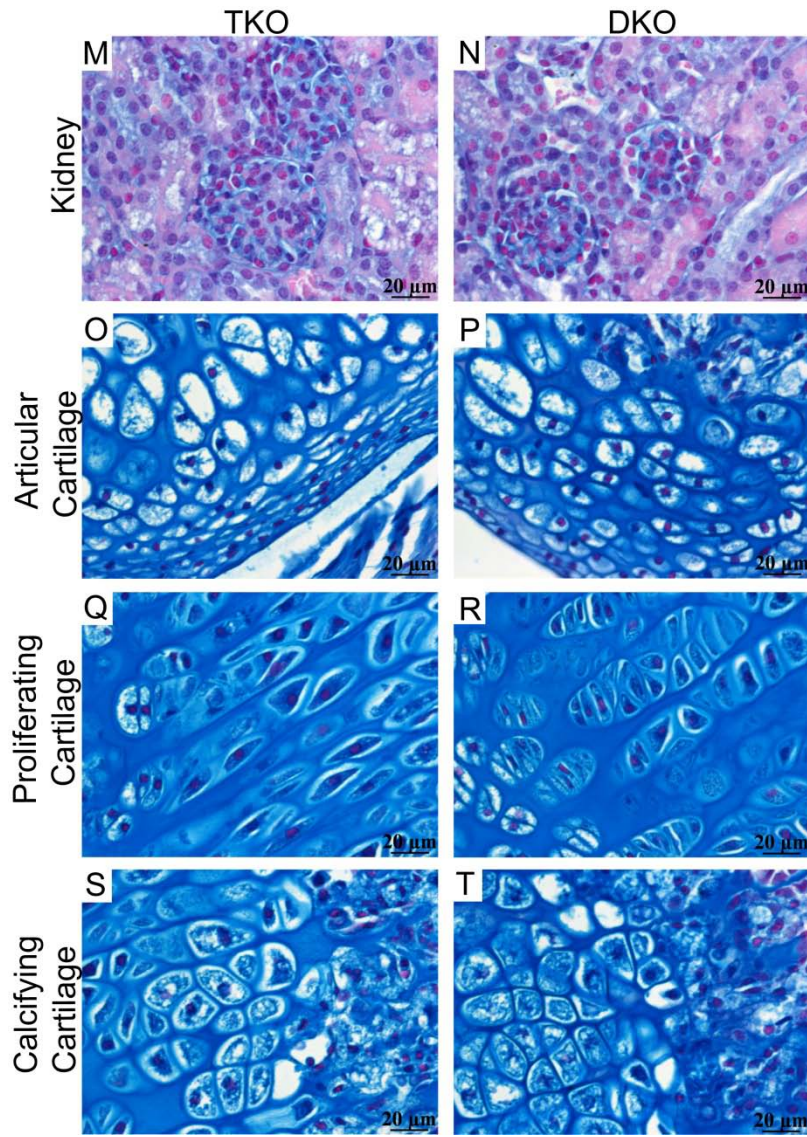
**Figure 10: Analysis of tissue morphology in TKO mice and DKO controls.** (A-T) H&E staining was completed to assess tissue morphology at 63x magnification. Intracellular vacuolization was apparent in both TKO and DKO sections in many tissues including liver (A and B), lymph node (C and D), brain (G and H), spleen (K and L), kidney (M and N), and in the cartilage of the knee joint (O-T), suggesting the accumulation of substrates. The observed vacuolization appeared similar in the TKO and respective DKO tissue control. However, the lacunae of the proliferative cartilage in the TKO mice (Q) appeared less organized than in the DKO mice (R). Intracellular vacuolization was not observed in skin (E and F) or lung (I and J) of the TKO and DKO mice.

To assess GAG accumulation after the loss of both HYAL1 and  $\beta$ -hexosaminidase, alcian blue staining was performed. Using this stain, an intense and specific blue signal was detected in both TKO and DKO tissues (Fig. 11). This staining was more intense in some of the TKO tissues, including liver, lymph node, skin, brain, and spleen, indicating a greater level of GAGs were present when compared to DKO tissues. As shown in Figure 11, staining intensities in TKO and DKO lung, kidney, and chondrocytes of the articular and epiphyseal cartilage were similar, suggesting the level of GAGs was similar.

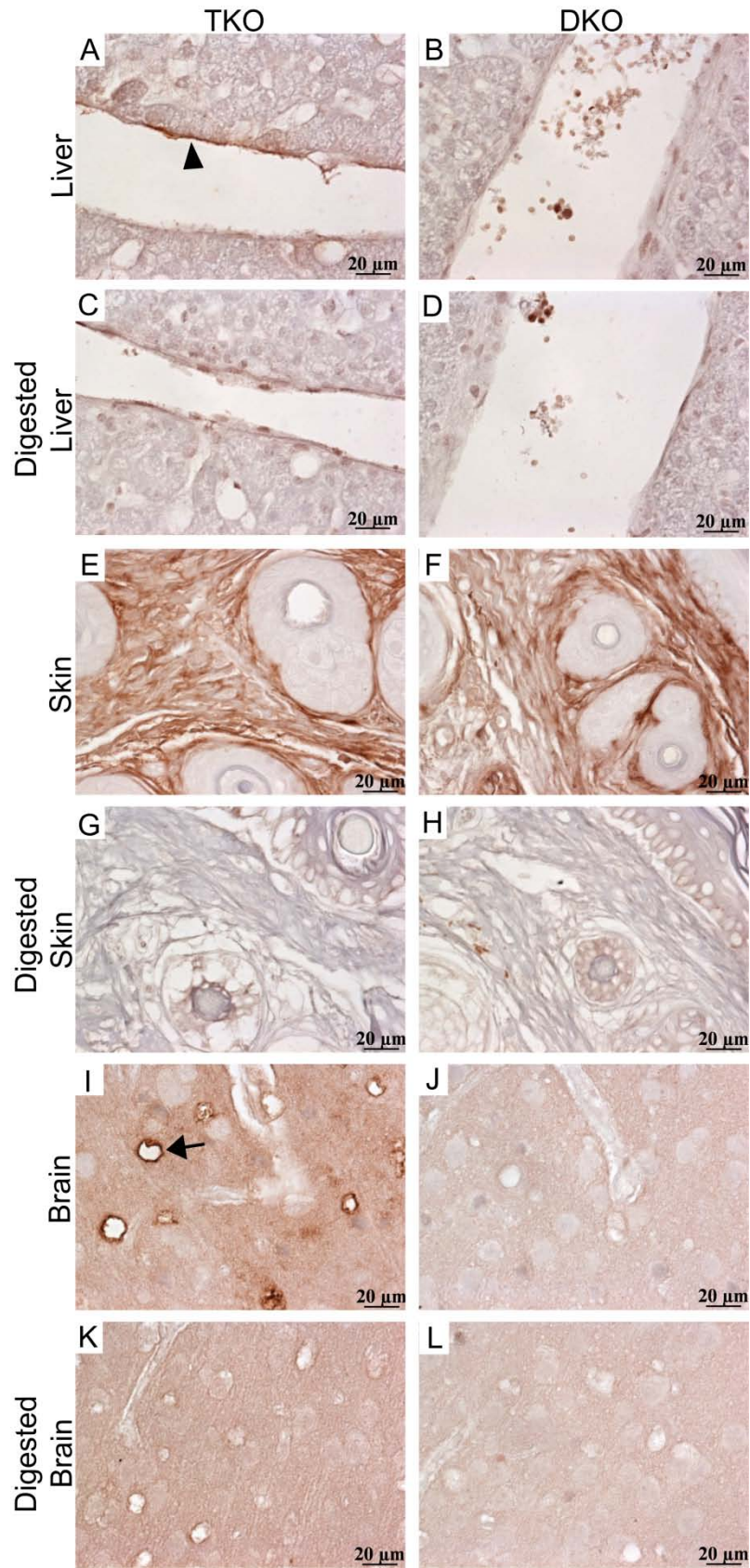
#### **4.5 Localization and accumulation of HA in TKO tissues:**

Given that little to no HA accumulation was seen in DKO mice after completing HABP staining (Fig. 5 and 6) and FACE (Fig. 8 and 9) and that GAG accumulation was not detected in HYAL1-deficient mice<sup>101</sup>, we wanted to assess HA accumulation in tissues from mice lacking both HYAL1 and  $\beta$ -hexosaminidase activity. Figure 12 and 13 show the distribution of HA in vascular and avascular tissues, respectively. HA accumulation was apparent in the endothelial cells of the liver (Fig. 12A), around the periphery of vacuolated neural cells in the brain (Fig. 12I), and in the mucosal folds of the bronchiole (Fig. 12M) in the TKO mice. DKO tissue controls (Fig. 12B, J, and N) for liver, brain, and lung lacked the distinct staining patterns observed in the TKO mice. In skin (Fig. 12E and F), HA levels appeared to be similar in the TKO mice and DKO controls. Negative controls showing the signal remaining after digestion with hyaluronidase was completed on all vascular tissues and is shown in Figure 12.





**Figure 11: GAG distribution in TKO mice and DKO controls.** Tissue sections were stained with alcian blue and the presence of GAGs was observed (blue staining) at 63x magnification. Compared to the corresponding DKO controls, TKO mice displayed more intense staining in several tissues, including, in the endothelial cells (arrowhead) of liver (A), the lymph node (C), skin (E), in the cytoplasm (arrowhead) as well as around vacuolated neural cells (arrow) in the brain (G), and spleen (K), suggesting the presence of more GAGs. Similar intensities of staining were seen in lung (I and J), kidney (M and N), and in the articular (O and P), proliferating (Q and R), and calcifying cartilage (S and T) sections of the TKO and DKO mice.



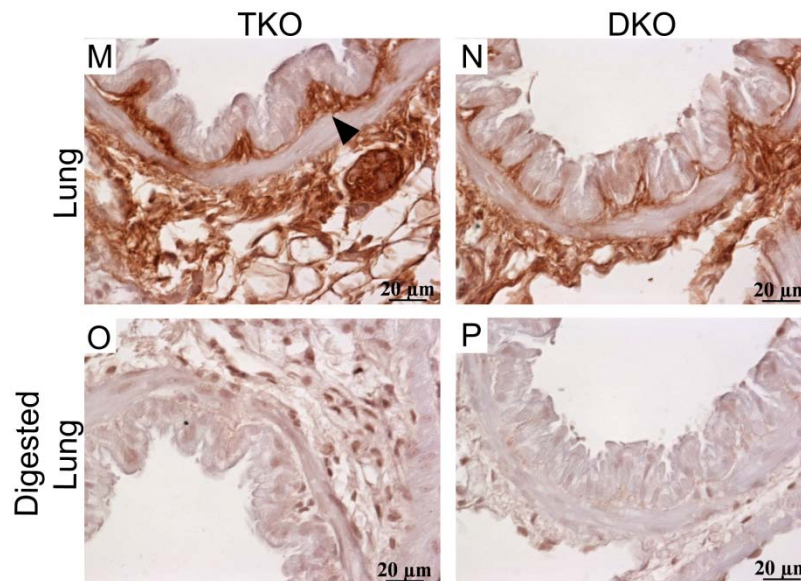


**Figure 12: HA localization in vascular tissues of TKO mice and DKO controls.** HA was detected in tissue sections of TKO mice and DKO controls by staining with HABP, followed by viewing at 63x magnification (A-P). Liver sections from TKO mice (A) displayed increased endothelial staining (arrowhead) when compared to DKO controls (B). Skin (E and F) was positive for HA but the levels were similar to one another. TKO brain sections (I) showed a distinct pattern of HA staining in the periphery of vacuolated neural cells (arrow) which was absent in DKO controls (J). HA accumulation was also apparent in mucosal folds of the bronchiole (arrowhead) in TKO mice (M) when compared to DKO controls (N). (C, D, G, H, K, L, O, and P) served as negative controls as the HA signal was not present after treatment with hyaluronidase from *Streptomyces hyalurolyticus*.

Avascular TKO and DKO tissues, including articular, proliferating, and calcifying cartilage, are shown in Figure 13. An increase in extracellular, pericellular, and intracellular staining was apparent in the TKO articular cartilage (Fig. 13A) when compared to that of DKO mice (Fig. 13B). A slight increase in staining was also observed in TKO proliferative (Fig. 13E) and calcifying cartilage (Fig. 13I) when compared to DKO cartilage (Fig. 13F and J). Avascular sections digested with a hyaluronidase are also shown in Figure 13 and account for the binding specificity of HABP.

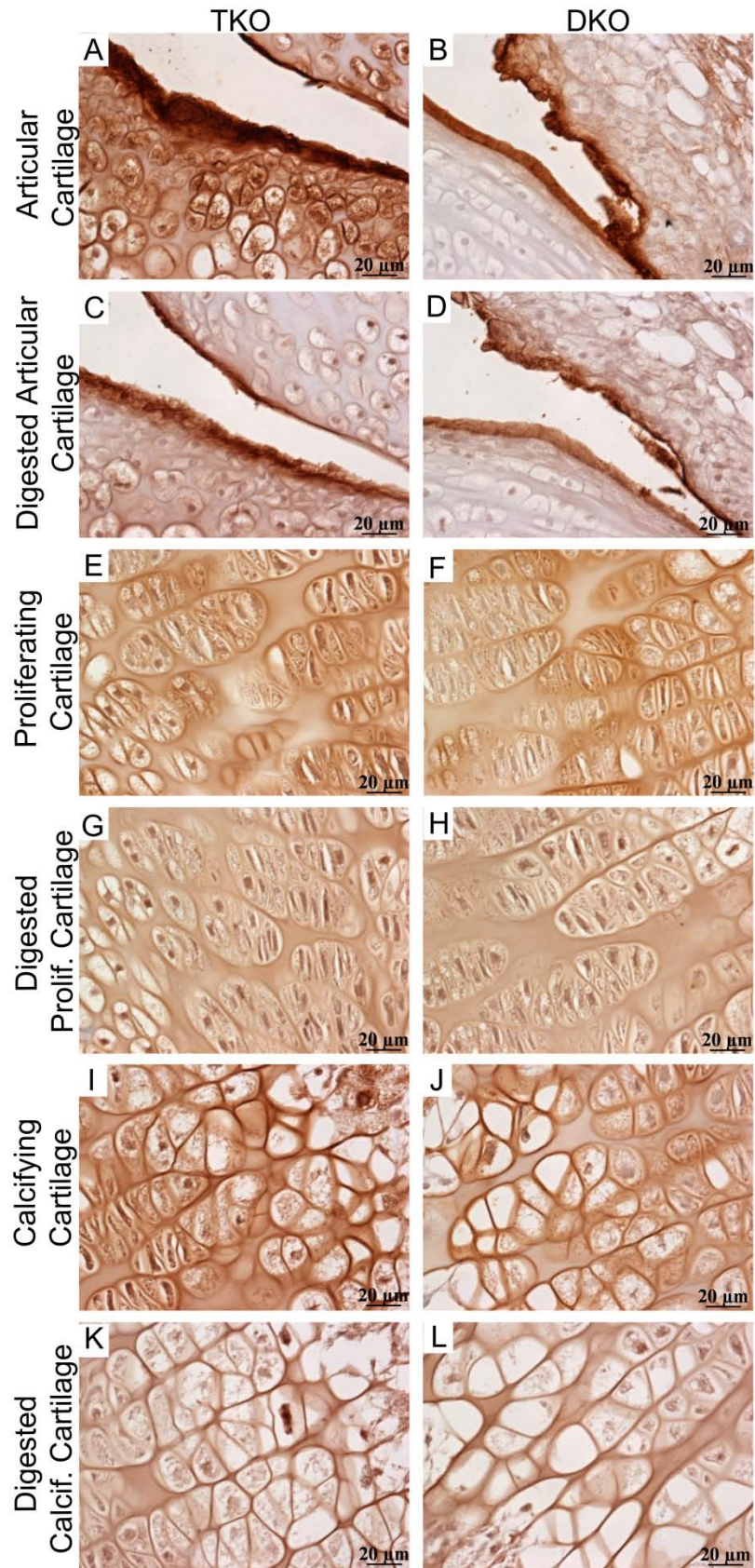


**Figure 13: HA localization in avascular tissues of TKO mice and DKO controls.** HA was detected in tissue sections of TKO mice and DKO controls by staining with HABP, followed by viewing at 63x magnification (A-L). Articular cartilage sections from TKO mice (A) displayed increased extracellular, pericellular, and intracellular staining when compared to DKO controls (B). A slight increase in HA staining was observed in the TKO proliferating (E) and calcifying (I) cartilage when compared to the respective DKO controls (F and J). Tissue sections treated with hyaluronidase from *Streptomyces hyalurolyticus* served as a negative control. The remaining signal after digestion is shown (C, D, G, H, K, and L).

#### 4.6 Identification and quantification of GAGs in TKO tissues using FACE:

FACE was performed to identify and quantify the levels of various GAGs, including HA, in the tissues of TKO and DKO control mice. GAGs were isolated from tissues and digested to their unique disaccharide units for quantification. A representative gel is shown in Figure 14.

Given that liver and lymph node are major turnover tissues for displaced HA<sup>83, 84</sup> we wanted to quantify HA levels in these tissues from TKO mice using FACE (Fig. 15A). HA levels were found to have reached an average of 78 ng/mg of tissue in the liver, far higher than the average level of 0.8 ng/mg of tissue detected in DKO controls ( $p=0.003$ ,  $n=3$ ). Extensive accumulation was also seen in the lymph node, with levels reaching 48 ng/mg of tissue compared to 4 ng/mg of tissue in DKO controls ( $p=0.02$ ,  $n=3$ ). Interestingly, HA levels observed in TKO liver and lymph node were approximately 3.6 and 2.2 fold higher, respectively, than those of TKO skin (Fig. 16A), a tissue known to have a high concentration of HA.

To determine if the catabolism of other GAGs was affected by the loss of both HYAL1 and  $\beta$ -hexosaminidase activity, levels of chondroitin and sulphated chondroitin were also analyzed in TKO liver and lymph node. It was found that accumulation in TKO liver and lymph node was not limited to HA, as chondroitin (OS), a GAG very similar in structure to HA was higher in the liver ( $p=0.001$ ,  $n=3$ ) and lymph node ( $p=0.0005$ ,  $n=3$ ) of TKO compared to DKO mice (Fig. 15B). In addition to HA and chondroitin accumulation, TKO liver samples displayed significant accumulation of various sulphated chondroitin derivatives (Fig. 15C) including UA2S ( $p=0.005$ ,  $n=3$ ), and S<sub>E</sub> ( $p=0.02$ ,  $n=3$ ).

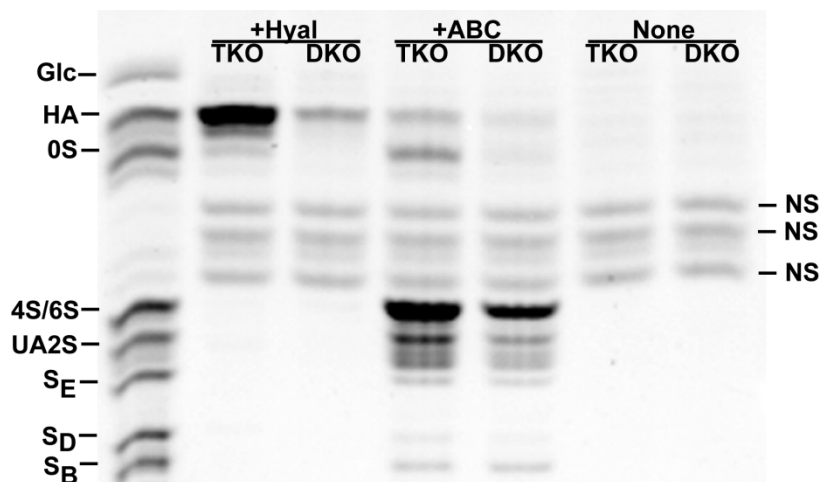


**Figure 14: FACE of various GAG disaccharides in TKO and DKO mouse tissue.** GAG disaccharides in TKO and DKO mouse tissue samples were analyzed using FACE. After treatment with hyaluronidase SD (+Hyal) elevated levels of HA were apparent in the TKO sample when compared to the DKO control. Chondroitinase ABC (+ABC) treatment revealed that OS along with several sulphated derivatives of chondroitin were accumulating. To serve as a negative control, an aliquot of each tissue homogenate was not digested (None). Bands labeled as NS are non-specific and are a result of the labeling agent 2-aminoacridone.

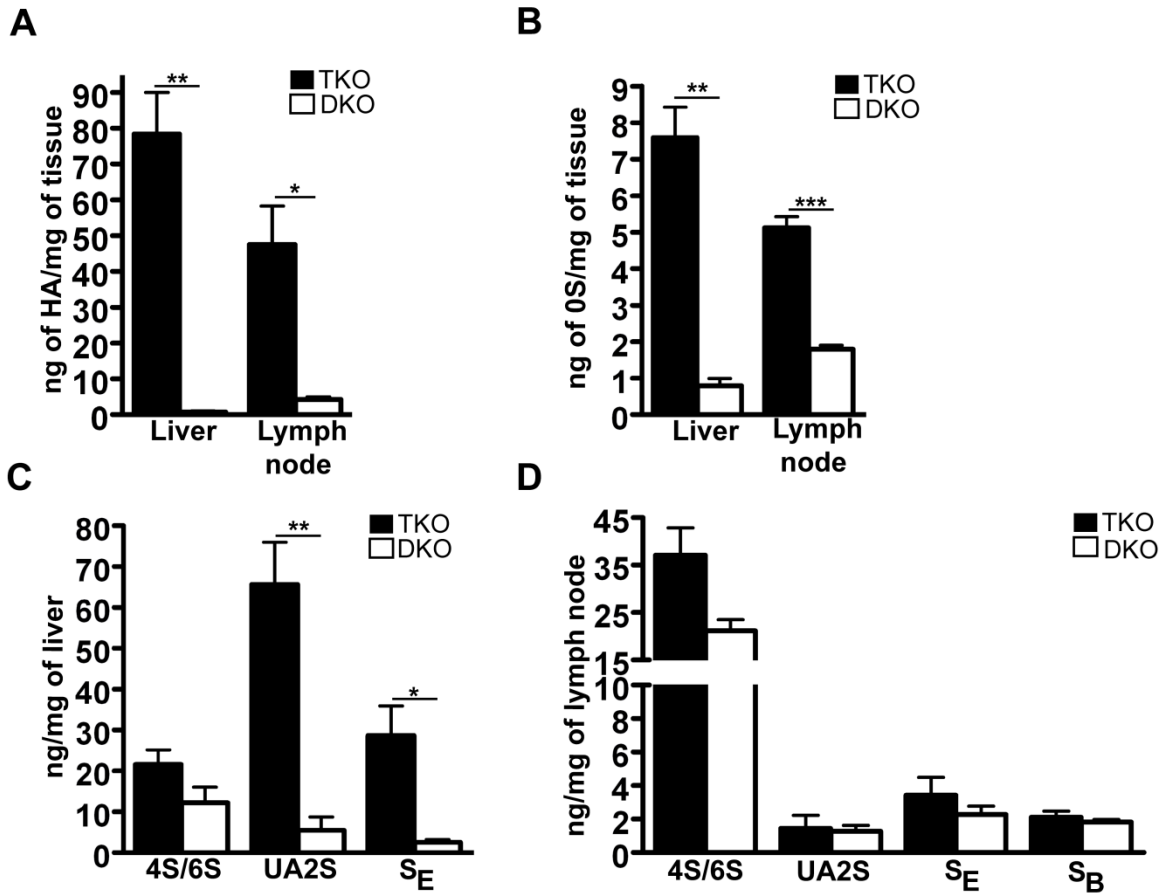


**Figure 15: Quantification of GAGs in TKO high HA turnover tissues.** FACE was used to quantify HA (A), chondroitin (0S) (B), and sulphated chondroitin in (C) liver (n=3) and (D) lymph node (n=3). (A) The level of HA was found to be significantly higher in TKO liver (p=0.003) and lymph node (p=0.02) when compared to DKO controls. (B) TKO liver (p=0.001) and lymph node (p=0.0005) also had significantly higher levels of 0S than that found in DKO controls. (C) TKO liver samples displayed significantly higher levels of chondroitin UA2S (p=0.005) and S<sub>E</sub> (p=0.02). Chondroitin 4S/6S (p=0.1) was not significantly accumulating in TKO liver samples. (D) 4S/6S (p=0.06, n=3), UA2S (p=0.8, n=3), S<sub>E</sub> (p=0.4, n=3), and S<sub>B</sub> (p=0.5, n=3) chondroitin sulphate levels in TKO lymph node were higher than DKO controls. However, the differences were not found to be significant. Average levels of GAGs are shown in ng/mg of tissue with standard error of the mean (\*p<0.05, \*\*p<0.01, \*\*\*p<0.001).

In contrast, levels of chondroitin sulphate derivatives detected in TKO lymph node were similar to DKO samples (Fig. 15D), taking into consideration that DKO levels were shown previously to significantly differ from WT controls (Fig. 8D). The accumulation of HA and other GAGs suggests that both HYAL1 and  $\beta$ -hexosaminidase have multiple substrates in the GAG family.

Given the drastic increase in HA accumulation in the TKO liver and lymph node, we wanted to determine if the loss of both HYAL1 and  $\beta$ -hexosaminidase activity affected other tissues not normally involved in HA turnover. FACE was completed on TKO and DKO brain, lung, and skin. Significant levels of HA accumulation was identified in TKO brain ( $p=0.03$ ,  $n=3$ ), and lung ( $p=0.02$ ,  $n=4$ ) compared to DKO controls (Fig. 16A). The concentration of HA observed in these tissues was 5 ng/mg of tissue and 3 ng/mg of tissue respectively; DKO controls displayed much lower levels in brain (0.9 ng/mg of tissue), and lung (1 ng/mg of tissue). Due to variation within the group, TKO skin ( $p=0.06$ ,  $n=5$ ) was not found to accumulate significant levels of HA, although average TKO levels (22 ng/mg of tissue) were approximately 4.4 fold higher than DKO controls (5 ng/mg of tissue;  $n=4$ ). Similar to TKO liver and lymph node, there was also significant chondroitin accumulation in TKO skin, brain, and lung samples (Fig. 16B). Interestingly, brain TKO samples displayed significant accumulation of sulphated chondroitin derivatives when compared to DKO controls (Fig. 16C). However, levels of sulphated chondroitin derivatives in skin (Fig. 16D), and lungs (Fig. 16E) were similar to DKO controls. Nonetheless, DKO lung chondroitin sulphate levels were previously shown to be significantly higher than that found in lung of WT mice (Fig. 9B).

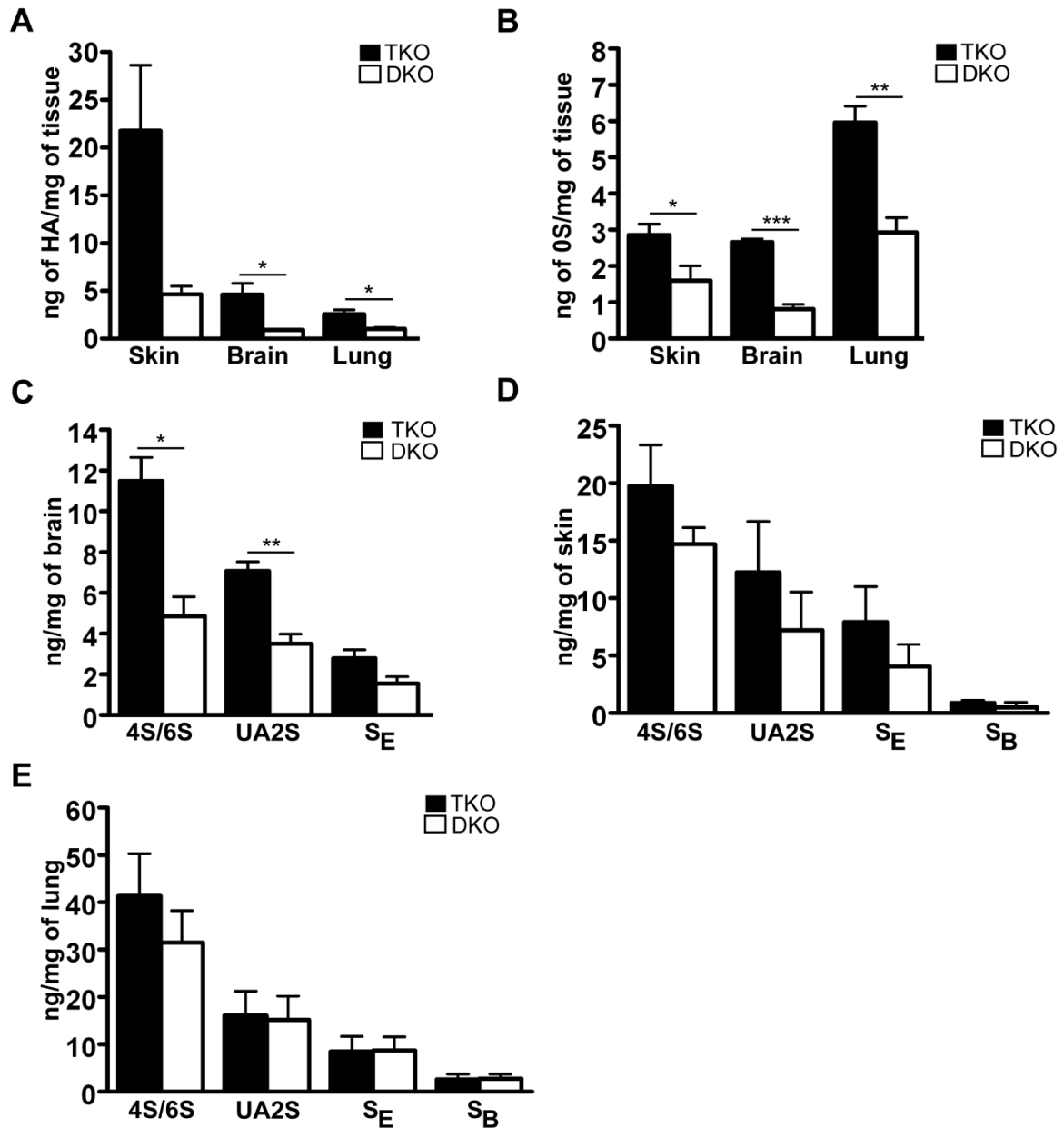


**Figure 16: Quantification of GAG accumulation in other TKO tissues.** FACE was used to quantify HA (A), chondroitin (0S) (B), and sulphated chondroitin (C-E) in skin, brain, and lung. (A) HA levels were significantly higher in TKO brain ( $p=0.03$ ,  $n=3$ ), and lung ( $p=0.02$ ,  $n=4$ ) than DKO controls. HA was not significantly accumulating in TKO skin samples ( $p=0.06$ ,  $n=5$ ). (B) TKO skin ( $p=0.04$ ,  $n=5$ ), brain ( $p=0.0003$ ,  $n=3$ ), and lung ( $p=0.003$ ,  $n=4$ ) displayed higher levels of 0S compared to DKO controls. (C) TKO brain samples had significantly higher levels of chondroitin 4S/6S ( $p=0.01$ ,  $n=3$ ) and UA2S ( $p=0.006$ ,  $n=4$ ). S<sub>E</sub> levels were similar in TKO and DKO samples ( $p=0.09$ ,  $n=4$ ). (D) TKO skin ( $n=4$ ) was not accumulating any chondroitin sulphate derivatives ( $p>0.05$ ) compared to DKO controls ( $n=3$ , with exception of S<sub>B</sub>,  $n=2$ ). (E) TKO lung was also not accumulating any sulphated derivatives of chondroitin ( $p>0.05$ ;  $n=4$ ). Average levels of GAGs are shown in ng/mg of tissue with standard error of the mean (\* $p<0.05$ , \*\* $p<0.01$ , \*\*\* $p<0.001$ ).

#### 4.7 Quantification of GAGs in *C57BL6* and *C57BL6;C129* HYAL1-deficient mice:

The identification of extensive HA accumulation in TKO tissues using FACE (Fig. 15A and 16A), was unexpected given the modest levels of HA accumulation detected by immunohistochemistry using the HABP (Fig. 12 and 13). Given that previous studies focused on total GAG levels in *C57BL6 Hyal1*<sup>-/-</sup> mice<sup>101</sup> and since our TKO and DKO studies were completed using mice on a *C57BL6;C129* background, GAG levels from both *C57BL6* and *C57BL6;C129* HYAL1-deficient tissues were analyzed using FACE. This would allow us to verify that the increase in HA seen in TKO tissues was a product of the loss of both HYAL1 and  $\beta$ -hexosaminidase activities.

There was no significant accumulation of HA in any of the tested *C57BL6;C129 Hyal1*<sup>-/-</sup> tissues when compared to *C57BL6;C129* WT controls (Fig. 17A). However, a definite trend was apparent, such that HYAL1-deficient tissues had consistently higher levels of HA in tested tissues than observed in WT controls. Further, levels of HA in the *C57BL6;C129 Hyal1*<sup>-/-</sup> tissues were much lower than those observed in the TKO tissues (Fig. 15A and 16A). Similar to DKO mice (Fig. 8), higher levels of HA were seen in the *C57BL6;C129 Hyal1*<sup>-/-</sup> lymph node compared to liver (Fig. 17A), although the increase was not significantly different. Unlike TKO tissues, accumulation of other GAGs in *C57BL6;C129 Hyal1*<sup>-/-</sup> tissues was not observed, as levels of chondroitin sulphate derivatives detected in liver, lymph node, skin, brain, and lung (Fig. 17B-E) were similar to WT controls.

Of the tissues tested, significant HA accumulation was seen in liver (p=0.006, n=4) of *C57BL6 Hyal1*<sup>-/-</sup> mice when compared to *C57BL6* WT controls (Fig. 18A). However, at a concentration of 0.1 ng/mg of tissue, *C57BL6 Hyal1*<sup>-/-</sup> HA liver levels were

approximately 660 fold lower than that observed in the TKO mice (Fig. 15A). Further, this statistically significant elevation in HA was from tissues isolated from 1 year-old *Hyal1*<sup>-/-</sup> mice as part of a previous study<sup>101</sup>. No tissues at early time points were available from the *C57BL6* line, and it is possible that the observed accumulation in the liver would not be present at earlier time points. At the time of necropsy of the *C57BL6 Hyal1*<sup>-/-</sup> mice, lymph nodes were only isolated for histological studies and were therefore not available for FACE studies. As shown in Figure 18B and C, *C57BL6 Hyal1*<sup>-/-</sup> tissues were not accumulating significant levels of any type of chondroitin sulphate in the liver, skin, brain, or lung.

#### **4.8 Summary of results part 2:**

Cellular vacuolization due to the accumulation of gangliosides and GAGs was evident in several TKO and DKO tissues however, there was no apparent difference in the overall vacuolization of the TKO mouse tissues when compared to DKO tissues. Alcian blue staining showed more intense staining in some of the TKO tissues, indicating a greater level of GAGs were present when compared to DKO tissues. HABP staining displayed HA accumulation in the liver, brain, lung, and in the cartilage of the knee joint of the TKO mice which was absent in the DKO mice. TKO and DKO tissue HA levels were quantified and it was shown that TKO liver, lymph node, brain, and lung were accumulating HA with the highest levels observed in the liver and lymph node. Along with HA accumulation, all tissues tested displayed accumulation of non-sulphated chondroitin when compared to DKO control samples. Further, TKO liver and brain displayed additional accumulation of sulphated chondroitin derivatives when compared to DKO liver and brain. FACE was also completed on HYAL-1-deficient tissues from 2

backgrounds, *C57BL6;C129* (current study) and *C57BL6* (previous study). Of all the tissues tested, significant HA accumulation was only seen in liver of *C57BL6 Hyal1<sup>-/-</sup>* mice when compared to *C57BL6* WT controls. Further, the level of HA accumulation seen in the *C57BL6 Hyal1<sup>-/-</sup>* liver was approximately 660 fold lower than that observed in the TKO mice.

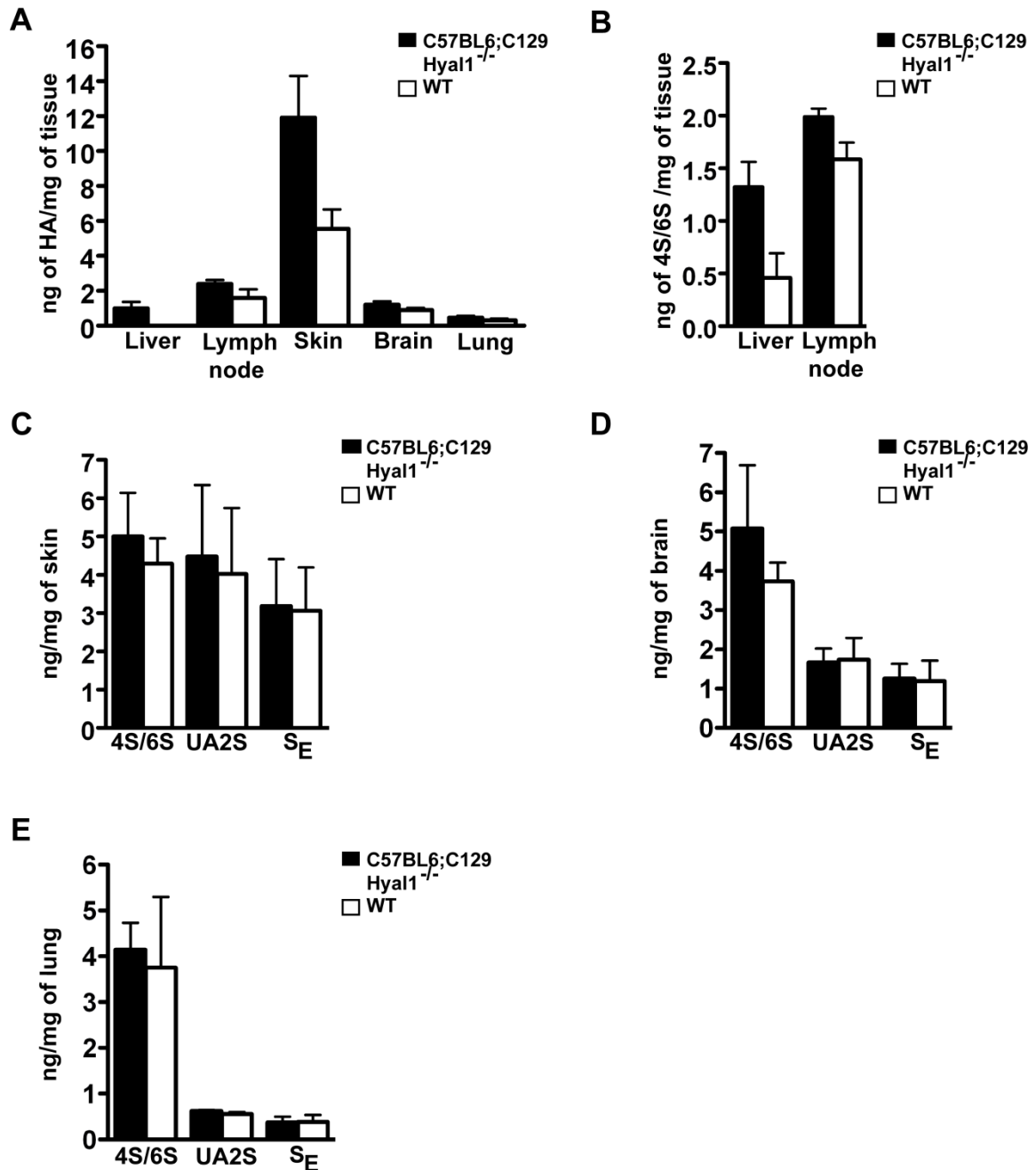


**Figure 17: Analysis of HA and chondroitin sulphate levels in *C57BL6;C129* HYAL1-deficient tissues.** Levels of HA (A) and chondroitin sulphate (B-E) were determined in *C57BL6;C129 Hyal1<sup>-/-</sup>* mice using FACE. (A) *C57BL6;C129 Hyal1<sup>-/-</sup>* mice (n=3) were not significantly accumulating HA in liver (p=0.06), lymph node (p=0.2), skin (p=0.07), brain (p=0.3), or lung (p=0.4), however levels were consistently higher in the HYAL1-deficient tissues than levels found in *C57BL6;C129* WT. (B) In liver (p=0.06) and lymph node (p=0.09), chondroitin 4S/6S was the only detected chondroitin sulphate derivative, but was not significantly accumulating. Various types of sulphated chondroitin were detected in *C57BL6;C129 Hyal1<sup>-/-</sup>* skin (C), brain (D), and lung (E). However, levels were similar to *C57BL6;C129* WT (p>0.05, n=3). Average levels of GAGs are shown in ng/mg of tissue with standard error of the mean.

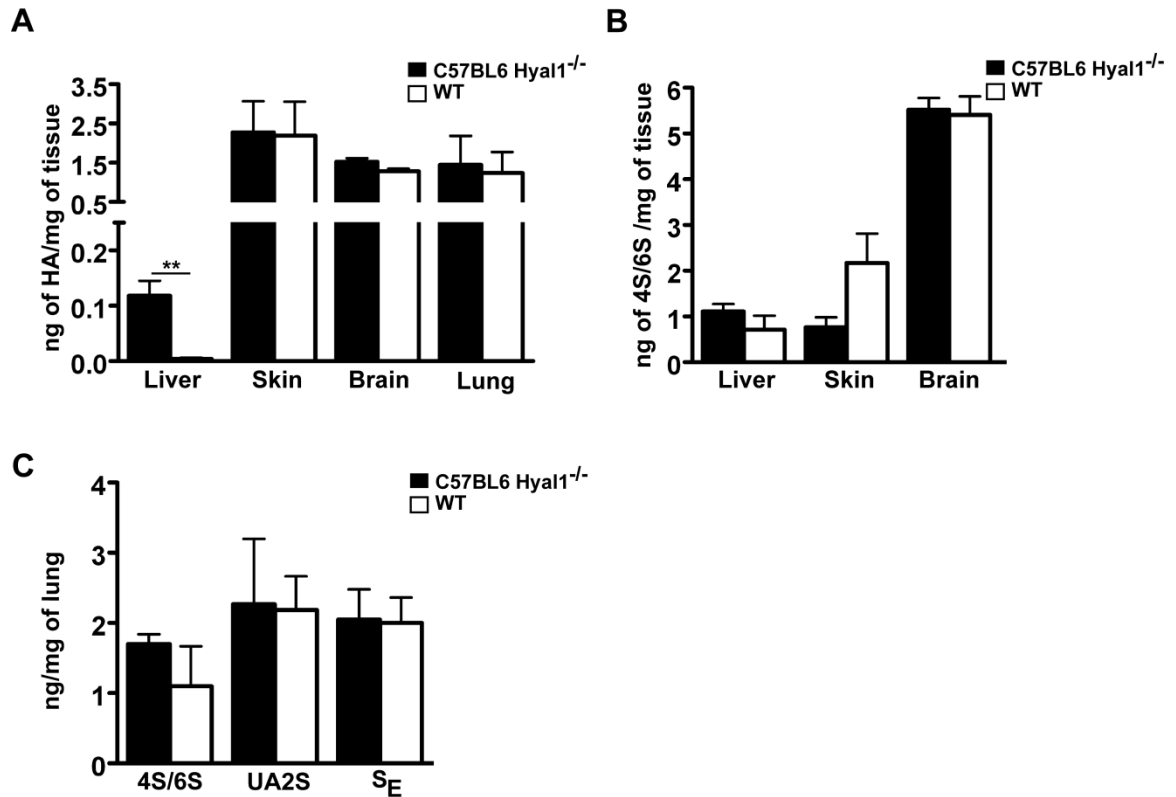


**Figure 18: Analysis of HA and chondroitin sulphate levels in *C57BL6 HYAL1*-deficient tissues.** Levels of HA (A) and chondroitin sulphate (B and C) were determined in *C57BL6 Hyal1*<sup>-/-</sup> mice using FACE. (A) Of the tissues tested, *C57BL6 Hyal1*<sup>-/-</sup> liver ( $p=0.006$ ,  $n=4$ ) was significantly accumulating low levels of HA compared to *C57BL6 WT* controls. *C57BL6 Hyal1*<sup>-/-</sup> skin, brain and lung samples ( $n=3$ ) had HA levels similar to those in *C57BL6 WT* ( $p>0.05$ ). (B) Chondroitin 4S/6S was detected in liver, skin, and brain in *C57BL6 Hyal1*<sup>-/-</sup> and *C57BL6 WT* samples at similar levels ( $p>0.05$ ,  $n=3$ ). (C) Levels of sulphated chondroitin in *C57BL6 Hyal1*<sup>-/-</sup> and *C57BL6 WT* lung were alike ( $p>0.05$ ,  $n=3$ ). Average levels of GAGs are shown in ng/mg of tissue with standard error of the mean (\*\* $p<0.01$ ).

## **Chapter 5: Discussion and Future Directions**

## 5.1 Discussion:

The important structural and functional roles of HA make it a critical component of the ECM. Study of the degradation of this macromolecule within tissues has attracted interest from the ECM field for several years<sup>52, 55, 79, 85</sup>. However, despite the development of several mouse models<sup>67, 101, 102, 108, 109</sup>, the extent to which individual hyaluronidases and exoglycosidases participated in HA turnover was largely unknown. To gain further insight into the contribution of individual hyaluronidases and exoglycosidases in this process, we focused on two lysosomal enzymes proposed to be involved in the breakdown of HA using multiple mouse models. These models included a *Hexb*<sup>-/-</sup> mouse model, a model deficient in all isoforms of  $\beta$ -hexosaminidase, a HYAL1-deficient model, and a model with a combined deficiency of  $\beta$ -hexosaminidase and HYAL1. Using these mouse models it was demonstrated *in vivo* that the exoglycosidase,  $\beta$ -hexosaminidase, and the endoglycosidase, HYAL1, are able to degrade HA fragments and other GAGs. Further, our results give *in vivo* evidence that supports the model for HA turnover proposed by Stern<sup>55, 103</sup>.

### 5.1.1 Functional redundancy between $\beta$ -hexosaminidase and HYAL1:

Global accumulation of HA was found in mice genetically modified to have a combined deficiency of both  $\beta$ -hexosaminidase and HYAL1 activities. However, studies conducted in mice deficient in solely  $\beta$ -hexosaminidase or HYAL1 showed tissue-specific accumulation of HA, albeit at dramatically lower levels than those seen in the combined deficiency. The extensive HA accumulation observed after the loss of both  $\beta$ -hexosaminidase and HYAL1 activities, can thus be attributed to a functional redundancy between the lysosomal hyaluronidase and the exoglycosidase,  $\beta$ -hexosaminidase. This

functional redundancy could potentially provide an explanation of the lack of HA accumulation observed in previous studies using HYAL1-deficient mice<sup>101</sup>.

### **5.1.2 Clinical relevance of a functional redundancy:**

Given the similarities of organ systems between mice and humans, the enzymatic redundancy, such that mouse  $\beta$ -hexosaminidase and HYAL1 can cleave HA and supplement one another *in vivo*, can be extrapolated to humans. Therefore, the above redundancy may account for the relatively mild, but still debilitating, phenotype seen in human HYAL1-deficient patients<sup>54, 91, 92</sup>, as  $\beta$ -hexosaminidase would still be functional and able to degrade HA. Given the above redundancy, treatments such as small molecule therapy that increase the amount of  $\beta$ -hexosaminidase could supplement HA degradation in the joint and would be useful in patients with HYAL1 deficiency as, in the 4 known human cases, the phenotype is limited to the cartilaginous tissue.

### **5.1.3 Major tissues involved in HA metabolism:**

Many studies have identified lymph node and liver as principal sites of HA uptake and turnover<sup>12, 13, 83-85</sup>; our results support these findings. Although TKO mice displayed global tissue accumulation of HA, the liver and lymph node showed much more extensive accumulation than the other tissues tested. Interestingly, a prior study of tissue HA distribution<sup>13</sup> showed that liver and lymph node normally have low levels of HA, whereas skin has high levels of HA. Therefore, since the accumulated HA in the TKO liver and lymph node exceeded the concentration of that in tissues with high HA levels such as skin, the HA is likely to have been transported to these tissues.

HA turnover studies suggest that peripheral tissue HA is brought to the lymph node where it is degraded and recycled. Residual HA that reaches the blood is then sequestered by the liver and degraded<sup>13, 86</sup>. TKO mice, deficient in both HYAL1 and  $\beta$ -hexosaminidase, displayed the highest levels of HA accumulation in the liver, followed by the lymph node. However, mice deficient only in  $\beta$ -hexosaminidase displayed the greatest HA accumulation in the lymph node, with only a small accumulation in the liver. Similarly, the same trend, with higher HA levels in the lymph node as opposed to the liver, was also observed in *C57BL6;C129* HYAL1-deficient mice. The findings seen in mice deficient in either  $\beta$ -hexosaminidase or HYAL1 support previous work suggesting that peripheral HA is first brought through the lymph to the lymph nodes, with a minor amount entering the bloodstream. Consequently, the organ distribution of HA accumulation in the TKO mice contradicts previous findings. However, based on the immense accumulation of HA globally in the TKO mice, the extensive amount of HA accumulated in the liver may just be a result of the liver having a greater overall HA storage capacity. Thus, with the lymphatic system at threshold, the efficiency of HA removal from the lymph would subsequently be hindered and allow more HA to be passed through the efferent lymphatics to the bloodstream and accumulate in the liver as a secondary site. Alternatively, it may be that the level of the compensating enzyme is lower in the lymph node than liver and is insufficient to deal with the HA levels in this tissue in the absence of either  $\beta$ -hexosaminidase or HYAL1.

A recent study focused on HA turnover in *C57BL6* mice by injecting fluorescently labeled HA subcutaneously as well as intravenously<sup>85</sup>. As expected, a strong fluorescent signal was detected in the endothelium of the lymph node and liver, which co-localized

with multiple HA receptors localized to the endothelium. Surprisingly, a strong signal was also observed in the spleen. From prior studies it is known that HA receptors including LYVE-1<sup>112</sup> and HARE<sup>33</sup> are distributed along the splenic endothelium. Our studies did not include spleen as one of the organs tested for HA accumulation after the loss of both  $\beta$ -hexosaminidase and HYAL1 activity. We predict that HA accumulation would be present in mice with a combined deficiency of  $\beta$ -hexosaminidase and HYAL1 because the spleen endothelium has been shown to be very similar to that of lymph node, being lined with multiple HA receptors<sup>85</sup>. Further, we propose spleen as a possible tertiary site of HA accumulation in the TKO mice as it is possible that blood would not be properly filtered by the lymph node and liver due to the accumulation of GAGs. Thus, blood entering the spleen could still have the residual presence of GAGs, which would then be taken up in the spleen by receptor mediated endocytosis.

#### **5.1.4 Role of HYAL1 in brain:**

The broad HA accumulation observed in the TKO mice affected many tissues including the brain. TKO mice displayed similar neurological deterioration as seen in the DKO controls, but the symptoms appeared approximately 10 days earlier. We suggest that the observed early deterioration is the result of neuronal toxicity due to the accumulation of multiple GAGs, including HA, as this accumulation was not seen in brain samples from mice deficient in either  $\beta$ -hexosaminidase or HYAL1. The accumulation of other GAGs, primarily heparin sulphate, has previously been hypothesized as the cause of the neuropathy associated with several other mucopolysaccharidoses<sup>113</sup>. Another possibility for the decreased lifespan is that the extensive accumulation of GAGs reduced the efficacy of the lysosomal breakdown of

other cellular material, resulting in cell toxicity. Regardless of the cause of early deterioration, the accumulation of HA after the loss of both  $\beta$ -hexosaminidase and HYAL1 indicates that HYAL1 plays an important role in HA degradation in the brain; this was surprising as HYAL1 was previously thought to be weakly expressed in the brain<sup>54</sup>. This finding suggests that the supplemental relationship between HYAL1 and  $\beta$ -hexosaminidase is critical for the proper breakdown of HA in brain.

#### **5.1.5 $\beta$ -hexosaminidase and HYAL1 take part in the degradation of multiple GAGs:**

Along with HA accumulation, TKO mice also displayed global accumulation of non-sulphated chondroitin. Chondroitin is a GAG very similar to HA, but is not a normal component of mouse tissues. This suggests that the chondroitin found in the TKO tissues may be derived from intermediates of chondroitin sulphate metabolism that have already been acted on by sulphatases. The presence of chondroitin in TKO, but not DKO or HYAL1-deficient tissues, provides evidence that a combined loss of  $\beta$ -hexosaminidase and HYAL1 activity affected the degradation pathways of multiple GAGs. Specifically, it suggests that  $\beta$ -hexosaminidase and HYAL1 are not only involved in HA degradation, but in chondroitin sulphate turnover as well.

Previous studies have shown that like HA, sulphated chondroitin degradation occurs in the lysosome<sup>114, 115</sup>, and that the same cell surface receptors for endocytosis are possibly shared<sup>35, 116</sup>. Once within the lysosome, the contribution of each lysosomal enzyme to the degradation of sulphated chondroitin is unknown, but both a hyaluronidase<sup>117</sup> and an exoglycosidase<sup>118</sup> have been suggested to have a role. Recently, human HYAL4, thought to be a chondroitinase, was further characterized and confirmed to be

the only known human chondroitin sulphate-specific hydrolyase with little to no activity towards HA and dermatan sulphate <sup>69</sup>. However, HYAL4 displayed tissue-specific expression primarily in placenta and skeletal muscle <sup>50</sup>, suggesting that other enzymes also play a role in chondroitin sulphate degradation.

In our study, sulphated derivatives of chondroitin were found to be accumulating in a tissue-specific manner in mice lacking just  $\beta$ -hexosaminidase activity and in mice with the combined loss of  $\beta$ -hexosaminidase and HYAL1. However, no accumulation was found in mice lacking only HYAL1 activity.  $\beta$ -Hexosaminidase-deficient mice displayed accumulation of several sulphated types of chondroitin including that of dermatan sulphate, providing evidence that  $\beta$ -hexosaminidase has the ability to cleave multiple types of sulphated chondroitin *in vivo*. Furthermore, accumulation of chondroitin sulphate in brain, and additional accumulation in liver after the combined loss of  $\beta$ -hexosaminidase and HYAL1, shows for the first time *in vivo* that sulphated chondroitin derivatives are also substrates of HYAL1. Accumulation in the brain and liver suggests that HYAL1 and  $\beta$ -hexosaminidase compensate for one another in a tissue-specific manner. In addition, the lack of chondroitin sulphate accumulation in other tissues, such as skin, after the combined loss of both  $\beta$ -hexosaminidase and HYAL1, indicates that other enzymes may also play a role, with HYAL4 being a possible candidate.

#### **5.1.6 Substrate specificity of the $\beta$ -hexosaminidase isoforms:**

The accumulation of various forms of sulphated chondroitin in multiple tissues of  $\beta$ -hexosaminidase-deficient mice, and the lack of chondroitin sulphate accumulation in HYAL1-deficient mice, indicates that chondroitin sulphate is a preferred substrate of  $\beta$ -

hexosaminidase. The majority of our study used mice deficient in all isoforms of  $\beta$ -hexosaminidase, and therefore the isoform(s) cleaving the accumulating GAGs could not be determined from solely the DKO studies. However, because FACE was completed in some *Hexb*<sup>-/-</sup> mouse tissues, some speculation as to which of the isoforms of  $\beta$ -hexosaminidase are involved in GAG degradation, and their relative contributions, was possible. Liver and lung from *Hexb*<sup>-/-</sup> mice displayed HA and most chondroitin sulphate levels at approximately half the amount of the levels observed in DKO liver and lung, suggesting that some enzyme activity towards GAGs is present. Given the definite trend seen in *Hexb*<sup>-/-</sup> liver and lung, it can be speculated that HEXB does contribute to HA and chondroitin sulphate degradation. However, it is not the sole contributor, since the levels of GAGs were not equivalent to DKO levels. In *Hexb*<sup>-/-</sup> mice the only isoform of  $\beta$ -hexosaminidase still forming a functioning dimer is  $\beta$ -hexosaminidase S. Previously characterized *in vitro*, recombinant  $\beta$ -hexosaminidase S was shown to preferentially cleave sulphated GAGs<sup>78</sup>. Our study provides *in vivo* evidence that suggests that  $\beta$ -hexosaminidase S may cleave not only sulphated GAGs, but HA as well, given that the levels of HA and chondroitin sulphate in *Hexb*<sup>-/-</sup> liver and lung were between that of WT and DKO values.

## **5.2 Conclusion:**

To conclude, this study describes extensive global accumulation of HA in mice that were modified to have a combined loss of  $\beta$ -hexosaminidase and HYAL1 activities. The lack of broad HA accumulation in mice deficient in either an exoglycosidase or a hyaluronidase suggests that there is a functional redundancy among the lysosomal HA degrading enzymes, HYAL1 and  $\beta$ -hexosaminidase. Moreover, the loss of both  $\beta$ -

hexosaminidase and HYAL1 activity creates an obstacle in overall GAG degradation, as noted by the broad accumulation of chondroitin in the TKO mice. Thus, providing further evidence that HA and chondroitin sulphate share a common degradation route. Furthermore, for the first time *in vivo*, both HYAL1 and  $\beta$ -hexosaminidase were shown to degrade multiple types of chondroitin sulphate. However, chondroitin sulphate was proposed as a preferential substrate for  $\beta$ -hexosaminidase, based on the lack of chondroitin sulphate accumulation in HYAL1-deficient mice.

### **5.3 Future directions:**

The present study gives further insight into the enzymes and tissues involved in GAG metabolism. However, given the recent findings of strong HA uptake in spleen<sup>85</sup>, it would be interesting to complete FACE on spleen samples from mice deficient in either  $\beta$ -hexosaminidase or HYAL1 and mice with a combined deficiency of both enzymes. It is possible that spleen also has a role in the constitutive degradation of HA and other GAGs, given that HA receptors line its endothelium and co-localize with fluorescently labeled HA undergoing endocytosis<sup>85</sup>.

The tissue specific functional redundancy found within the lysosome between  $\beta$ -hexosaminidase and HYAL1, along with the lack of GAG accumulation in TKO skin, suggests that other enzymes are present to degrade GAGs in the absence of both of these enzymes. Two possible candidates are HYAL3 and HYAL4.

Although HYAL3 is expressed at low levels, it is broadly distributed in tissues and therefore, it would be interesting to create other mouse models of combined deficiencies including that of HYAL1 and HYAL3,  $\beta$ -hexosaminidase and HYAL3, as

well as a combined mouse model deficient in HYAL1, HYAL3, and  $\beta$ -hexosaminidase. This would provide further knowledge of the contribution of the lysosomal enzymes involved in GAG catabolism and may provide *in vivo* answers to whether HYAL3 is in fact involved in GAG degradation. The other possible candidate to cleave sulphated GAGs is HYAL4. Using a HYAL4 knockout model, along with combined deficiency models of HYAL4 with the other enzymes above, would provide further *in vivo* data about the contributions of each enzyme to the catabolism of multiple GAGs.

To further validate the proposed model of HA degradation, another mouse model of interest would be a model deficient in the three hyaluronidases, HYAL1, HYAL2, and HYAL3. Information gained from a model completely deficient in hyaluronidases would give a broader knowledge of the overall turnover of GAGs and insight to other possible mechanisms of GAG turnover. Furthermore, it is possible that not all actively degrading GAG enzymes are known in humans and mice. Therefore, a search for novel HA and other GAG degrading enzymes is another possible direction. A potential method to determine novel enzymes would be to employ sequence homology studies.

HA accumulation was not detected in previous studies using *C57BL6* HYAL1-deficient mice<sup>101</sup>. Our study found that these mice were accumulating low, but significant, levels of HA in the liver. As FACE was not completed in the previous study, it is possible that HA accumulation in other tissues was missed. Therefore, it would be interesting to apply FACE to other *C57BL6* HYAL1-deficient tissues, including that of lymph node, which was not available for our study. Furthermore, in our study *C57BL6* wild-type liver had approximately a 2.5 fold lower level of HA than that found in the liver of *C57BL6;C129* wild-type mice, suggesting a difference in overall HA metabolism

between mouse strains. It is unknown if this difference is the result of HA synthesis or degradation. Thus, it would be interesting to complete experiments, similar to previous studies<sup>85</sup>, using fluorescently labeled HA as a marker for turnover in each strain. Knowing the differences in overall GAG metabolism between mouse strains is critical as the same strain of mouse is not consistently used in GAG research.

Lastly, a drawback of using mice deficient in all isoforms of  $\beta$ -hexosaminidase was that it is unclear as to which isoform(s) were contributing to GAG turnover. Thus, only speculations about the contributions could be generated from trends observed in the limited *Hexb*<sup>-/-</sup> data. Further studies using tissues from WT, *Hexa*<sup>-/-</sup>, *Hexb*<sup>-/-</sup>, and DKO mice would be required to provide solid evidence of the extent to which the individual isoforms contribute to GAG degradation. Knowing the preferred GAG substrate for each isoform of  $\beta$ -hexosaminidase would allow for the treatment of some mucopolysaccharidoses to be tailored to the particular GAG that is accumulating.

## References:

1. Hascall, V. & Esko, J. D. in *Essentials of Glycobiology* (eds Varki, A. et al.) (The Consortium of Glycobiology Editors, La Jolla, California, Cold Spring Harbor (NY), 2009).
2. Esko, J. D., Kimata, K. & Lindahl, U. in *Essentials of Glycobiology* (eds Varki, A. et al.) (The Consortium of Glycobiology Editors, La Jolla, California, Cold Spring Harbor (NY), 2009).
3. Hellstrom, M., Mattsson, C., Hellstrom, S. & Engstrom-Laurent, A. Hyaluronan is differently located in arteries and veins. An immunohistochemical study in the rat. *Cells Tissues Organs* **173**, 227-233 (2003).
4. Archer, G. T. Release of heparin from the mast cells of the rat. *Nature* **191**, 90 (1961).
5. Hassell, J. R. *et al.* Isolation of a heparan sulfate-containing proteoglycan from basement membrane. *Proc. Natl. Acad. Sci. U. S. A.* **77**, 4494-4498 (1980).
6. Melrose, J., Smith, S. M., Appleyard, R. C. & Little, C. B. Aggrecan, versican and type VI collagen are components of annular translamellar crossbridges in the intervertebral disc. *Eur. Spine J.* **17**, 314-324 (2008).
7. Bespalov, M. M. *et al.* Heparan sulfate proteoglycan syndecan-3 is a novel receptor for GDNF, neurturin, and artemin. *J. Cell Biol.* **192**, 153-169 (2011).
8. Meyer, K. & Palmer, J. The Polysaccharide of the Vitreous Humor. *J. Biol. Chem.* **107**, 629 (1934).
9. Stern, R., Asari, A. A. & Sugahara, K. N. Hyaluronan fragments: an information-rich system. *Eur. J. Cell Biol.* **85**, 699-715 (2006).
10. Laurent, T. C., Laurent, U. B. & Fraser, J. R. The structure and function of hyaluronan: An overview. *Immunol. Cell Biol.* **74**, A1-7 (1996).
11. Hardingham, T. E. & Muir, H. The specific interaction of hyaluronic acid with cartilage proteoglycans. *Biochim. Biophys. Acta* **279**, 401-405 (1972).
12. Reed, R. K., Lilja, K. & Laurent, T. C. Hyaluronan in the rat with special reference to the skin. *Acta Physiol. Scand.* **134**, 405-411 (1988).
13. Fraser, J. R. & Laurent, T. C. Turnover and metabolism of hyaluronan. *Ciba Found. Symp.* **143**, 41-53; discussion 53-9, 281-5 (1989).
14. Comper, W. D. & Laurent, T. C. Physiological function of connective tissue polysaccharides. *Physiol. Rev.* **58**, 255-315 (1978).

15. Jiang, D., Liang, J. & Noble, P. W. Hyaluronan as an immune regulator in human diseases. *Physiol. Rev.* **91**, 221-264 (2011).
16. Russell, D. L. & Salustri, A. Extracellular matrix of the cumulus-oocyte complex. *Semin. Reprod. Med.* **24**, 217-227 (2006).
17. Volpi, N., Schiller, J., Stern, R. & Soltes, L. Role, metabolism, chemical modifications and applications of hyaluronan. *Curr. Med. Chem.* **16**, 1718-1745 (2009).
18. Feinberg, R. N. & Beebe, D. C. Hyaluronate in vasculogenesis. *Science* **220**, 1177-1179 (1983).
19. Sattar, A. *et al.* Application of angiogenic oligosaccharides of hyaluronan increases blood vessel numbers in rat skin. *J. Invest. Dermatol.* **103**, 576-579 (1994).
20. Camenisch, T. D. *et al.* Disruption of hyaluronan synthase-2 abrogates normal cardiac morphogenesis and hyaluronan-mediated transformation of epithelium to mesenchyme. *J. Clin. Invest.* **106**, 349-360 (2000).
21. Toole, B. P. Hyaluronan and its binding proteins, the hyaladherins. *Curr. Opin. Cell Biol.* **2**, 839-844 (1990).
22. Kohda, D. *et al.* Solution structure of the link module: a hyaluronan-binding domain involved in extracellular matrix stability and cell migration. *Cell* **86**, 767-775 (1996).
23. Day, A. J. & Prestwich, G. D. Hyaluronan-binding proteins: tying up the giant. *J. Biol. Chem.* **277**, 4585-4588 (2002).
24. Culty, M., Nguyen, H. A. & Underhill, C. B. The hyaluronan receptor (CD44) participates in the uptake and degradation of hyaluronan. *J. Cell Biol.* **116**, 1055-1062 (1992).
25. Harada, H. & Takahashi, M. CD44-dependent intracellular and extracellular catabolism of hyaluronic acid by hyaluronidase-1 and -2. *J. Biol. Chem.* **282**, 5597-5607 (2007).
26. Clark, R. A., Alon, R. & Springer, T. A. CD44 and hyaluronan-dependent rolling interactions of lymphocytes on tonsillar stroma. *J. Cell Biol.* **134**, 1075-1087 (1996).
27. Matou-Nasri, S., Gaffney, J., Kumar, S. & Slevin, M. Oligosaccharides of hyaluronan induce angiogenesis through distinct CD44 and RHAMM-mediated signalling pathways involving Cdc2 and gamma-adducin. *Int. J. Oncol.* **35**, 761-773 (2009).
28. Wrobel, T. *et al.* LYVE-1 expression on high endothelial venules (HEVs) of lymph nodes. *Lymphology* **38**, 107-110 (2005).

29. Mouta Carreira, C. *et al.* LYVE-1 is not restricted to the lymph vessels: expression in normal liver blood sinusoids and down-regulation in human liver cancer and cirrhosis. *Cancer Res.* **61**, 8079-8084 (2001).
30. Gordon, E. J., Gale, N. W. & Harvey, N. L. Expression of the hyaluronan receptor LYVE-1 is not restricted to the lymphatic vasculature; LYVE-1 is also expressed on embryonic blood vessels. *Dev. Dyn.* **237**, 1901-1909 (2008).
31. Lee, H. W. *et al.* Expression of lymphatic endothelium-specific hyaluronan receptor LYVE-1 in the developing mouse kidney. *Cell Tissue Res.* **343**, 429-444 (2011).
32. Prevo, R., Banerji, S., Ferguson, D. J., Clasper, S. & Jackson, D. G. Mouse LYVE-1 is an endocytic receptor for hyaluronan in lymphatic endothelium. *J. Biol. Chem.* **276**, 19420-19430 (2001).
33. Zhou, B., Weigel, J. A., Fauss, L. & Weigel, P. H. Identification of the hyaluronan receptor for endocytosis (HARE). *J. Biol. Chem.* **275**, 37733-37741 (2000).
34. Politz, O. *et al.* Stabilin-1 and -2 constitute a novel family of fasciclin-like hyaluronan receptor homologues. *Biochem. J.* **362**, 155-164 (2002).
35. Harris, E. N. & Weigel, P. H. The ligand-binding profile of HARE: hyaluronan and chondroitin sulfates A, C, and D bind to overlapping sites distinct from the sites for heparin, acetylated low-density lipoprotein, dermatan sulfate, and CS-E. *Glycobiology* **18**, 638-648 (2008).
36. Gale, N. W. *et al.* Normal lymphatic development and function in mice deficient for the lymphatic hyaluronan receptor LYVE-1. *Mol. Cell. Biol.* **27**, 595-604 (2007).
37. Hardwick, C. *et al.* Molecular cloning of a novel hyaluronan receptor that mediates tumor cell motility. *J. Cell Biol.* **117**, 1343-1350 (1992).
38. Turley, E. A., Austen, L., Moore, D. & Hoare, K. Ras-transformed cells express both CD44 and RHAMM hyaluronan receptors: only RHAMM is essential for hyaluronan-promoted locomotion. *Exp. Cell Res.* **207**, 277-282 (1993).
39. Assmann, V., Jenkinson, D., Marshall, J. F. & Hart, I. R. The intracellular hyaluronan receptor RHAMM/IHABP interacts with microtubules and actin filaments. *J. Cell. Sci.* **112** ( Pt 22), 3943-3954 (1999).
40. Savani, R. C. *et al.* Migration of bovine aortic smooth muscle cells after wounding injury. The role of hyaluronan and RHAMM. *J. Clin. Invest.* **95**, 1158-1168 (1995).
41. Ahrens, T. *et al.* CD44 is the principal mediator of hyaluronic-acid-induced melanoma cell proliferation. *J. Invest. Dermatol.* **116**, 93-101 (2001).

42. Assmann, V. *et al.* The pattern of expression of the microtubule-binding protein RHAMM/IHABP in mammary carcinoma suggests a role in the invasive behaviour of tumour cells. *J. Pathol.* **195**, 191-196 (2001).
43. Prehm, P. Synthesis of hyaluronate in differentiated teratocarcinoma cells. Mechanism of chain growth. *Biochem. J.* **211**, 191-198 (1983).
44. Prehm, P. & Schumacher, U. Inhibition of hyaluronan export from human fibroblasts by inhibitors of multidrug resistance transporters. *Biochem. Pharmacol.* **68**, 1401-1410 (2004).
45. Schulz, T., Schumacher, U. & Prehm, P. Hyaluronan export by the ABC transporter MRP5 and its modulation by intracellular cGMP. *J. Biol. Chem.* **282**, 20999-21004 (2007).
46. Itano, N. *et al.* Three isoforms of mammalian hyaluronan synthases have distinct enzymatic properties. *J. Biol. Chem.* **274**, 25085-25092 (1999).
47. Bai, K. J. *et al.* The role of hyaluronan synthase 3 in ventilator-induced lung injury. *Am. J. Respir. Crit. Care Med.* **172**, 92-98 (2005).
48. Mack, J. A. *et al.* Enhanced inflammation and accelerated wound closure following tetraphorbol ester application or full-thickness wounding in mice lacking hyaluronan synthases has1 and has3. *J. Invest. Dermatol.* **132**, 198-207 (2012).
49. Stern, R. & Jedrzejewski, M. J. Hyaluronidases: their genomics, structures, and mechanisms of action. *Chem. Rev.* **106**, 818-839 (2006).
50. Csoka, A. B., Scherer, S. W. & Stern, R. Expression analysis of six paralogous human hyaluronidase genes clustered on chromosomes 3p21 and 7q31. *Genomics* **60**, 356-361 (1999).
51. Csoka, A. B. *et al.* The hyaluronidase gene HYAL1 maps to chromosome 3p21.2-p21.3 in human and 9F1-F2 in mouse, a conserved candidate tumor suppressor locus. *Genomics* **48**, 63-70 (1998).
52. Csoka, A. B., Frost, G. I. & Stern, R. The six hyaluronidase-like genes in the human and mouse genomes. *Matrix Biol.* **20**, 499-508 (2001).
53. Kim, E. *et al.* Identification of a hyaluronidase, Hyal5, involved in penetration of mouse sperm through cumulus mass. *Proc. Natl. Acad. Sci. U. S. A.* **102**, 18028-18033 (2005).
54. Triggs-Raine, B., Salo, T. J., Zhang, H., Wicklow, B. A. & Natowicz, M. R. Mutations in HYAL1, a member of a tandemly distributed multigene family encoding

- disparate hyaluronidase activities, cause a newly described lysosomal disorder, mucopolysaccharidosis IX. *Proc. Natl. Acad. Sci. U. S. A.* **96**, 6296-6300 (1999).
55. Stern, R. Devising a pathway for hyaluronan catabolism: are we there yet? *Glycobiology* **13**, 105R-115R (2003).
56. Frost, G. I., Csoka, A. B., Wong, T. & Stern, R. Purification, cloning, and expression of human plasma hyaluronidase. *Biochem. Biophys. Res. Commun.* **236**, 10-15 (1997).
57. Gasingirwa, M. C. *et al.* Endocytosis of hyaluronidase-1 by the liver. *Biochem. J.* **430**, 305-313 (2010).
58. Strobl, B., Wechselberger, C., Beier, D. R. & Lepperdinger, G. Structural organization and chromosomal localization of Hyal2, a gene encoding a lysosomal hyaluronidase. *Genomics* **53**, 214-219 (1998).
59. Rai, S. K. *et al.* Candidate tumor suppressor HYAL2 is a glycosylphosphatidylinositol (GPI)-anchored cell-surface receptor for jaagsiekte sheep retrovirus, the envelope protein of which mediates oncogenic transformation. *Proc. Natl. Acad. Sci. U. S. A.* **98**, 4443-4448 (2001).
60. Andre, B. *et al.* Hyal2 is a glycosylphosphatidylinositol-anchored, lipid raft-associated hyaluronidase. *Biochem. Biophys. Res. Commun.* **411**, 175-179 (2011).
61. Duterme, C., Mertens-Strijthagen, J., Tammi, M. & Flamion, B. Two novel functions of hyaluronidase-2 (Hyal2) are formation of the glycocalyx and control of CD44-ERM interactions. *J. Biol. Chem.* **284**, 33495-33508 (2009).
62. de la Motte, C. *et al.* Platelet-derived hyaluronidase 2 cleaves hyaluronan into fragments that trigger monocyte-mediated production of proinflammatory cytokines. *Am. J. Pathol.* **174**, 2254-2264 (2009).
63. Tan, J. X. *et al.* Upregulation of HYAL1 expression in breast cancer promoted tumor cell proliferation, migration, invasion and angiogenesis. *PLoS One* **6**, e22836 (2011).
64. Bourguignon, L. Y., Singleton, P. A., Diedrich, F., Stern, R. & Gilad, E. CD44 interaction with Na<sup>+</sup>-H<sup>+</sup> exchanger (NHE1) creates acidic microenvironments leading to hyaluronidase-2 and cathepsin B activation and breast tumor cell invasion. *J. Biol. Chem.* **279**, 26991-27007 (2004).
65. Tan, J. X. *et al.* HYAL1 overexpression is correlated with the malignant behavior of human breast cancer. *Int. J. Cancer* **128**, 1303-1315 (2011).
66. Hemming, R. *et al.* Mouse Hyal3 encodes a 45- to 56-kDa glycoprotein whose overexpression increases hyaluronidase 1 activity in cultured cells. *Glycobiology* **18**, 280-289 (2008).

67. Atmuri, V. *et al.* Hyaluronidase 3 (HYAL3) knockout mice do not display evidence of hyaluronan accumulation. *Matrix Biol.* **27**, 653-660 (2008).
68. Cherr, G. N. *et al.* The PH-20 protein in cynomolgus macaque spermatozoa: identification of two different forms exhibiting hyaluronidase activity. *Dev. Biol.* **175**, 142-153 (1996).
69. Kaneiwa, T., Mizumoto, S., Sugahara, K. & Yamada, S. Identification of human hyaluronidase-4 as a novel chondroitin sulfate hydrolase that preferentially cleaves the galactosaminidic linkage in the trisulfated tetrasaccharide sequence. *Glycobiology* **20**, 300-309 (2010).
70. Longas, M. O. & Meyer, K. Sequential hydrolysis of hyaluronate by beta-glucuronidase and beta-N-acetylhexosaminidase. *Biochem. J.* **197**, 275-282 (1981).
71. Chern, C. J. & Croce, C. M. Assignment of the structural gene for human beta glucuronidase to chromosome 7 and tetrameric association of subunits in the enzyme molecule. *Am. J. Hum. Genet.* **28**, 350-356 (1976).
72. Swank, R. T., Paigen, K. & Ganschow, R. E. Genetic control of glucuronidase induction in mice. *J. Mol. Biol.* **81**, 225-243 (1973).
73. Paigen, K. Acid hydrolases as models of genetic control. *Annu. Rev. Genet.* **13**, 417-466 (1979).
74. Tomino, S., Paigen, K., Tulsiani, D. R. & Touster, O. Purification and chemical properties of mouse liver lysosomal (L form) beta-glucuronidase. *J. Biol. Chem.* **250**, 8503-8509 (1975).
75. Linker, A., Meyer, K. & Weissmann, B. Enzymatic formation of monosaccharides from hyaluronate. *J. Biol. Chem.* **213**, 237-248 (1955).
76. Yamanaka, S., Johnson, O. N., Norflus, F., Boles, D. J. & Proia, R. L. Structure and expression of the mouse beta-hexosaminidase genes, Hexa and Hexb. *Genomics* **21**, 588-596 (1994).
77. Zwierz, K., Zalewska, A. & Zoch-Zwierz, A. Isoenzymes of N-acetyl-beta-hexosaminidase. *Acta Biochim. Pol.* **46**, 739-751 (1999).
78. Hepbildikler, S. T., Sandhoff, R., Kolzer, M., Proia, R. L. & Sandhoff, K. Physiological substrates for human lysosomal beta -hexosaminidase S. *J. Biol. Chem.* **277**, 2562-2572 (2002).
79. Hascall, V. C., Sandy, J. D. & Handley, C. J. in *Biology of the synovial joint* 101 (Harwood Academic Publishers, Amsterdam , the Netherlands, 1999).

80. Banerji, S. *et al.* LYVE-1, a new homologue of the CD44 glycoprotein, is a lymph-specific receptor for hyaluronan. *J. Cell Biol.* **144**, 789-801 (1999).
81. Rome, L. H. & Hill, D. F. Lysosomal degradation of glycoproteins and glycosaminoglycans. Efflux and recycling of sulphate and N-acetylhexosamines. *Biochem. J.* **235**, 707-713 (1986).
82. Bastow, E. R. *et al.* Hyaluronan synthesis and degradation in cartilage and bone. *Cell Mol. Life Sci.* **65**, 395-413 (2008).
83. Eriksson, S., Fraser, J. R., Laurent, T. C., Pertoft, H. & Smedsrod, B. Endothelial cells are a site of uptake and degradation of hyaluronic acid in the liver. *Exp. Cell Res.* **144**, 223-228 (1983).
84. Fraser, J. R., Kimpton, W. G., Laurent, T. C., Cahill, R. N. & Vakakis, N. Uptake and degradation of hyaluronan in lymphatic tissue. *Biochem. J.* **256**, 153-158 (1988).
85. Jadin, L., Bookbinder, L. H. & Frost, G. I. A comprehensive model of hyaluronan turnover in the mouse. *Matrix Biol.* (2011). doi:10.1016/j.matbio.2011.11.002
86. Laurent, U. B. & Laurent, T. C. On the origin of hyaluronate in blood. *Biochem. Int.* **2**, 195 (1981).
87. Schultz, M. L., Tecedor, L., Chang, M. & Davidson, B. L. Clarifying lysosomal storage diseases. *Trends Neurosci.* **34**, 401-410 (2011).
88. Coutinho, M. F., Lacerda, L. & Alves, S. Glycosaminoglycan storage disorders: a review. *Biochem. Res. Int.* **2012**, 471325 (2012).
89. Boomkamp, S. D. & Butters, T. D. Glycosphingolipid disorders of the brain. *Subcell. Biochem.* **49**, 441-467 (2008).
90. Sandhoff, K. & Christomanou, H. Biochemistry and genetics of gangliosidoses. *Hum. Genet.* **50**, 107-143 (1979).
91. Imundo, L. *et al.* A complete deficiency of Hyaluronoglucosaminidase 1 (HYAL1) presenting as familial juvenile idiopathic arthritis. *J. Inherit. Metab. Dis.* **34**, 1013-1022 (2011).
92. Natowicz, M. R. *et al.* Clinical and biochemical manifestations of hyaluronidase deficiency. *N. Engl. J. Med.* **335**, 1029-1033 (1996).
93. Sly, W. S., Quinton, B. A., McAlister, W. H. & Rimoin, D. L. Beta glucuronidase deficiency: report of clinical, radiologic, and biochemical features of a new mucopolysaccharidosis. *J. Pediatr.* **82**, 249-257 (1973).

94. Storch, S. *et al.* Mutational analysis in longest known survivor of mucopolysaccharidosis type VII. *Hum. Genet.* **112**, 190-194 (2003).
95. Sewell, A. C., Gehler, J., Mittermaier, G. & Meyer, E. Mucopolysaccharidosis type VII (beta-glucuronidase deficiency): a report of a new case and a survey of those in the literature. *Clin. Genet.* **21**, 366-373 (1982).
96. Delbecque, K., Gaillez, S. & Schaaps, J. P. Histopathological diagnosis of a type vii mucopolysaccharidosis after pregnancy termination. *Fetal. Pediatr. Pathol.* **28**, 1-8 (2009).
97. Vogler, C. *et al.* Mucopolysaccharidosis VII: postmortem biochemical and pathological findings in a young adult with beta-glucuronidase deficiency. *Mod. Pathol.* **7**, 132-137 (1994).
98. Jeyakumar, M., Butters, T. D., Dwek, R. A. & Platt, F. M. Glycosphingolipid lysosomal storage diseases: therapy and pathogenesis. *Neuropathol. Appl. Neurobiol.* **28**, 343-357 (2002).
99. Bolhuis, P. A. *et al.* Ganglioside storage, hexosaminidase lability, and urinary oligosaccharides in adult Sandhoff's disease. *Neurology* **37**, 75-81 (1987).
100. Kornfeld, M. Neuropathology of chronic GM2 gangliosidosis due to hexosaminidase A deficiency. *Clin. Neuropathol.* **27**, 302-308 (2008).
101. Martin, D. C. *et al.* A mouse model of human mucopolysaccharidosis IX exhibits osteoarthritis. *Hum. Mol. Genet.* **17**, 1904-1915 (2008).
102. Jadin, L. *et al.* Skeletal and hematological anomalies in HYAL2-deficient mice: a second type of mucopolysaccharidosis IX? *FASEB J.* **22**, 4316-4326 (2008).
103. Stern, R. Hyaluronan catabolism: a new metabolic pathway. *Eur. J. Cell Biol.* **83**, 317-325 (2004).
104. Birkenmeier, E. H. *et al.* Murine mucopolysaccharidosis type VII. Characterization of a mouse with beta-glucuronidase deficiency. *J. Clin. Invest.* **83**, 1258-1266 (1989).
105. Vogler, C. *et al.* A murine model of mucopolysaccharidosis VII. Gross and microscopic findings in beta-glucuronidase-deficient mice. *Am. J. Pathol.* **136**, 207-217 (1990).
106. Phaneuf, D. *et al.* Dramatically different phenotypes in mouse models of human Tay-Sachs and Sandhoff diseases. *Hum. Mol. Genet.* **5**, 1-14 (1996).
107. Sango, K. *et al.* Mouse models of Tay-Sachs and Sandhoff diseases differ in neurologic phenotype and ganglioside metabolism. *Nat. Genet.* **11**, 170-176 (1995).

108. Sango, K. *et al.* Mice lacking both subunits of lysosomal beta-hexosaminidase display gangliosidosis and mucopolysaccharidosis. *Nat. Genet.* **14**, 348-352 (1996).
109. Suzuki, K., Sango, K., Proia, R. L. & Langaman, C. Mice deficient in all forms of lysosomal beta-hexosaminidase show mucopolysaccharidosis-like pathology. *J. Neuropathol. Exp. Neurol.* **56**, 693-703 (1997).
110. Lehrman, M. A. & Gao, N. Alternative and sources of reagents and supplies of fluorophore-assisted carbohydrate electrophoresis(FACE). *Glycobiology* **13**, 1G-3G (2003).
111. Evers, M. *et al.* Targeted disruption of the arylsulfatase B gene results in mice resembling the phenotype of mucopolysaccharidosis VI. *Proc. Natl. Acad. Sci. U. S. A.* **93**, 8214-8219 (1996).
112. Jackson, D. G. Biology of the lymphatic marker LYVE-1 and applications in research into lymphatic trafficking and lymphangiogenesis. *APMIS* **112**, 526-538 (2004).
113. Wegrzyn, G. *et al.* Why are behaviors of children suffering from various neuronopathic types of mucopolysaccharidoses different? *Med. Hypotheses* **75**, 605-609 (2010).
114. Wood, K. M., Wusteman, F. S. & Curtis, C. G. The degradation of intravenously injected chondroitin 4-sulphate in the rat. *Biochem. J.* **134**, 1009-1013 (1973).
115. Fischer, J. Tilorone-induced lysosomal storage of glycosaminoglycans in cultured corneal fibroblasts: biochemical and physicochemical investigations. *Biochem. J.* **312 ( Pt 1)**, 215-222 (1995).
116. Kawashima, H. *et al.* Binding of a large chondroitin sulfate/dermatan sulfate proteoglycan, versican, to L-selectin, P-selectin, and CD44. *J. Biol. Chem.* **275**, 35448-35456 (2000).
117. Aronson, N. N., Jr & Davidson, E. A. Lysosomal hyaluronidase from rat liver. II. Properties. *J. Biol. Chem.* **242**, 441-444 (1967).
118. Glaser, J. H. & Conrad, H. E. Chondroitin SO<sub>4</sub> catabolism in chick embryo chondrocytes. *J. Biol. Chem.* **254**, 2316-2325 (1979).